PALACKÝ
UNIVERSITY
OLOMOUC

Mgr. Mikuláš Kocman

Intermolecular Interactions in Nanomaterials

Ph.D. Thesis

Supervisor: doc. RNDr. Petr Jurečka, Ph.D.

Department of Physical Chemistry, 2014

Declaration of the author

I declare that I have worked out this thesis by myself using cited references. Neither the thesis nor any of its part was previously used for obtaining academic degree.

Olomouc, July 2014

_____

Mikuláš Kocman

To my beloved Irenka
and Emil

Acknowledgement

There are a number of people without whom this thesis might not be written and to whom I am greatly indebted. At first I would like to thank my supervisor Petr Jurečka for introducing me the world of computational chemistry and for being a good friend who had never regret to help me.

To Pavel Banáš from whom I keep learning how to quickly solve any problem of any difficulties in elegant way.

I am also grateful to Michal Otyepka as he turned the Department of Physical chemistry into inspiring, open and excellently equipped environment, where was pleasure to work.

I have to mention my desk-mate Vojtech Mlynsky as we have spent Ph.D. studies together from beginning to the end.

Most of all I would like to thank my family for the continuous support and trust in me during my whole studies.

Contents

Motivation **1**

1. Graphene **3**

1.1. Properties of Graphene 6

1.2. Synthesis of Graphene 7

2. Theory and Methods **9**

2.1. Intermolecular Interactions 11

2.2. Computational Chemistry 16

2.2.1. Quantum Mechanics approach 16

2.2.2. Classical Mechanics approach 19

2.3. Comparison with experiment 22

2.4. Connection to the world of nanomaterials 24

3. Results **27**

3.1. Electric Quadrupole Moment of Graphene and its Effect on Intermolecular Interactions 29

3.2. Adsorption of small organic molecules on graphene 37

3.3. Choosing a Density Functional for Modelling of Adsorptive Hydrogen Storage 41

Summary **45**

References **47**

List of publications **53**

Apendix **55**

Abbreviations

AFM – atomic force microscope
B97D – Becke-Johnson functional with dispersion correction
BLYP, B3LYP – Becke-Lee-Yang-Par functional
BSSE – basis set superposition error
C478 – rectangular graphene of 478 carbon atoms
CBS – complete basis set
CC – coupled cluster
cc-pVXZ – correlation consistent polarization X-zeta basis
CCSD(T) – CC single, double, triple perturbatively
CHARMM – Chemistry at HARvard Molecular Mechanics package
CP – counter poise
CVD – chemical vapor deposition
DFT – density functional theory
DFT-D3 – DFT-corrected with empirical dispersion
DNA – deoxyribonucleic acid
DOE – department of energy
ESP – electrostatic potential
FF – force field
GGA – generalized gradient approximation
GTO – Gaussian type orbital
HF – Hartree Fock
HOPG – highly oriented pyrolitic graphite
LDA – local density approximation
LJ – Lennard Jones
M06 – Truhlar's functional
MD – molecular mynamics
MM – molecular mechanics
MPX – Moller Plesset of X-th order
OPLS – optimized potentials for liquid simulations
OPLS-AA – OPLS - all atom
Parm99 – Amber forcefield, 1999
PBE – Perdew-Burke-Ernzerhof functional
PBE+TS – PBE with Tkatchenko Scheffler correction
PMF – potential of mean force
PW91 – Pee-Wang functional
QM – quantum mechanics
SAPT – symmetry adapted perturbation theory
STO – Slater type orbital
SVWN – Slater-Vosko-Wilk-Nusair functional
TPSS – Tao-Perdew-Staroverov-Scuseria functional
vdW – van der Waalse
ZPVE – zero point vibrational energy

Motivation

Graphene is a novel two-dimensional material consisting of carbon atoms arranged in a honeycomb lattice. Its discovery provoked the imagination of scientific community and aroused great interest in usage and design of new materials based on graphene structure. The main topics of research are graphene electronics, photonics, energy generation and storage, composite materials, bio-application and mass production of graphene.

Liquid phase exfoliation is one of the most promising methods for preparation of large amounts of graphene in solution. Unfortunately, graphene flakes tend to stick together and quickly form graphite aggregates. Finding a suitable solvent that would be able to keep the graphene sheets apart remains a challenge. An interesting problem related to this arose when two solvents with similar solubility parameters showed opposite effect on the exfoliation process. The aim of the first part of my PhD thesis is to describe the mechanism of exfoliation process in various solvents with the tools of molecular modelling, investigate the role of (often neglected) electrostatic interactions and propose the way these interactions should be treated in molecular dynamics simulations involving graphene.

Graphene has a surface density of 2.62 A^2/atom which leads to theoretical surface area of 2600 m^2/g. Due to this huge surface area, graphene-based structures may find applications as a sorption material, e. g., in hydrogen storage. However, some kind of chemical modification is required, because hydrogen adsorbs to pristine graphene only weakly. Second part of this thesis will focuse on obtaining accurate intermolecular interaction energies of graphene and its derivatives with molecular hydrogen and assessment of accuracy of current DFT functionals including empirical and nonempirical dispersion corrections.

Understanding adsorption properties of graphene may be important in various nanotechnological and sensing applications. In the third part of my thesis I will focus on describing intermolecular interactions of graphene with small organic molecules and possibility of accurate predictions of adsorption enthalpies by means of theoretical calculations.

Graphene

Graphene

On 22nd of October 2004 two relatively young scientists, Alexander Geim and Konstantin Novoselov published an article in Science, and shared with scientific community their discovery of graphene.[1] The two-dimensional sheet of six membered carbon rings was prepared simply by scotch tape peeling of highly oriented pyrolitic graphite (HOPG). Their discovery immediately aroused great scientific interest, which can be demonstrated by more than 100,000 scientific articles published in peer-reviewed journals in past ten years.[2] This explosion of interest had two reasons. First, until their discovery it was believed, that none of the two-dimensional crystals could be thermodynamically stable in its free form. Second, graphene has several properties that are dramatically different from those of bulk graphite.[3] The main research areas will be discussed below.

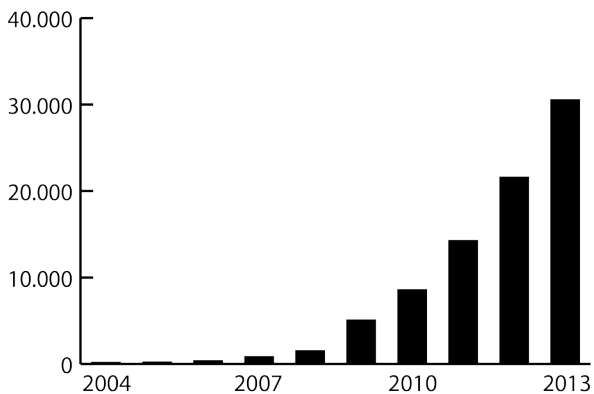

Figure 1. Rise of the graphene publications in recent years.

Besides experimental approaches, properties of graphene can be studied also theoretically, with the use of computational chemistry tools. Detailed theoretical insight can provide better understanding of many important phenomena, including intermolecular interactions. In the following I will briefly review basic properties of graphene, experimental methods of graphene preparation and theoretical approaches for description of intermolecular interactions with graphene. Emphasis will be placed on treatment of intermolecular interactions by empirical force fields and their description by computationally efficient quantum mechanical (QM) methods.

1.1. Properties of Graphene

Electronic properties. Graphene is a semi-metal with very high electrical conductivity. Carbon atoms have four electrons in their valence shells, three of which are used for bonding to the neighbouring atoms in lattice and one remaining, the π electron, is involved in the π system delocalized above and below the graphene plane. This electron is free to move and can travel through the graphene sheet as if it carried no mass. Its actual velocity is equivalent to about 1/300 of velocity of light. This results in unique electronic and transport properties, such as absence of backscattering, which causes that graphene behaves as a perfect conductor.[4]

Mechanical properties. Elastic properties of graphene have been measured with atomic force microscope by pressing the microscope tip against the graphene surface placed on silicon support with holes. The group of J. Hone measured the maximum load and corresponding Young modulus of graphene, which is about 1TPa (compare to 200GPa for steel)[5] Graphene is also very flexible and the deflection before braking is more than 20% of its initial length. Combination of favourable mechanical and electronic properties makes graphene a perspective material for flexible electronics such as transparent conductive coatings or rollable e-paper.

Thermal properties. Thermal conductivity of a single graphene layer was experimentally determined by confocal micro-Raman spectroscopy.[6] The room temperature value was as high as 5300 W/m/K, which is higher than the values measured in other carbon structures, such as graphite nanotubes and diamond. Compared with semiconductors, where thermal conductivity is 150 W/m/K for bulk Si and 10 W/m/K for Si nanowires at room temperature,[7] the outstanding thermal and electrical conductivity of graphene might push this material towards being used as nano-interconnects as well as for thermal dissipation in integrated circuits.[8]

Optical properties. One atom thick graphene sheet is found to absorb only a small fraction of light; graphene opacity is about 2.3%. Optical spectroscopy shows that absorbance of visible light is independent of wavelength and is proportional to the number of layers. Reflectance is almost negligible (<0.1%).[9] Additionally, single and double layer graphene become completely transparent if the optical energy is smaller than double the Fermi level.10 Such properties could be used in many photonic devices, e.g., photodetectors, optical modulators, optical polarization controllers or mode-locked lasers.[8]

Sorption properties. As a material with large surface area, graphene can - simi-

larly to graphite - adsorb various gases, for example H_2, NO_2, CO_2.[11] Large molecular structures, such as DNA or proteins can also be adsorbed on to the graphene surface; while the carrier concentration changes, graphene remains highly conductive, and therefore it can be used as a chemical detector or even as a DNA sequencing tool.[12] It is also possible to dope graphene with various elements like F, O, B, Li or Mg to increase adsorption energy of hydrogen (with applications in hydrogen storage), or to change electric properties of graphene.[13] Unless exposed to reasonably harsh reaction conditions, graphene is a fairly inert material, and does not react readily despite every atom being exposed to it's surroundings.[8]

1.2. Synthesis of Graphene

Bulk graphite is composed of graphene sheets tight together by weak non-covalent interactions. In the past there were attempts to lower the number of graphene layers - for example Ruoff's group peeled away the layers with an atomic force microscope (AFM) tip.14 However, they were not able to prepare less than 100-layers thick graphite. The "big" discovery came with a much simpler method. The Manchaster group led by Geim used only simple scotch tape to peel a single graphene layer off the graphite.[1] Interesting and important part was to locate the single layer in a microscope. Graphene itself has optical absorbance of 2.3% and visual observation is not possible. Cleaving the prepared sample on a SiO_2/Si wafer and taking advantage of interference the single layers could be distinguished across the sample. *See Figure 2.*

Nowadays, there are several methods used for single-layer graphene preparation.

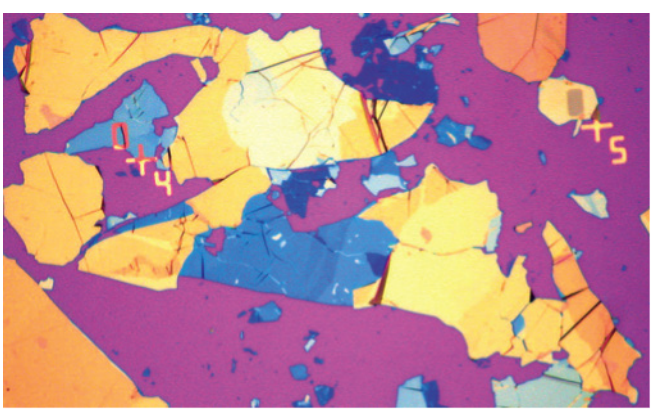

Figure 2. Interference used to distinguish single, double and multi layers of graphene surface.[15]

These can be divided into two groups. First is exfoliation of graphite, either mechanical or liquid phase exfoliation, and second is bottom up chemical synthesis.

Chemical vapour deposition (CVD) is a widely used process for growing crystals on a substrate under well-controlled temperature and pressure. Nowadays it is possible to grow graphene sheets with very large areas (square metres),[16] despite the fact that graphene typically requires transport from the substrate onto a dielectric support. The main advantage of the CVD method is controlled production of large high-quality graphene sheets. However, this method will likely remain very costly.

Liquid phase exfoliation is based on sonication of graphite in a suitable solvent. During sonication weak intermolecular interactions between graphene layers are broken and single graphene layers are dispersed into solvent. Only relatively small graphene flakes may be prepared, with area of about 1 μm, and the product may contain flakes with multiple graphene layers. However, liquid phase exfoliation allows for production of large amounts of graphene flakes, which makes it highly promising for large-scale industrial applications. The main challenge is to find a suitable solvent that would keep the layers dispersed as long as possible. We have to keep in mind that graphene aggregation is a thermodynamically favoured process and therefore it is eventually inevitable. N-methyl-pyrrolidone, dimethylformamide and C_6F_6, are examples of typical solvents used in this process.[17,18] The thermodynamics and kinetics of exfoliation process in various solvents will be discussed in Results.

Theory and Methods

Theory and Methods

Besides experimental studies there is a significant increase in number of theoretical works studying graphene. In my thesis I focused on weak intermolecular interactions with graphene. In this section, I will provide a short overview of intermolecular interactions and then briefly describe the main theoretical approaches used, with focus on their accuracy and computational demands.

2.1. Intermolecular Interactions

According to Symmetry Adapted Perturbation Theory (cite, see below), intermolecular interaction energy can be decomposed into four basic components: electrostatic, induction, dispersion and repulsion. The electrostatic energy arises between two molecules as a sum of their permanent multipole interactions. At short intermolecular distances, overlap electrostatics adds to the multipolar interactions. The induction energy assumes the presence of polar molecule that induces an induced multipole moment in interacting molecule, resulting in attractive interaction. The dispersion interaction arises from the fluctuating electron density of one molecule that results in a temporary multipole, which induces an induced multipole in the interacting molecule. Repulsion is a destabilizing interaction arising from Pauli exclusion principle, which prohibits two electrons being found in same quantum state simultaneously. *See figure 3.*

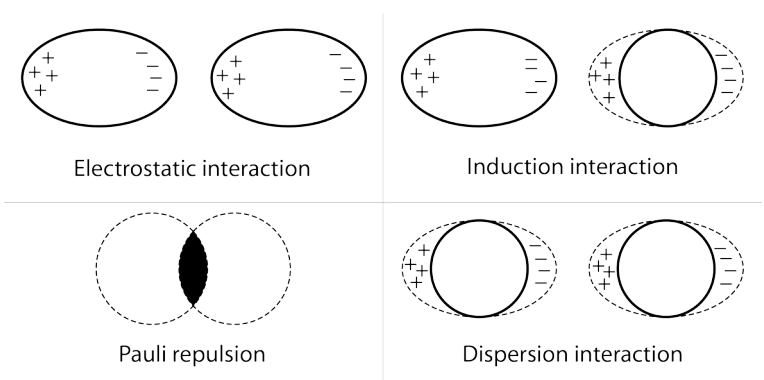

Figure 3. Schematic representation of intermolecular interactions.

Except electrostatic interaction none of the interactions is pairwise additive. There is a nonzero term for each component of interaction energy, which describes many-body corrections.

Electrostatic energy. The Coulomb law describes the electrostatic potential between two charged particles of charge q_A and q_B, which are separated by distance r as:

$$V = k\frac{q_A q_B}{r} \tag{1}$$

where $k=1/4\pi\varepsilon_0$. At the molecular level, the electrostatic field of a molecule can be described by multipolar expansion. The electrostatic field of the molecule is represented as monopole (ions), dipole, quadrupole, octupole, etc; the first non-vanishing term is the leading one. The electrostatic interaction of non-overlapping sufficiently distant electron distributions is given by interactions of these multipoles. The order of multipole controls the interaction energy decay as a function of the intermolecular distance and mutual orientation of the multipoles controls the magnitude and sign of the electrostatic intermolecular energy. The interaction energy decay as a function of distance can be expressed as:

$$V \propto \frac{1}{r^{n+m-1}} \tag{2}$$

where r is the distance between multipoles and the m and n represents order of interacting multipoles.[19]

At shorter distances, which are comparable to the typical van der Waals equilibrium separations, overlap electrostatic term contributes. This term is due to overlap of the molecular electron distributions and needs to be added to the multipolar interaction. It should be noted that when interacting molecules are of highly irregular shape allowing them to approach each other at the distances smaller than some of their dimensions (such as in graphene sheet interacting with a small molecule), electrostatic interaction may not be well described by molecular multipoles and more refined approaches need to be used.

Induction energy. Induction (or polarization) energy originates from deformation of electronic distribution of one molecule due to electrostatic field of other molecules. In the multipolar description, permanent electric multipole of one molecule induces an induced multipole moment in the second molecule. Induction energy is given by interaction between the permanent and induced multipoles. It is always

attractive and its magnitude depends on the order and magnitude of the permanent multipole moments of and on polarizabilities of the interacting molecules. As an example, in the case of molecule A with a permanent dipole μ_A interacting with a nonpolar molecule B characterized by polarizability volume α_B, the potential can be written as:

$$V = -\frac{1}{4\pi\varepsilon_0}\frac{\mu_A^2\alpha_B}{r^6} \tag{3}$$

where r is intermolecular separation.[20]

Dispersion energy. There is an attractive interaction between nonpolar molecules even if none of them exhibits permanent multipole moments. This interaction originates from continuous fluctuation of electron density. The fluctuating density gives rise to instantaneous multipoles, which induce induced multipoles in the neighbouring molecule and interact with them. Dispersion interaction depends on dynamic polarizabilities of given molecules; in a simple approximation, the interaction potential can be written as:

$$V = -\frac{C_6}{r^6} \quad \text{where} \quad C_6 = \frac{3}{2}\alpha_A\alpha_B\frac{I_A I_B}{I_A + I_B} \tag{4}$$

Here, α_A and α_B are dipole polarizabilities of interacting molecules, I_A and I_B are their ionization potentials and C_6 is so called dispersion coefficient. Dispersion energy is not pairwise additive and in the cases where nonadditivity is important it can be approximated by a simple Axilrod-Teller-Muto formula.[21]

Repulsion energy. Repulsive energy between closed shell molecules is a consequence of Pauli exclusion principle. It is a short range interaction which depends on overlap of electron clouds of the interacting molecules and vanishes as this overlap goes to zero. Repulsion is often approximated by the following empirical exponential formula:

$$V = Ae^{-Br} \tag{5}$$

The repulsive exponent B depends on the square of the overlap and A is an empirical constant.[22] Yet simpler approximations can be found in empirical force fields. *See below.*

Intermolecular interactions on surfaces. Although interactions of small molecules with surfaces obey the same principles as interactions between molecules, their description differs in several ways. For instance, distance dependence of various potentials changes as a result of integration over the surface area (or bulk volume), but also due to specific conditions, such as metallic character. Also anisotropy may play a very important role in 1D, 2D and 3D materials. While high-level quantum mechanical calculations take all these effects into account, empirical potentials and empirical corrections to mean field methods may provide less satisfactory results. Here I am concerned mainly with the electrostatic and dispersion interactions with graphene based materials, which I will discuss in more detail.

The electrostatic interaction is in classical pairwise additive force fields usually represented by point charges located on atoms. However, this representation is not suitable for description of electrostatic (quadrupolar) field of infinite graphene sheets, because their total charge must be zero. Also molecular multipoles cannot be used for larger graphene sheets, because the distance between surface and a molecule adsorbed on it does not fulfil the condition of multipolar expansion, where the intermolecular distance must be large compared to size of the objects. One way of representing the quadrupolar field of graphene is to use atom-centered local multipoles. This method has the advantage that it is capable of providing correct quadrupolar field for both finite and infinite graphene sheets, whether they are perfectly flat or corrugated. Unfortunately, this option is not available in most of the widely used codes for molecular dynamics simulations. The investigation of importance of graphene quadrupolar interactions described in this thesis was performed using my own parameterization of atom-centered multipoles for graphene implemented in Gromacs software.

The dispersion interaction potential of a molecule interacting with a surface of an infinite sheet decays with distance much slower ($\sim r^{-4}$) than that between two molecules ($\sim r^{-6}$). This is a simple consequence of the fact that interaction between the molecule and surface atoms must be integrated over the surface. For instance, when interaction of an adsorbed particle with an atom of the surface is approximated by the classical Lennard-Jones potential with well depth ε and separation σ

$$V = 4\varepsilon\left[\left(\frac{\sigma}{r}\right)^{12} - \left(\frac{\sigma}{r}\right)^{6}\right] \tag{6}$$

integration over one atom thick and perfectly flat infinite layer gives the following expression:

$$V = \left(\frac{C_{10}}{z}\right)^{10} - \left(\frac{C_4}{z}\right)^4 \quad (7)$$

in which z is the distance above surface, and $C_{10} = 4/5\pi\rho\sigma^{12}\varepsilon$ and $C_{10} = 2\pi\rho\sigma^6\varepsilon$, where ρ is the number of surface atoms per unit area. This interaction energy distance dependence is correctly recovered by classical empirical potentials. Nevertheless, it should be noted that parameters of current force fields are parameterized on small organic molecules and may not be directly transferable to nanomaterials like graphene. This may introduce inaccuracies in nanomaterial modelling.

However, the real asymptotics for graphene is in fact yet different, because of the graphene's conductive character. Comparison of asymptotic scalings obtained for co-parallel infinite layers by classical (LJ) and quantum-mechanical (random phase approximation)[23,24] descriptions is shown in Table 1. Note, that asymptotics of molecule interacting with an infinite layer is the same as that of two layers.

Table 1. The asymptotic behaviour of two infinite layers.

System	QM	Classical
1D metals	$(\log(KD))^{-3/2}D^{-2}$	D^{-5}
2D metals	$D^{-5/2}$	D^{-4}
1D insulators	D^{-5}	D^{-5}
2D insulators	D^{-4}	D^{-4}
Pi-conjugated layers (graphene)	D^{-3}	D^{-4}

From the above it can be seen that the classical force fields may not describe the asymptotics and binding strength of the intermolecular interactions with graphene accurately. The same applies also to empirical corrections to density functional theory, which are also based on pairwise corrections of the C_6 / r^6 type. Accuracy of these approximations is also a topic of this thesis.

2.2. Computational chemistry

Computational chemistry is a powerful tool, which allow us to study chemical properties and structures on the molecular level. With rapid increase of computer power computational studies become still more common. The whole group of computational methods can be divided into two main groups: The quantum mechanical approaches and approaches based on empirical force fields and classical mechanics. The quantum mechanical methods describe electronic structure of molecules; they are suitable for modelling of the electronic properties, intermolecular interactions, vibrational spectra and many other properties. The main limitation of quantum mechanical approaches is in the computational demands and, consequently, the size of system that can be treated. Current density functional methods can treat several hundreds of atoms, while very accurate coupled cluster calculations are reserved for systems containing maximum of 30 to 40 atoms. Using the classical empirical force field/molecular dynamics approach it is possible to simulate very large structures, such proteins, nucleic acids or large nanostructures even with explicit solvent. Molecular dynamics uses the time propagation of Newtonian equation and it is possible to evaluate thermodynamic properties using the tools of statistical thermodynamics.

2.2.1. Quantum Mechanical approach

The quantum mechanics is an exact mathematical description of the behaviour of electrons nuclei in molecules. In theory, it is possible to predict any property of atom or molecule with the use of QM. In practise, analytic solution of QM equations is possible only for one-electron systems. For larger systems, approximations must be necessarily applied. The QM methods can be (arbitrarily) divided into three groups: ab-initio methods, semiempirical methods and Density functional theory (DFT). All of them are based on solving the Schrödinger equation

$$\hat{H}\psi = E\psi \tag{8}$$

$\hat{H}_n$ is an operator of the total energy (Hamiltonian), ψ represents wave function, and E is energy. The Hamiltonian operator can be written as following

$$\hat{H} = \hat{K}_n + \hat{K}_e + \hat{V}_{nn} + \hat{V}_{ee} + \hat{V}_{ne} \tag{9}$$

$\hat{K}_n$ and $\hat{K}_E$ are kinetic energy operators for nuclear and electron motion, $\hat{V}_{nn}$,$\hat{V}_{ee}$,$\hat{V}_{ne}$ are

potential energy operators of nucleus-nucleus, electron-electron and nucleus-electron interactions. According to the Born-Oppenheimer approximation, Hamiltonian can be simplified if we separate the nuclear and electronic motions. Plenty of other approximations follow, that define the rich family of QM methods.

Hartre-Fock (HF) method is among the simplest ab-initio methods, characteristic by a relatively low computational cost. It is based on an assumption that the N-electron wave function can be approximated as an (antisymmetric) product of N one-electron functions, called orbitals (atomic or molecular). Importantly, each electron moves in an average field of the other electrons. One-electron wave functions are described as a linear combination of Slater-type orbitals (STO) or more often Gaussian-type orbitals (GTO). To obey Pauli principle the orbitals are written in the form of a Slater determinant. In a complete basis set the energy converges to so called Hartree-Fock limit. The HF method is variational, which means that the obtained energy is always greater than the exact energy. The most serious error of this approximation comes from the lack of electron correlation. The HF wave function is used as a starting point for other theories called post Hartree-Fock methods. The correlation energy may be obtained either variationally (e.g., through configuration interaction expansion) or perturbatively. *See bellow.*[25]

Moller-Plesset Pertubation Theory (MP) treats electron correlation as a small perturbation with respect to the HF result. The HF becomes the first order perturbation, MP2 second, MP3 third, etc. More accurate results can be usually expected at higher order of the MP method. MP2 method is most commonly used, being one of the least computationally demanding options for reliable estimates of correlation energy. However, in the case of intermolecular interactions MP2 is known to overestimate the dispersion contribution.[26] Therefore, this method cannot be used when very accurate description of intermolecular interactions is required.

Coupled Cluster Theory (CC) constructs wave function as a linear combination of many excited determinants, which account for electron correlation. The determinants are chosen so that they gradually include single, double, triple excitations, etc. (CCS, CCSD,CCSDT). The method is variational, but it can be combined with perturbation theory. For example the CCSD(T) method, where T in parentheses stands for triple excitations calculated perturbatively is currently considered as a golden standard of computational chemistry. The CCSD(T) method provides benchmark quality results for intermolecular interactions, however, at a prize of high computational cost. Currently, complexes as large as 30-40 atoms can be treated by a combination of com-

plete basis set extrapolation at the MP2 level and a CCSD(T) correction for higher order correlation calculated using a smaller basis set.[27]

Density Functional Theory (DFT). In contrast with the above mentioned methods based on wave function description, DFT works predominantly with electron density, which entails all information necessary to calculate any molecular property. In the Kohn-Sham formulation, DFT calculations are very similar to the HF calculations and also the computer time demands are comparable. The main difference is that DFT calculations include large portion of the short-range correlation energy through the use of a correlation functional. Inclusion of correlation energy at a cost of a HF calculation made DFT the most popular computational method nowadays. Unfortunately, exact correlation (and exchange) functionals are not known and currently used approximations, such as LDA, GGA, meta-GGA or hybrid functionals are not perfect. One of their major shortcomings is that they do not describe long-range correlations – the dispersion energy. Therefore, they cannot be used for accurate calculations of intermolecular interactions. There are numerous attempts to design a new "dispersion" functional (see, e.g., ref. 28–30) or to correct for the missing dispersion empirically (see, e.g., ref. 31,32). However, these efforts require extensive validation, because their accuracy is not known a priori. Validation of the latest dispersion-corrected density functionals for weak intermolecular interactions with graphene is one of the goals of this thesis.

Symmetry Adapted Perturbation Theory (SAPT)[33] was developed to calculate the intermolecular energy directly, without the need to evaluate total electronic energies of the interacting molecules and the resulting complex. The intermolecular interaction is treated as a small perturbation with respect to the noninteracting monomers. An important advantage of this method is that the intermolecular interaction energy can be decomposed into physically meaningful components. In its DFT based variant, DFT-SAPT,[34] the monomer is described by density functional theory and the intermolecular interaction is treated perturbatively. The total interaction energy is sum of the following terms (Eq. 10)

$$E^{\mathrm{SAPT}} = E_{\mathrm{elst}}^{(1)} + E_{\mathrm{exch}}^{(1)} + E_{\mathrm{ind}}^{(2)} + E_{\mathrm{exch\text{-}ind}}^{(2)} + E_{\mathrm{disp}}^{(2)} + E_{\mathrm{exch\text{-}disp}}^{(2)} + \delta(\mathrm{HF}) \qquad (10)$$

where $E_{elst}^{(1)}$ is electrostatic, $E_{exch}^{(1)}$ exchange repulsion, $E_{ind}^{(2)}$ induction or polarization and $E_{disp}^{(2)}$ dispersion contribution and $E_{exch\text{-}ind}^{(2)}$ and $E_{exch\text{-}disp}^{(2)}$ are exchange-induction and exchange-dispersion mixing terms. The δ(HF) term approximates higher order

induction contributions. It is customary to contract the above contributions into four terms: $E_{elst} = E_{elst}^{(1)}$, $E_{exch} = E_{exch}^{(1)}$, $E_{ind} = E_{ind}^{(2)} + E_{exch\text{-}ind}^{(2)} + \delta(HF)$ and $E_{disp} = E_{disp}^{(2)} + E_{exch\text{-}disp}^{(2)}$. These terms may be used to investigate type of binding in various intermolecular complexes and accuracy of individual interaction components in empirical force fields.

Accurate intermolecular interactions in QM methods. Besides SAPT, intermolecular interactions are usually calculated with the use of some of the above-mentioned QM methods. Intaraction energy is calculated as a difference between energy of the whole complex and energies of the isolated subsystems. There is a hidden source of error in this approach, called basis set superposition error (BSSE). BSSE is a mathematical artifact and can be eliminated by counter poise correction (CP) scheme.[35] Very large basis sets are necessary to obtain well converged values of interactions energies. In practice, complete basis set (CBS) extrapolation is used to estimate the basis set limit from two or more calculations in systematically increasing basis sets, such as, for instance, cc-pVTZ and cc-pVQZ (see, e.g., ref. 36,37). CCSD(T) method is a well established highly accurate approach providing benchmark quality results. Because CCSD(T) is excessively demanding for larger basis sets, some kind of correction for higher order correlation effects may be calculated using a smaller basis set and added, for instance, to the MP2/CBS energy.[27] This type of calculation may be used as a reliable reference for assessing quality of less rigorious approaches, such as those based on DFT theory.

2.2.2. Classical Mechanical approach

Classical (Newtonian) mechanics is the basis of methods of computational chemistry often referred as molecular mechanics (MM) or molecular dynamics (MD). MM methods were developed and are used for studying large systems. The basic concept of MM is approximation of atoms and interatomic forces as a "balls and springs". The electronic structure is not considered. The potential energy is expressed as a parametric function for a given nuclear configuration. All non-bonded interactions are usually pairwise additive (coulomb and vdW interactions). The bonded interactions are described as quadratic potentials (bond stretching and angle bending) or sums of cosine series (torsional angles). The set of parameters for all these terms is called Force Field (FF). The FF parameters can be obtained either from QM calculations or by fitting experimental results. The main application of such force fields is in molecular dynamics simulations, where masses are assigned to the particles (usually atoms) and their positions are propagated in time. In this way it is possible to simulate struc-

tural changes, thermodynamic properties, solvation effects, diffusion coefficients, etc.

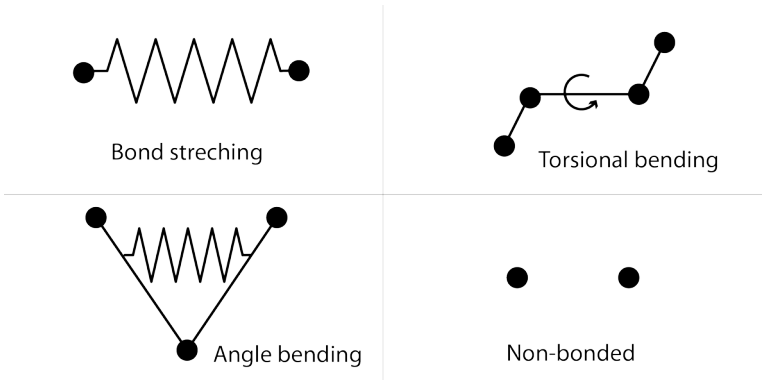

Figure 4. The schematic picture of basics interactions in molecular mechanics.

Quality of the empirical force field is crucial for obtaining reliable predictions from the molecular dynamics simulations. The total potential V of a system is a sum of all the above-described components: the bonded terms:

$$V_{\text{bonded}} = V_{\text{bond}} + V_{\text{angle}} + V_{\text{tors}} \tag{11}$$

and the non-bonded interactions, which consist of the coulomb and vdW terms, and, in some force fields, also the polarization term:

$$V_{\text{non-bonded}} = V_{\text{coulomb}} + V_{\text{vdw}} \; (+ V_{\text{pol}}) \tag{12}$$

As mentioned in the Intermolecular interaction section above, polarization might be important when considering surfaces of nanomaterials. Therefore, I will briefly mention the basic concepts of polarizable force fields. Polarization may be included through: (i) polarizable dipoles, (ii) Drude model or (iii) electronegativity equalization.

Polarizable dipoles model is exactly what it says. Each atom is assigned polarizability α_i, which allows for emergence of induced dipole moment μ_i, whose orientation is given by the external field $\boldsymbol{E}_i^q$: $\boldsymbol{\mu}_i = \alpha_i \boldsymbol{E}_i^q$. Drude model is based on adding an auxiliary massless particle (Drude particle) to each polarizable atom. The particle

has its own charge, q_D, and is bonded to the atom by a harmonic potential with force constant k_D. When external field $\boldsymbol{E}_i^q$ is applied, movement of the Drude particle creates an average dipole moment $\boldsymbol{\mu}_i = q_D^2 \boldsymbol{E}_i^q / k_D$ and polarizability of such particle equals $\alpha_i = {}_D^2 / k_D$. Electronegativity equalization method allows the dynamic charge fluctuation within the same molecule. There are no explicit dipoles.

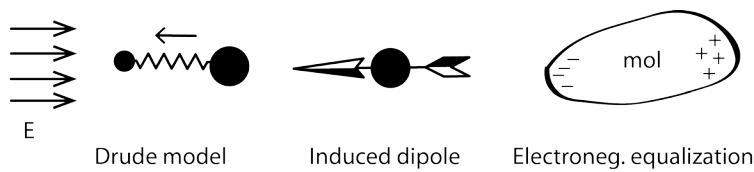

Figure 5. Schematic model of polarizable FF.

Unfortunately, except for a few exceptions,[38] most of the published MD simulation studies of nanomaterials uses additive (non-polarizable) force fields and does not consider polarization.

Popular Force Fields used in MD simulations. Molecular dynamics simulations of nanomaterials is an unexplored field. The common force fields are usually parameterized on small organic molecules and it is not clear whether the parameters are suitable for graphene and nanomaterials in general. A major concern is that most current force fields seem to provide too strong vdW binding. Some groups use modified force field parameters with reduced vdW strength when simulating graphene surface.[39] Comparison of widely used force field vdW parameters for graphene carbon atoms is shown in Table 2. In all my simulations I have used the same parameters as Cheng and Steele for non-bonded vdw interactions.

Table 2. List of non-bonded vdW parameters in current FF.

Force Field	Sigma [nm]	Epsilon [kJ/mol]
Parm 99[40]	0.34	0.36
OPLS[41]	0.35	0.29
CHARMM[42]	0.36	0.29
Ulbricht[43]	0.38	0.25
Cheng & Steele[39]	0.34	0.23

In addition to it, electrostatic interaction with grapehene is usually not considered in MD simulations, which might lead to unpredictable errors when simulating interactions with polar molecules.

2.3. Comparison with experiment

The ability to accurately predict outcomes of the processes taking place at the surfaces is critically dependent on our knowledge of both entropies and enthalpies of the adsorbed species.[44]

Enthalpy of adsorption. When describing adsorption of molecules or gases, experimentalists refer to heat of adsorption, or, in other words, the enthalpy of adsorption. Therefore, the enthalpy of adsorption has to be calculated when comparing experimental data with theory. The enthalpy of adsorption is defined as:

$$\Delta H = \Delta U + \Delta(pV) \tag{13}$$

Under constant pressure condition the last term can be written as:

$$\Delta(pV) = p\left(V_{ad} - V_s - V_g\right) \tag{14}$$

where V_{ad} is volume of the adsorbent with the adsorbed gas, V_s is volume of the free adsorbent and V_g is volume of the gas. The first two volume terms are much smaller than V_g and can be neglected. The only remaining term, V_g, is pressure-volume work of gas, which equals RT. The resulting expression for the adsorption enthalpy is:

$$\Delta H = \Delta U - RT \tag{15}$$

ΔU is an internal energy, which consists of electronic energy, zero-point vibration energy (ZPVE) and thermal vibration energy. In the molecular dynamics simulations with empirical force fields the internal energy can be approximated as a mean value of internal energy throughout the MD trajectory, $\Delta U = \Delta U_{MD}$. This approach does not include ZPVE, but it samples all possible conformations.

Entropy of adsorption. Estimating the magnitude of entropy change upon adsorption on surface remained elusive for a long time. Recently Campbell and Sellers[45] showed that entropies of the adsorbed molecules are surprisingly high and linearly dependent on entropy of molecules in gaseous state. The explanation of this effect is not straightforward. In small molecules, the adsorption entropy arises mostly from the translation and rotation part of the partition function. When a molecule is adsorbed on a surface it loses translational entropy corresponding to 1D translations (i.e., it is allowed to move almost freely on 2D surface after adsorption) and usually two thirds of its rotational entropy (while the helicopter rotations are allowed on the surface, both cartwheel rotations are strongly hindered). The magnitude of the translational partition function is equally distributed in x, y and z directions in the gas phase. However, the rotational contributions from the three main rotational axes depend on shape, and the entropy also depends on the point group of symmetry of a given molecule. In small compact molecules, the rotational entropy is much smaller than the translational entropy and therefore the ration between adsorbed and gas phase entropies is close to 2/3. For larger molecules the contribution of the vibrational entropy exceeds the other contributions and the loss of entropy upon adsorption is marginal. In this case, is the ratio between adsorbed and gas phase entropies is close to 1. Indeed, for small molecules it was measured that the relation between gas phase and adsorbed phase is approximately $S_{ad}(T) = 0.70S_{gas}(T) - 3.3RT$, while for linear alkenes with more than 10 atoms it is $S_{ad}(T) = 0.99S_{gas}(T) - 20RT$.[45] Using these relations, adsorption entropies may be estimated with reasonably accuracy. For detailed discussion see ref. 46.

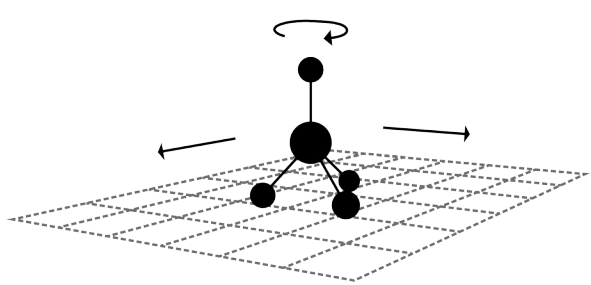

Figure 6. Molecule at the surface is capable to translate only in x-y and rotate in helicopter rotation.

2.4. Connection to the world of nanomaterials

In 1959, Richard Feynman gave a talk named "There is plenty of room at the bottom" at the American Physical Society meeting,[47] in which he explored the possibilities of downsizing materials. He pointed out that with the current knowledge of physical laws we should be able to theoretically predict the properties of nano-world objects and materials, which differ from the properties of bulk systems. It is often referred as beginning of nanotechnology development.* Nevertheless, while correctly predicting the role dawnsizing will play in computer technology, even Feynman did not foresee the role computers will play in investigating nanoworld.

This thesis aims at describing the beauty and complexity of nanoworld with the help of computational chemistry. It focuses mainly on intermolecular interactions on graphene surface. One of the possible applications of my research could be in development of graphene-based chemical detectors, which would provide such a high sensitivity, that a single molecule adsorbed on the graphene surface could be detected. The knowledge of the nature of the interactions of adsorbed molecules with graphene may help to propose and design such a detector.

One of the other possible applications of graphene is in hydrogen storage devices. In order to be practical these devices should fulfil the U.S. Department of Energy (DOE) target gravimetric capacity. In addition, molecular hydrogen should be able to adsorb and desorb reversibly. The optimal adsorption energy of molecular hydrogen should be around 15 kJ/mol per H_2 to be strong enough to achieve target capacity and weak enough to allow hydrogen release without applying extreme conditions.[48] Since the interaction energy of molecular hydrogen with pristine graphene surface is only about 4 kJ/mol, several modifications of graphene were proposed to increase strength of interaction.[49–55] Among all the elements, which can be used for graphene surface doping, it is necessary to choose from light elements such as boron, lithium, calcium or magnesium to achieve required gravimetric capacity. A modification of graphene with boron and lithium suggested in this work increased the binding energy of molecular hydrogen to the desired target. The structures designed with the use of highly accurate calculations or carefully calibrated and validated DFT calculations can inspire experimental community into producing highly efficient hydrogen storage materials.

Still growing is also the interest in simulating graphene with molecular dynamics tools. The popular force fields are not widely tested for nanomaterials and there are doubts that the approximations used for simulating biomolecules can be used for

* Actually this is not correct. The Feynman's article had been cited only seven times in two decades after it was published. However, at the time of invention of the scanning tunnelling microscope in 1981, when the nanotechnology emerged as a research area, there was need for "an authoritative account of its origin".[62]

also for nanomaterials. One of the frequently applied approximations is the neglect of electrostatics in graphene. Validity of this approximation will be discussed in detail in this thesis.

Results

3.1. Electric Quadrupole Moment of Graphene and its Effect on Intermolecular Interactions

Liquid phase exfoliation is a method of producing medium size graphene flakes at a large scale and low cost. The key to this technology is to find an efficient solvent able to solubilize graphene to a desired concentration. Number of solvents have been studied and it has been suggested, that the best solvents are those with Hansen solubility parameters close to certain values.[56] An interesting pair of exfoliation solvents is benzene and C_6F_6. Both have very similar Hansen solubility parameters, therefore they would be expected to exhibit similar exfoliation efficiency. Nevertheless experiments have shown that whereas C_6F_6 is quite good exfoliation solvent, benzene is rather poor one.[13] Interestingly, both molecules exhibit electric quadrupole moment with similar magnitude, but opposite sign. The carbon atoms in aromatic compounds also exhibit a permanent electric quadrupole moment due to the aromatic π electron distribution. The purpose of this study is to theoretically describe the exfoliation process and to find out whether the quadrupolar electrostatic interactions between solvent molecules and graphene may be responsible for strikingly different exfoliation behaviour of these two solvents.

To study the electrostatic contribution to the exfoliation process we have chosen molecular dynamics with an empirical potential. It is clear that in MD simulations there are other important sources of errors, such as lack of polarization, which are not considered here. However, empirical force field provides a unique opportunity to isolate solely the effect electric quadrupole, by running separate simulations with and without inclusion of quadrupole.

In addition, to investigate the electrostatic potential close to the graphene surface analytically, we derived analytical models of electrostatics of finite and corrugated graphene surfaces. We have studied the electrostatic potential (ESP) above the center of a flake, at the edges of a flat surface and on peaks and in the valleys of the corrugated surface. Secondly, we used molecular dynamics to study the effect of quadrupole moment by: (i) pulling off graphene from graphite surface – to evaluate size dependence thermodynamic stabilization; (ii) potential of mean force of two co-parallel graphene plates with the help of thermodynamic integration – to evaluate association barriers (iii) alchemical transformation – to evaluate the effect of quadrupole moment on solvation energies.

Analytical model. The electrostatic potential of a quadrupole can be expressed using Coulomb law as a potential of a group of three point charges arranged as shown in Figure 7; the potential at point P is:

$$V_Q = kq\left(\frac{2}{r} - \frac{1}{r_1} - \frac{1}{r_2}\right) = kq\frac{2r_1r_2 - r(r_1 + r_2)}{r \cdot r_1 \cdot r_2} \tag{16}$$

where k is the Coulomb's constant $k=1/(4\pi\varepsilon_0)$. The r_1 and r_2 distances are obtained with the help of cosine rule and because $r \gg p$ they can be approximated by a second degree Taylor polynomial:

$$r_1 = \sqrt{r^2 + p^2 - 2rp\cos\theta} \approx r - p\cos\theta + p^2\frac{1 - \cos^2\theta}{2r} \tag{17}$$

$$r_2 = \sqrt{r^2 + p^2 + 2rp\cos\theta} \approx r + p\cos\theta + p^2\frac{1 - \cos^2\theta}{2r} \tag{18}$$

The product of the last terms of polynomials, $r_1 \cdot r_2$, becomes very small and can be safely neglected. Assuming $r \cdot r_1 \cdot r_2 \approx r^3$, the expression for electrostatic potential at point P due to quadrupole moment is:

$$V_Q = -k\frac{qp^2(3\cos^2\theta - 1)}{r^3} \tag{19}$$

The z component of traceless quadrupole due to n-point charges q_n in the z direction is defined as:

$$Q_{zz} = \frac{1}{2}\sum_n q_n\,(3z_n^2 - r_n^2) \tag{20}$$

where r_n is the position of n-th point charge q_n and z_n is the z-component of r_n position vector.

Within this definition, $Q_{zz} = -2qp^2$, independent on choosing the origin. The final expression for electrostatic potential due to quadrupole moment is:

$$V_Q = \frac{1}{2}kQ_{zz}\frac{(3\cos^2\theta - 1)}{r^3} \tag{21}$$

To calculate electrostatic potential above the graphene surface, represented by a field of localized atomic quadrupoles, we need to integrate expression (21) over the whole surface. First, we express all variables using the surface x-y coordinates:

$$V_Q^{xy} = \frac{1}{2} k Q_{zz} \frac{3\frac{h^2}{(x^2+y^2+h^2)} - 1}{(x^2+y^2+h^2)^{\frac{3}{2}}} \tag{22}$$

where h is the distance above surface. Next, the quadrupole moment Q_{zz} is expressed as quadrupole density $Q_{zz}^{\text{dens}} = Q_{zz} \cdot A^{\text{dens}}$. A^{dens} is the density of carbon atoms of the graphene surface (~40 atoms/nm^2). Then we can integrate over x and y:

$$V_Q^{\text{surf}} = \frac{1}{2} k Q_{zz}^{\text{dens}} \iint \frac{3h^2 - (x^2+y^2+h^2)}{(x^2+y^2+h^2)^{\frac{5}{2}}} dx\, dy \tag{23}$$

If the point P is placed above the center of the graphene flake, transformation into polar coordinates can be used and integral can be solved analytically:

$$V_Q^{\text{surf}} = \pi k Q_{zz}^{\text{dens}} \frac{R^2}{(R^2+h^2)^{\frac{3}{2}}} \tag{24}$$

where R is the radius of graphene flake.

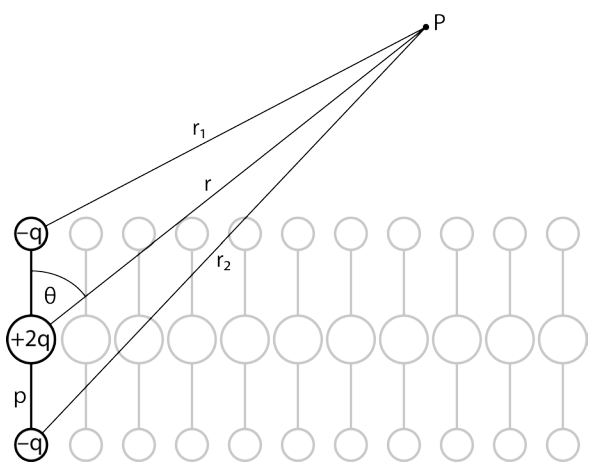

Figure 7. The model of quadrupole.

Now we can investigate two cases. First, when the graphene flake radius is much larger than the distance from graphene surface, h, expression (24) can be rewritten as:

$$V_Q^{\text{surf}}(h \ll r) \approx \pi k Q_{ZZ}^{\text{dens}} \frac{1}{R} \tag{25}$$

h can be neglected and therefore the electric field becomes constant at a short distance above the surface and approaches zero as the surface area goes to infinity.

Second, for finite graphene flakes, whose radius is much smaller than the distance from the surface the potential exhibits the typical h^{-3} dependence known from the multipolar expansion:

$$V_Q^{\text{surf}}(r \ll h) \approx \pi k Q_{ZZ}^{\text{dens}} \frac{R^2}{h^3} \tag{26}$$

Investigation of the electrostatic potential around the edges or corners of rectangular graphene flakes can be carried by numerical solution of integral (23) within desired boundaries. Results of these calculations are described below.

As a model of corrugation of the graphene surface we have chosen two-dimensional cosine function with amplitude A and period l; the z coordinate of graphene sheet is:

$$z = A\cos\left(\frac{2\pi}{l}x\right)\cos\left(\frac{2\pi}{l}y\right) \tag{27}$$

The direction of the quadrupole moment at each point on the surface is given by a normal vector of the tangent plane:

$$\vec{n} = \left(-\frac{\partial z}{\partial x}, -\frac{\partial z}{\partial y}, 1\right) \tag{28}$$

To calculate electrostatic potential above the graphene surface, represented by a field of localized atomic quadrupoles, we need to integrate expression (21) over the whole surface. First, we express all variables using the surface x-y coordinates:

$$\cos^2\theta = \frac{\left[-(x-x_0)\frac{\partial z}{\partial x} - (y-y_0)\frac{\partial z}{\partial x} + (z-z_0)\right]^2}{\left[\left(\frac{\partial z}{\partial x}\right)^2 + \left(\frac{\partial z}{\partial y}\right)^2 + 1\right]\left[(x-x_0)^2 + (y-y_0)^2 + (z-z_0)^2\right]} \tag{29}$$

Final integral, which has to be treated numerically, is:

$$V_Q^{\mathrm{surf}}(P) = \frac{1}{2} k Q_{ZZ}^{\mathrm{dens}} \iint \frac{3\cos^2\theta - 1}{((x-x_0)^2 + (y-y_0)^2 + (z-z_0)^2)^{\frac{3}{2}}} dx\, dy \qquad (30)$$

Let me summarize the basic results of the analytical model. For a finite and flat graphene flakes, ESP just above the surface becomes almost negligible when the flake size is 1000×1000 Å or larger. However, around the graphene edges ESP is nonzero even for very large flakes. It converges to a value of –3.6 kcal/mol above the graphene edge and +7.2 kcal/mol right next to the graphene edge (in graphene plane). This behavior may result in in preferencial absorption of polar molecules near graphene edges.[57]

The analytical model of corrugated graphene showed that ESP does not converge to zero even for very large surfaces, but it converges to a finite value. The sign and magnitude of ESP depends on position above the corrugated surface. Above the peaks ESP converges to +2 kcal/mol and above the valleys to –4.5 kcal/mol for our model (amplitude A and period l corresponding to experimental measurements). In Figure 9 the quadrupolar electrostatic potential of corrugated graphene is compared with that of benzene and selected polyaromatic molecules to put it into perspective. Note that

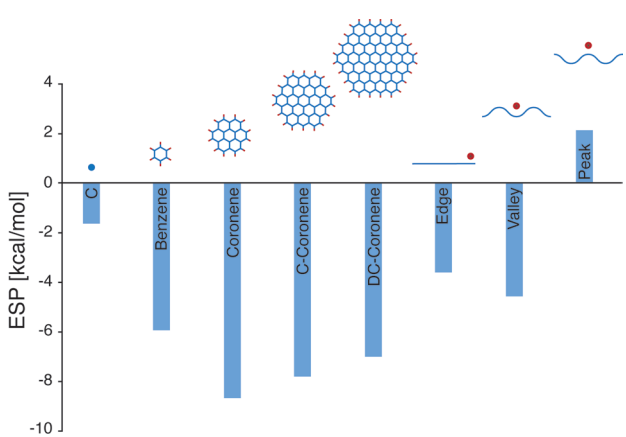

Figure 8. Comparison of ESP near a graphene edge and of corrugated graphene with ESPs of aromatic hydrocarbons.

this is just a rough estimate, because corrugation in real graphene is irregular and probably highly environment-dependent.

Nevertheless, the electric field of graphene's quadrupole may become sizeable not

only near edges or due to corrugation, but every time the graphene sheet is disturbed from planarity. This happens at graphene folds or wrinkles but also in processes in which the graphene sheet is mechanically stressed, e.g., during sonication induced exfoliation. In all these cases, quadrupolar interactions may need to be considered.

Role of the graphene quadrupole in MD simulations. In the conventional software packages for molecular simulations and common force fields the quadrupole moment of graphene is not accounted for. In our simulations graphene's quadrupole was represented by a pair of virtual sites placed above and below each carbon atom as shown in Figure 7. The distance p and charge q were chosen to reproduce experimentally measured graphite quadrupole moment $Q_{zz} = (-3.03 \pm 0.10) \times 10^{-40}$ Cm^2 by Whitehouse and Buckingham.[58]

Graphene peeling. The mechanism of liquid phase exfoliation is not yet fully understood and many different pathways may be possible. One idealized pathway is that the leaving sheet is gradually peeled from the support. To model this process, we pulled two small model molecules (circumcoronene and the rectangular flake C478, Figure 9) from the support by one of the outer carbon atoms and calculated PMF of this process by the umbrella integration technique. The exfoliation energy in C_6F_6 per carbon atom was about –0.61 kcal/mol for the circumcoronene model and –0.69 kcal/mol for C478, when quadrupole moment was not applied.

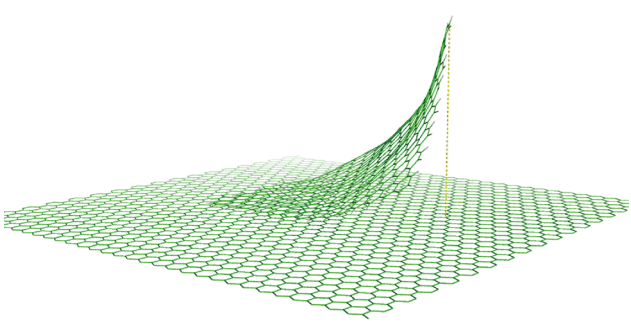

Figure 9. Peeling of the graphene flake from an infinite graphene sheet.

Apparently, the quadrupolar contribution is relatively small in C_6F_6 and tends to decrease with the size of the simulated flake. Therefore, neglect of quadrupole moment is probably a reasonable approximation in this case.

Solvation energy. The contribution of the quadrupolar moment to graphene's solvation energy was estimated by thermodynamic integration of alchemical trans-

formation. Here we gradually grew atomic quadrupoles and integrated the accompanying change of Gibbs energy. The graphene flake models were not constrained, and thus were free to form ripples.

For benzene and C_6F_6, the quadrupolar contribution to solvation was relatively small and decreased with the flake size. In C_6F_6 it was estimated to be only about 12 % and is expected to be much smaller for larger graphene flakes. Higher results for water indicate that electrostatic interactions are more important in polar solvents, as expected. Nevertheless, it appears that neglecting quadrupolar interactions in force field calculations introduces only a relatively minor error in solvation energies and is probably a justified approximation.

PMF of co-paralel graphene flakes. Two circumcoronene molecules, which were kept planar and coparallel modeled the graphene flakes. One of the circumcoronenes bore atomic quadrupoles, whereas the other did not. The circumcoronene without quadrupoles represented a flat support, for which the electrostatic field cancels out due to its planarity. The circumcoronene with atomic quadrupoles mimicked the approaching (or leaving) graphene sheet, which may be corrugated or bent, and thus exhibit a local quadrupolar field. For comparison, we also calculated PMF for a model in which both circumcoronene molecules were without quadrupoles, as in the classical force field.

Inclusion of quadrupoles had notable effects on several characteristics of the PMF curves. Consistent with the results shown above (using a different exfoliation trajectory), the exfoliation energy in C_6F_6 decreased only slightly (by about 3 kcal/mol, or 5 %) when quadrupoles were included. However, inclusion of quadrupoles had a more pronounced effect on the barrier heights. When quadrupoles were neglected, benzene provided a slightly larger barrier height than C_6F_6, which suggests slower aggregation in benzene. Interestingly, when quadrupoles were considered, the height of this barrier increased by 4.2 kcal/mol (17 %) in C_6F_6, whereas in benzene it is decreased by 2.7 kcal/mol (11 %) (note that these are rough estimates only as they are model-dependent).

The height of this barrier has been shown to play an important role in kinetic theory of graphene colloid aggregation because it contributes to colloid stability.[59] As a result, the expected association rate would be slower in C_6F_6 than in benzene when quadrupoles are included, as opposed to the situation when quadrupoles are neglected.

Because of the sensitivity of reaction rates to barrier heights, the almost 7 kcal/mol increase may lead to a significant decrease of aggregation rate in C_6F_6, resulting in better kinetic stability of graphene colloid in this solvent. Thus, kinetic aspects may partially explain the experimentally observed better exfoliation capabilities of C_6F_6,

which cannot be explained by thermodynamic considerations, as discussed above.

Conclusion. In this study, we investigated the effect of graphene's electric quadrupole moment arising from its π electron distribution on intermolecular interactions. The results indicate that quadrupolar interactions may need to be considered

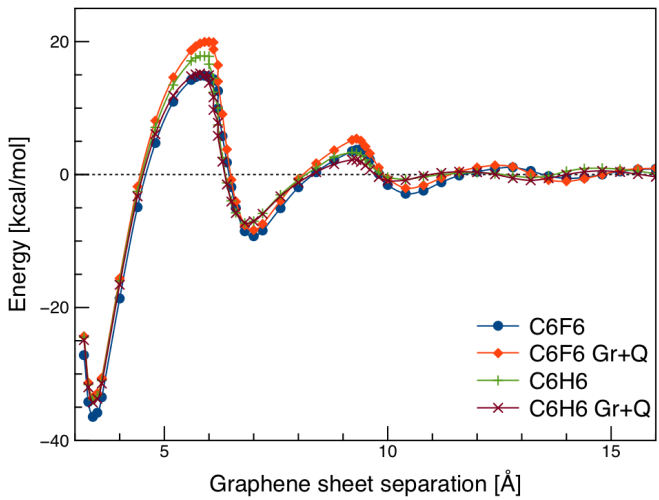

Figure 10. PMF of separation of two circumcoronene molecules calculated in C6F6 and benzene with and without quadrupoles on the approaching circumcoronene.

when modeling intermolecular interactions with corrugated or bent graphene.

It should be noted that current pairwise additive empirical potentials neglect also other effects which may play important role in molecular interactions with graphene, such as polarization, charge redistribution in graphene upon corrugation, or charge transfer between interacting molecules. Some of these effects may be sizeable and comparable in magnitude with the quadrupolar contribution. The main purpose of this work was to isolate the quadrupolar contribution and estimate its magnitude separate from the above mentioned effects.

In conclusion, corrugated or bent graphene exhibits an electric quadrupole moment that may be important for intermolecular interactions. Our results will help to assess errors due to omission of quadrupolar electrostatic interactions in force field MD simulations and improve general understanding of the importance of quadrupolar moments on molecular interactions with graphene.

3.2. Adsorption of small organic molecules on graphene

One of the possible applications for graphene-based nanomaterials is in chemical detectors. It has been shown that sensors made of graphene are capable of detecting individual adsorption events when molecules are adsorbed to or desorbed from graphene's surface.[60] When constructing a chemical detector, one of the important quantities that need to be known is adsorption enthalpy of the detected molecule.

In our study (Appendix) we presented a combined experimental and theoretical quantification of the adsorption enthalpies of seven organic molecules (acetone, acetonitrile, dichloromethane, ethanol, ethyl acetate, hexane, and toluene) on graphene. Adsorption enthalpies were measured by inverse gas chromatography. The interaction energy between graphene and the organic molecules was obtained by DFT methods, wave function theory based methods, and empirical molecular mechanics calculations.

The nature of the interaction between graphene and the adsorbed molecule was studied by Symmetry Adapted Perturbation Theory method. Our results demonstrated that contribution of the dispersion energy to the overall stabilization was dominant for all studied molecules, even those with marked polar character, such as ethanol. In all cases, dispersion contributed more than 60 % of the total attractive energy. The remaining came mainly from electrostatics (on average 30 %) and polarization (on average 10 %).

It is perhaps not surprising that the QM calculations at the well established CCSD(T)/CBS level predicted interaction energies that correlate very well with the experimental results (Table 3). However, it would be interesting to see whether a classical pairwise additive force is also able to model adsorption process with reasonable accuracy. The force field simulations were performed using all atom optimal potentials for liquid simulations (OPLS-AA) by Jorgensen et al.[41] The simulation was carried under periodic boundary conditions to simulate infinite graphene. Graphene surface was kept flat and therefore there was no need to account for electrostatics of graphene, because it would cancel out anyway. Therefore, the intermolecular interaction of graphene with small molecule was simulated only by using the Lennard – Jones (LJ) potential (with parameters by Chang & Steele[61]). The interaction energy U between graphene surface and adsorbed molecule was averaged over the molecular dynamics trajectory. The enthalpy of adsorption was then calculated as $\Delta H = \Delta U - RT$ (see also discussion in the Introduction).

One of the possible applications for graphene-based nanomaterials is in chemical detectors. It has been shown that sensors made of graphene are capable of detecting individual adsorption events when molecules are adsorbed to or desorbed from

graphene's surface.[60] When constructing a chemical detector, one of the important quantities that need to be known is adsorption enthalpy of the detected molecule.

In our study (Appendix) we presented a combined experimental and theoretical quantification of the adsorption enthalpies of seven organic molecules (acetone, acetonitrile, dichloromethane, ethanol, ethyl acetate, hexane, and toluene) on graphene. Adsorption enthalpies were measured by inverse gas chromatography. The interaction energy between graphene and the organic molecules was obtained by DFT methods, wave function theory based methods, and empirical molecular mechanics calculations.

The nature of the interaction between graphene and the adsorbed molecule was studied by Symmetry Adapted Perturbation Theory method. Our results demonstrated that contribution of the dispersion energy to the overall stabilization was dominant for all studied molecules, even those with marked polar character, such as ethanol. In all cases, dispersion contributed more than 60 % of the total attractive energy. The remaining came mainly from electrostatics (on average 30 %) and polarization (on average 10 %).

Table 3. Experimentally measured adsorption Enthalpies compared with the FF simulation and CCSD(T)/CBS energies in kcal/mol.

System	ΔHFF	CCSD(T)/CBS	ΔHads
acetone	–6.6	–7.6	–8.2
acetonitrile	–5.0	–6.2	–7.6
dichloromethane	–6.3	–6.7	–5.9
ethanol	–5.0	–7.1	–7.3
ethyl acetate	–9.4	–9.7	–11.5
hexane	–10.2	–10.4	–12.2
toulene	–10.5	–11.9	–13.5

It is perhaps not surprising that the QM calculations at the well established CCSD(T)/CBS level predicted interaction energies that correlate very well with the experimental results (Table 3). However, it would be interesting to see whether a classical pairwise additive force is also able to model adsorption process with reasonable accuracy. The force field simulations were performed using all atom optimal potentials for liquid simulations (OPLS-AA) by Jorgensen et al.[41] The simulation was carried under periodic boundary conditions to simulate infinite graphene. Graphene surface was kept flat and therefore there was no need to account for electrostatics

of graphene, because it would cancel out anyway. Therefore, the intermolecular interaction of graphene with small molecule was simulated only by using the Lennard – Jones (LJ) potential (with parameters by Chang & Steele[61]). The interaction energy U between graphene surface and adsorbed molecule was averaged over the molecular dynamics trajectory. The enthalpy of adsorption was then calculated as $\Delta H = \Delta U - RT$. *See also discussion in the Introduction.*

Our calculations have shown that adsorption enthalpies obtained from molecular dynamics simulations agree with the experimental data fairly well; the correlation coefficient for all tested molecules is r = 0.93. The main discrepancy is that the theoretical enthalpies are underestimated with respect to the experimental values by about ~20 %. We can hypothesize that this is in part due to lack of polarization in force field simulations. Note that according to SAPT calculations the polarization contributes on average ~10 % of the total attractive interaction. Other effect that might play a role when comparing modelling with experiment is the irregularities of real graphene surface. Nevertheless, the force field simulations were able to distinguish the weakly and strongly adsorbed molecules and thus can be used as a semi-quantitative tool for estimating interaction energies of large molecules with graphene.

3.3. Choosing a Density Functional for Modeling of Adsorptive Hydrogen Storage

Hydrogen storage in carbonaceous materials and their derivatives is currently a widely investigated topic. Rational design of novel adsorptive materials is often attempted with the help of computational chemistry tools. In particular, hydrogen adsorption capacity is assessed using quantum mechanical (QM) calculations, usually density functional theory (DFT). However, it is well known that various exchange-correlation functionals provide a very wide range of hydrogen binding energies. In this work we calculated reference dissociation curves for physisorption of hydrogen molecule on two different model compounds, coronene and coronene modified with boron and lithium ($coroB_2Li_2$), shown in Figure 11. Whereas coronene represents weak adsorption typical for carbonaceous materials, the $coroB_2Li_2$ molecule simulates much stronger binding of molecular hydrogen in modified sorption materials.

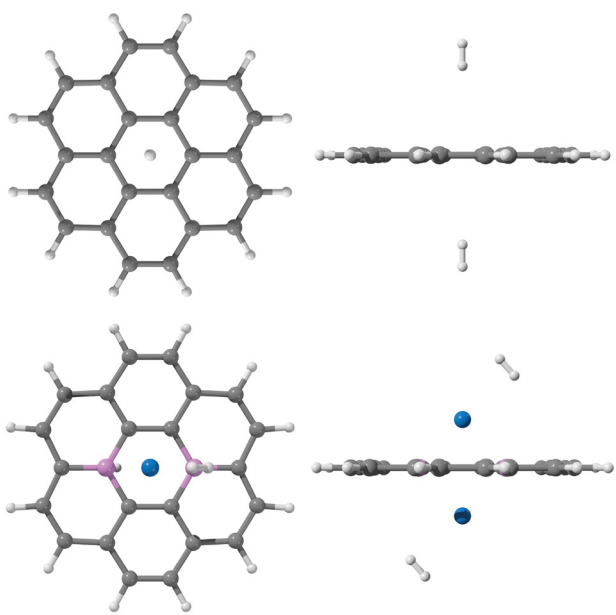

Figure 11. The coronene…H2 and the coroB2Li2…H2 structure.

In the first part of this study we performed the DFT-SAPT calculations on the two model complexes in order to decompose the intermolecular energy into physically meaningful components. The results confirmed our assumption, that the coronene…$2H_2$ complex is stabilized predominantly by dispersion interaction (75%), while the $coroB_2Li_2$…$2H_2$ complex is, apart from dispersion, stabilized also by induc-

tion, whose contribution is comparable. The different nature of binding in the non-polar and polar complexes can explain the observed differences in performance of various DFT functionals for the two binding situations, as discussed below.

As a reference for further comparisons we have chosen the high level QM CCSD(T) calculations with estimate of the complete basis set limit. Quality of this reference was further verified by a single point diffusion quantum Monte Carlo calculation for the coronene…H_2 complex at the optimal distance. The reference CCSD(T)/CBS curves are shown in Appendix and in the following I will discuss only the binding energies. Our calculations predicted the binding energy –4.68 kJ/mol for the coronene…$2H_2$ complex and –14.25 kJ/mol for the coroB_2Li_2…$2H_2$ complex. Note that the interaction energy in the second complex is relatively very high for an adsorptive interaction and is close to the optimal value for adsorptive storage suggested by Bathia et al.[48] Therefore, this complex should be a good model for assessing hydrogen storage in high capacity materials.

Comparison of the dissociation curves obtained with pure DFT functionals (without empirical correction) with the reference calculations (see appendix) showed that for the dispersion bound coronene…$2H_2$ all of these functionals fail to give reliable description (see Table 4). Some of the functionals do not bind molecular hydrogen at all (BLYP, B3LYP). The closest to the reference and the only functional which correctly predicted equilibrium distance is the Truhlar's M06 functional. Nevertheless, even M06 underestimated the binding energy by more than 50 %. In the case of the polar coroB_2Li_2…$2H_2$ complex, the pure DFT functionals correctly predicted equilibrium distances, but the underestimation of interaction energy is still notably large (20-55 %). The only exception is SVWN functional, which overestimates the binding energy in both complexes by about 50 %. Apparently, none of the standard and widely used functionals can be used for accurate estimation of hydrogen adsorption on carbonaceous materials, not even in the case of highly polar complexes.

Perhaps the simplest way to include dispersion interaction in DFT calculations is through an empirical dispersion correction. Here we have chosen one of the widely available dispersion corrections by Grimme, DFT-D3, , which is parameterized for a variety of commonly used DFT functionals. As expected, the dispersion correction significantly improved accuracy of both complexes. Interestingly, in the dispersion dominated complex the performance of the BLYP-D3 and B3LYP-D3 methods was remarkably good (interaction was overestimated by only 3 % with B3LYP-D3). However, in the case of the polar coroB_2Li_2…$2H_2$ complex the dispersion correction overestimated the interaction energy with all DFT functionals, on average by about ~15 %. We can only hypothesize that this is a consequence of using the dispersion parameters derived to work well for small organic molecules for description of interactions in large

conjugated molecules.

The last group of methods tested in our work were the density functionals in which dispersion correction is at least partially derived from the DFT electron density. Although the tested density based dispersion functionals are not as accurate as the best DFT-D3 combinations for the weakly bound coronene…$2H_2$, they better

Table 4. Interaction energies per H_2 molecule kJ/mol and error with respect to reference CCSD(T)/CBS calculation. In the cases denoted by an asterisk (*), the dissociation curve is purely repulsive and does not exhibit a minimum.

	Coronene…H_2		$CoroB_2Li_2$…H_2	
method	ΔE_0	%	ΔE_0	%
CCSD(T)/CBS	–4.68		–14.25	
BLYP	-*		–6.39	–55 %
PBE	–1.16	–75 %	–11.47	–19 %
TPSS	–0.54	–89 %	–9.61	–33 %
B3LYP	-*		–7.80	–45 %
LDA	–7.76	66 %	–20.65	45 %
PBE0	–0.95	–80 %	–11.26	–21 %
PW91	–2.00	–57 %	–10.15	–29 %
M06	–2.06	–56 %	–11.25	–21 %
BLYP+D3	–4.55	–3 %	–16.17	13 %
PBE+D3	–5.58	19 %	–17.16	20 %
TPSS+D3	–5.03	7 %	–16.81	18 %
B3LYP+D3	–4.83	3 %	–16.41	15 %
B97-D	–5.63	20 %	–16.05	13 %
PBE0+D3	–5.36	14 %	–16.72	17 %
PBE+TS	–6.02	29 %	–16.05	13 %
optB88+vdW	–5.85	25 %	–15.22	7 %
vdW-DF	–6.58	41 %	–14.54	2 %
vdW+DF2	–5.53	18 %	–15.05	6 %

describe stronger binding in the more polar $coroB_2Li_2$…$2H_2$ complex. Especially the optB88+vdW and vdW-DF2 functionals provided the best results for the intermolecular interaction energies (6 % error with vdW-DF2) and equilibrium distances of the

polar complex. Although the vdw-DF functional performed even better in estimating the intermolecular energy (2 % error) the equilibrium distance was too large. (see figures in appendix) Because the coroB_2Li_2…H_2 complex is probably a better model for high-capacity hydrogen storage materials, the recent functionals with density based dispersion correction may be a good choice in this case. It should be noted that these methods are less empirical and therefore potentially more robust for unusual binding situations, which are far from those considered in the empirical parameterizations like DFT-D3.

Conclusions. In our work we have calculated high level QM reference data (coupled-clusters singles and doubles with perturbative triple excitations, CCSD(T); complete basis set estimate) for two model systems for hydrogen storage and compared them with a selection of widely used density functional based methods, both with and without inclusion of dispersion energy. Our results may serve as a guide for choosing a suitable DFT method for quick assessment of hydrogen binding capacity of newly designed materials as well as reference for assessing accuracy of previously published DFT results.

Summary

The aim of this thesis was to study intermolecular interactions in graphene-based nanomaterials by means of computational chemistry. Variety of computational methods have been employed, from empirical force fields to highly accurate ab initio approaches. Among the investigated topics were hydrogen storage, liquid phase graphene exfoliation and adsorption on graphene in general.

In a work combining theoretical calculations with experiment we have shown that intermolecular interactions between graphene and small organic molecules can be well described by high level super-molecular methods, such as CCSD(T) combined with complete basis set estimate. Experimentally measured values of adsorption enthalpies of acetone, acetonitrile, dichloromethane, ethanol, ethyl acetate, hexane, and toluene agreed with the theoretically predicted values reasonably well.

Nevertheless, the high level wavefunction based methods are computationally demanding and other (more efficient) methods need to be considered, especially when modeling nanomaterials on a larger scale. One of the highly popular methods is Density Functional theory. In order to assess quality of the DFT based predictions, we have chosen two graphene-like structures interacting with molecular hydrogen. One of the structures (coronene) modeled weak binding, whereas the second (coronene/boron/lithium construct suggested by us) modeled very strong hydrogen adsorption close to the theoretical optimum for adsorptive hydrogen storage. On these two complexes we have tested the performance of the commonly used density functionals, such as LDA, GGA, and hybride meta-GGA, but also functionals with several empirical and nonempirical dispersion corrections. We have demonstrated that the more recent dispersion corrected methods are capable of reasonable estimates of hydrogen adsorption energies, although they generally tend to overestimate binding in the coronene/boron/lithium complex, which is more relevant to modeling of perspective hydrogen storage materials. This purely computational study also proposed a model compound that fulfills requirements for optimal adsorptive hydrogen storage.

There are tasks, which cannot be solved with the highly demanding tools of quantum chemistry; those are studies of graphene dynamics, its interactions with explicit solvent, molecular diffusion, etc. For such cases the methods based on classical mechanics are the only appropriate tool. We have simulated the process of graphene exfoliation in two polar (quadrupolar) solvents and investigated the importance of graphene electrostatics in it. We have found that while inclusion of graphene quadrupolar interactions has negligible effect on thermodynamic stabilization of exfoliated graphene, it may be important when describing the association barrier, which could partly explain the kinetic stabilization of exfoliated graphene in certain solvents.

References

(1) Novoselov, K. S.; Geim, a K.; Morozov, S. V; Jiang, D.; Zhang, Y.; Dubonos, S. V; Grigorieva, I. V; Firsov, a a. Electric Field Effect in Atomically Thin Carbon Films. *Science* **2004**, *306*, 666–669.

(2) Web Of Science, Institute for Scientific Information; http://isiknowledge.com.

(3) Geim, A. K.; Novoselov, K. S. The Rise of Graphene. *Nat. Mater.* **2007**, *6*, 183–191.

(4) Ando, T. The Electronic Properties of Graphene and Carbon Nanotubes. *NPG Asia Mater.* **2009**, *1*, 17–21.

(5) Lee, C.; Wei, X.; Kysar, J. W.; Hone, J. Measurement of the Elastic Properties and Intrinsic Strength of Monolayer Graphene. *Science* **2008**, *321*, 385–388.

(6) Balandin, A. a; Ghosh, S.; Bao, W.; Calizo, I.; Teweldebrhan, D.; Miao, F.; Lau, C. N. Superior Thermal Conductivity of Single-Layer Graphene. *Nano Lett.* **2008**, *8*, 902–907.

(7) Zou, J.; Balandin, A. Phonon Heat Conduction in a Semiconductor Nanowire. *J. Appl. Phys.* **2001**, *89*, 2932.

(8) Novoselov, K. S.; Fal'ko, V. I.; Colombo, L.; Gellert, P. R.; Schwab, M. G.; Kim, K. A Roadmap for Graphene. *Nature* **2012**, *490*, 192–200.

(9) Nair, R. R.; Blake, P.; Grigorenko, A. N.; Novoselov, K. S.; Booth, T. J.; Stauber, T.; Peres, N. M. R.; Geim, A. K. Fine Structure Constant Defines Visual Transparency of Graphene. *Science* **2008**, *320*, 1308.

(10) Li, Z. Q.; Henriksen, E. A.; Jiang, Z.; Hao, Z.; Martin, M. C.; Kim, P.; Stormer, H. L.; Basov, D. N. Dirac Charge Dynamics in Graphene by Infrared Spectroscopy. *Nat. Phys.* **2008**, *4*, 532–535.

(11) Leenaerts, O.; Partoens, B.; Peeters, F. Adsorption of H2O, NH3, CO, NO2, and NO on Graphene: A First-Principles Study. *Phys. Rev. B* **2008**, *77*, 1–6.

(12) Min, S. K.; Kim, W. Y.; Cho, Y.; Kim, K. S. Fast DNA Sequencing with a Graphene-Based Nanochannel Device. *Nat. Nanotechnol.* **2011**, *6*, 162–165.

(13) Bourlinos, A. B.; Georgakilas, V.; Zboril, R.; Steriotis, T. a; Stubos, A. K. Liquid-Phase Exfoliation of Graphite towards Solubilized Graphenes. *Small* **2009**, *5*, 1841–1845.

(14) Lu, X.; Yu, M.; Huang, H.; Ruoff, R. S. Tailoring Graphite with the Goal of Achieving Single Sheets. *Nanotechnology* **1999**, *10*, 269–272.

(15) Peres, N. M. R. Graphene, New Physics in Two Dimensions. *Europhys. News* **2009**, *40*, 17–20.

(16) Bae, S.; Kim, H.; Lee, Y.; Xu, X.; Park, J.-S.; Zheng, Y.; Balakrishnan, J.; Lei, T.; Kim, H. R.; Song, Y. Il; et al. Roll-to-Roll Production of 30-Inch Graphene Films for Transparent Electrodes. *Nat. Nanotechnol.* **2010**, *5*, 574–578.

(17) Coleman, J. N. Liquid Exfoliation of Defect-Free Graphene. *Acc. Chem. Res.* **2013**, *46*, 14–22.

(18) Ciesielski, A.; Samorì, P. Graphene via Sonication Assisted Liquid-Phase Exfoliation. *Chem. Soc. Rev.* **2014**, *43*, 381–398.

(19) Ilya, K. *Calculation of Intermolecular Interactions, in Intermolecular Interactions: Physical Picture, Computational Methods and Model Potentials*; John Wiley & Sons, Ltd: Chichester, UK, 2006.

(20) Stone, A. J. *The Theory of Intermolecular Forces*; Oxford University Press: Oxford, UK, 1997; p. 264.

(21) Axilrod, B. M.; Teller, E. Interaction of the van Der Waals Type Between Three Atoms. *J. Chem. Phys.* **1943**, *11*, 299.

(22) Rappe, A. K.; Casewit, C. J.; Colwell, K. S.; Goddard, W. A.; Skiff, W. M. UFF, a Full Periodic Table Force Field for Molecular Mechanics and Molecular Dynamics Simulations. *J. Am. Chem. Soc.* **1992**, *114*, 10024–10035.

(23) Dobson, J. F.; White, A.; Rubio, A. Asymptotics of the Dispersion Interaction: Analytic Benchmarks for van Der Waals Energy Functionals. *Phys. Rev. Lett.* **2006**, *96*, 073201.

(24) Gould, T.; Gray, E.; Dobson, J. Van Der Waals Dispersion Power Laws for Cleavage, Exfoliation, and Stretching in Multiscale, Layered Systems. *Phys. Rev. B* **2009**, *79*, 1–4.

(25) Young, D. *Computational Chemistry: A Practical Guide for Applying Techniques to Real World Problems*; John Wiley & Sons, 2004; p. 408.

(26) Hübner, O.; Glöss, A.; Fichtner, M.; Klopper, W. On the Interaction of Dihydrogen with Aromatic Systems †. *J. Phys. Chem. A* **2004**, *108*, 3019–3023.

(27) Jurecka, P.; Hobza, P. True Stabilization Energies for the Optimal Planar Hydrogen-Bonded and Stacked Structures of Guanine...cytosine, Adenine...thymine, and Their 9- and 1-Methyl Derivatives: Complete Basis Set Calculations at the MP2 and CCSD(T) Levels and Comparison with Ex. *J. Am. Chem. Soc.* **2003**, *125*, 15608–15613.

(28) Dion, M.; Rydberg, H.; Schröder, E.; Langreth, D. C.; Lundqvist, B. I. Van Der Waals Density Functional for General Geometries. *Phys. Rev. Lett.* **2004**, 92, 246401.

(29) Becke, A. D.; Johnson, E. R. Exchange-Hole Dipole Moment and the Dispersion Interaction Revisited. *J. Chem. Phys.* **2007**, *127*, 154108.

(30) Tkatchenko, A.; Scheffler, M. Accurate Molecular Van Der Waals Interactions from Ground-State Electron Density and Free-Atom Reference Data. *Phys. Rev. Lett.* **2009**, *102*, 073005.

(31) Grimme, S.; Antony, J.; Ehrlich, S.; Krieg, H. A Consistent and Accurate Ab Initio Parametrization of Density Functional Dispersion Correction (DFT-D) for the 94 Elements H-Pu. *J. Chem. Phys.* **2010**, *132*, 154104.

(32) Jurecka, P.; Cerný, J.; Hobza, P.; Salahub, D. R. Density Functional Theory Augmented with an Empirical Dispersion Term. Interaction Energies and Geometries of 80 Noncovalent Complexes Compared with Ab Initio Quantum Mechanics Calculations. *J. Comput. Chem.* **2007**, *28*, 555–569.

(33) Jeziorski, B.; Moszynski, R.; Szalewicz, K. Perturbation Theory Approach to Intermolecular Potential Energy Surfaces of van Der Waals Complexes. *Chem. Rev.* **1994**, *94*, 1887–1930.

(34) Hesselmann, A.; Jansen, G.; Schütz, M. Density-Functional Theory-Symmetry-Adapted Intermolecular Perturbation Theory with Density Fitting: A New Efficient Method to Study Intermolecular Interaction Energies. *J. Chem. Phys.* **2005**, *122*, 14103.

(35) Boys, S. F.; Bernardi, F. The Calculation of Small Molecular Interactions by the Differences of Separate Total Energies. Some Procedures with Reduced Errors. *Mol. Phys.* **1970**, *19*, 553–566.

(36) Halkier, A.; Helgaker, T.; Jørgensen, P.; Klopper, W.; Olsen, J. Basis-Set Convergence of the Energy in Molecular Hartree–Fock Calculations. *Chem. Phys. Lett.* **1999**, *302*, 437–446.

(37) Halkier, A.; Helgaker, T.; Jørgensen, P.; Klopper, W.; Koch, H.; Olsen, J.; Wilson, A. K. Basis-Set Convergence in Correlated Calculations on Ne, N2, and H2O. *Chem. Phys. Lett.* **1998**, *286*, 243–252.

(38) Ho, T. A.; Striolo, A. Polarizability Effects in Molecular Dynamics Simulations of the Graphene-Water Interface. *J. Chem. Phys.* **2013**, *138*, 054117.

(39) Cheng, A.; Steele, W. a. Computer Simulation of Ammonia on Graphite. I. Low Temperature Structure of Monolayer and Bilayer Films. *J. Chem. Phys.* **1990**, *92*, 3858.

(40) Wang, J.; Cieplak, P.; Kollman, P. A. How Well Does a Restrained Electrostatic Potential (RESP) Model Perform in Calculating Conformational Energies of Organic and Biological Molecules? *J. Comput. Chem.* **2000**, *21*, 1049–1074.

(41) Jorgensen, W. L.; Tirado-Rives, J. Potential Energy Functions for Atomic-Level Simulations of Water and Organic and Biomolecular Systems. *Proc. Natl. Acad. Sci. U. S. A.* **2005**, *102*, 6665–6670.

(42) Vanommeslaeghe, K.; Hatcher, E.; Acharya, C.; Kundu, S.; Zhong, S.; Shim, J.; Darian, E.; Guvench, O.; Lopes, P.; Vorobyov, I.; et al. CHARMM General Force Field: A Force Field for Drug-like Molecules Compatible with the CHARMM All-Atom Additive Biological Force Fields. *J. Comput. Chem.* **2010**, *31*, 671–690.

(43) Ulbricht, H.; Moos, G.; Hertel, T. Interaction of C60 with Carbon Nanotubes and Graphite. *Phys. Rev. Lett.* **2003**, *90*, 095501.

(44) Weaver, J. F. Chemistry. Entropies of Adsorbed Molecules Exceed Expectations. *Science* **2013**, *339*, 39–40.

(45) Campbell, C. T.; Sellers, J. R. V. The Entropies of Adsorbed Molecules. *J. Am. Chem. Soc.* **2012**, *134*, 18109–18115.

(46) Campbell, C. T.; Sellers, J. R. V. Enthalpies and Entropies of Adsorption on Well-Defined Oxide Surfaces: Experimental Measurements. *Chem. Rev.* **2013**, *113*, 4106–4135.

(47) Feynman, R. There's Plenty of Room at the Bottom. *Engineering and Science.* **1960**, pp. 22–36.

(48) Bhatia, S. K.; Myers, A. L. Optimum Conditions for Adsorptive Storage. *Langmuir* **2006**, *22*, 1688–1700.

(49) Kemp, K. C.; Seema, H.; Saleh, M.; Le, N. H.; Mahesh, K.; Chandra, V.; Kim, K. S. Environmental Applications Using Graphene Composites: Water Remediation and Gas Adsorption. *Nanoscale* **2013**, *5*, 3149–3171.

(50) Lee, H. M.; Kim, D. Y.; Pak, C.; Singh, N. J.; Kim, K. S. H 2 -Binding by Neutral and Multiply Charged Titaniums: Hydrogen Storage Capacity of Titanium Mono- and Dications. *J. Chem. Theory Comput.* **2011**, *7*, 969–978.

(51) Georgakilas, V.; Otyepka, M.; Bourlinos, A. B.; Chandra, V.; Kim, N.; Kemp, K. C.; Hobza, P.; Zboril, R.; Kim, K. S. Functionalization of Graphene: Covalent and Non-Covalent Approaches, Derivatives and Applications. *Chem. Rev.* **2012**, *112*, 6156–6214.

(52) Kim, Y.-H.; Zhao, Y.; Williamson, A.; Heben, M.; Zhang, S. Nondissociative Adsorption of H2 Molecules in Light-Element-Doped Fullerenes. *Phys. Rev. Lett.* **2006**, *96*, 016102.

(53) Du, A.; Zhu, Z.; Smith, S. C. Multifunctional Porous Graphene for Nanoelectronics and Hydrogen Storage: New Properties Revealed by First Principle Calculations. *J. Am. Chem. Soc.* **2010**, *132*, 2876–2877.

(54) Deng, W.-Q.; Xu, X.; Goddard, W. New Alkali Doped Pillared Carbon Materials Designed to Achieve Practical Reversible Hydrogen Storage for Transportation. *Phys. Rev. Lett.* **2004**, *92*, 166103.

(55) Kuchta, B.; Firlej, L.; Roszak, S.; Pfeifer, P. A Review of Boron Enhanced Nanoporous Carbons for Hydrogen Adsorption: Numerical Perspective. *Adsorption* **2010**, *16*, 413–421.

(56) Coleman, J. N. Liquid-Phase Exfoliation of Nanotubes and Graphene. *Adv. Funct. Mater.* **2009**, *19*, 3680–3695.

(57) Gan, C. K.; Srolovitz, D. J. First-Principles Study of Graphene Edge Properties and Flake Shapes. *Phys. Rev. B* **2010**, *81*, 125445.

(58) Whitehouse, D. B.; Buckingham, A. D. Experimental Determination of the Atomic Quadrupole Moment of Graphite. *J. Chem. Soc. Faraday Trans.* **1993**, *89*, 1909.

(59) Shih, C.; Lin, S.; Strano, M. S.; Blankschtein, D. Understanding the Stabilization of Liquid-Phase-Exfoliated Graphene in Polar Solvents: Molecular Dynamics Simulations and Kinetic Theory of Colloid Aggregation. *J. Am. Chem. Soc.* **2010**, *132*, 14638–14648.

(60) Schedin, F.; Geim, A. K.; Morozov, S. V; Hill, E. W.; Blake, P.; Katsnelson, M. I.; Novoselov, K. S. Detection of Individual Gas Molecules Adsorbed on Graphene. *Nat. Mater.* **2007**, *6*, 652–655.

(61) Cheng, A.; Steele, W. a. Computer Simulation of Ammonia on Graphite. I. Low Temperature Structure of Monolayer and Bilayer Films. *J. Chem. Phys.* **1990**, *92*, 3858.

(62) "Plenty of Room" Revisited. *Nat. Nanotechnol.* **2009**, *4*, 781.

List of publications

(1) **Kocman, M.**; Pykal, M.; Jurečka, P. Electric Quadrupole Moment of Graphene and Its Effect on Intermolecular Interactions. *Phys. Chem. Chem. Phys.* **2014**, 16, 3144–3152.

(2) Lazar, P.; Karlický, F.; Jurečka, P.; **Kocman, M.**; Otyepková, E.; Safářová, K.; Otyepka, M. Adsorption of Small Organic Molecules on Graphene. *J. Am. Chem. Soc.* **2013**, 135, 6372–6377.

(3) **Kocman, M.**; Jurečka, P.; Dubecký, M.; Otyepka, M.; Cho, Y.; Kim, S. K. Choosing a Density Functional for Modeling Adsorptive Hydrogen Storage: Reference Coupled Cluster and Diffusion Quantum Monte Carlo Calculations, and a Comparison of Dispersion-Corrected Density Functionals. *In Preparation.*

Appendix

Appendix I

Electric Quadrupole Moment of Graphene and Its Effect on Intermolecular Interactions.

Appendix II

Adsorption of Small Organic Molecules on Graphene

Appendix III

Choosing a Density Functional for Modeling Adsorptive Hydrogen Storage: Reference Coupled Cluster and Diffusion Quantum Monte Carlo Calculations, and a Comparison of Dispersion-Corrected Density Functionals.

PCCP

PAPER

View Article Online
View Journal | View Issue

Electric quadrupole moment of graphene and its effect on intermolecular interactions

Cite this: *Phys. Chem. Chem. Phys.*, 2014, **16**, 3144

Mikuláš Kocman, Martin Pykal and Petr Jurečka*

Carbon atoms in aromatic compounds exhibit a permanent electric quadrupole moment due to the aromatic π electron distribution. In the case of small aromatic hydrocarbons, this quadrupole contributes significantly to their intermolecular interactions, but when the honeycomb lattice is expanded to infinity, the quadrupolar field sums to zero and its significance vanishes. Therefore, electrostatic interactions with graphene are often omitted in force field molecular modeling. However, for a finite sheet, the electrostatic field decays only slowly with increasing size and is always non-negligible near edges. In addition, in a corrugated graphene sheet, the electrostatic field near the surface does not vanish completely and remains sizeable. In the present study, we investigated the magnitude of the graphene quadrupolar field as a function of model size and graphene corrugation, and estimated the error resulting from its neglect in molecular dynamics simulations. Exfoliation energies in benzene and hexafluorobenzene were calculated using the potential of mean force method with and without explicit quadrupoles. The effect on exfoliation energies was found to be quite small. However, the quadrupole moment may be important for graphene sheet association (aggregation) as it affects barrier heights, and consequently kinetics of association. Our results indicate that quadrupolar interactions may need to be considered in molecular modeling when graphene is corrugated or bent.

Received 6th November 2013,
Accepted 2nd December 2013

DOI: 10.1039/c3cp54701a

www.rsc.org/pccp

1. Introduction

Recent progress in graphene-related nanotechnologies has fuelled interest in theoretical modeling of graphene-based materials. Different levels of theory can provide important information about various material properties, its behavior and chemistry.[1] Electronic, mechanical, optical and other properties related to electronic structure are usually obtained from quantum chemical calculations. Detailed atomistic information about dynamical processes occurring on longer time scales, such as interactions with biomolecules or the surrounding environment, is typically modeled using molecular mechanics and force fields. The chosen level of theory determines the computational cost and also accuracy of the resulting description of individual properties and features.

The feature of graphene that is of interest in this article is its electric quadrupole moment. Whereas quantum mechanical treatments are in general capable of providing an accurate description of the graphene quadrupolar field, in empirical force fields, it is usually ignored. Typically, carbon atoms in force field calculations are treated as van der Waals spheres and are not assigned any charge or multipole moment. As we will discuss below, ignoring the quadrupole moment is in most applications a reasonable approximation. However, in some cases, this neglect may result in error, the importance of which is difficult to prejudge. Here, we focus on modeling the quadrupole moment of graphene using empirical potentials and molecular dynamics (MD) simulations and discuss its influence on intermolecular interactions with finite and corrugated graphene sheets. Note that there are other important sources of errors in force field calculations which we do not consider here, such as lack of explicit polarization in pairwise additive potentials. Although the effect of missing polarization is expected to be important, it is beyond the scope of this work, which aims to estimate errors that result solely from neglecting the quadrupolar interaction in force field calculations. Another problem is that not only quadrupolar, but also dipolar electric field may arise in real graphene upon its deformation. This effect, however, cannot be modeled by a classical force field, therefore we also do not consider it here.

Let us first examine the origin of graphene's quadrupole moment in more detail. Molecules of aromatic hydrocarbons have strong molecular electric quadrupole moments arising from two different sources. First, carbon atoms in aromatic rings exhibit a permanent quadrupole moment due to the aromatic π electron distribution. High electron densities above and below the graphene layer generate a quadrupolar field characterized by a negative Q_{zz} component of the quadrupolar tensor perpendicular to the aromatic ring (z direction in Fig. 1a).

Regional Centre of Advanced Technologies and Materials, Department of Physical Chemistry, Faculty of Science, Palacky University, 17. listopadu 12, 77146 Olomouc, Czech Republic. E-mail: petr.jurecka@upol.cz

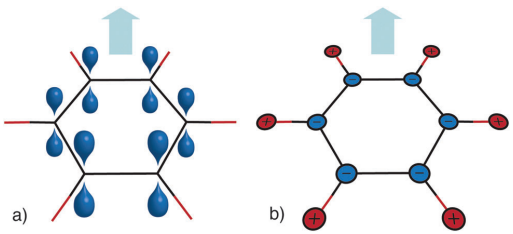

Fig. 1 Two components of the quadrupole moment in a benzene molecule. Similar components contribute to the quadrupole of finite graphene flakes.

Henceforth, we will refer to this contribution as the "atomic quadrupole". The remaining elements of the quadrupolar tensor are much smaller and vanish on the inner carbon atoms for larger molecules (see also ref. 2). Second, in aromatic hydrocarbons, a molecular quadrupole may arise due to the polarity of C–H bonds. For instance, in benzene, the Q_{zz} molecular component due to partial charges on hydrogen and carbon atoms is of the same sign as the atomic quadrupole (Fig. 1b). We will refer to this component as the "CH polarity quadrupole". Note that a quadrupole of the latter type may also arise due to other substitutions. For instance, hexafluorobenzene exhibits a CF polarity quadrupole, with a Q_{zz} sign opposite to that of the CH polarity quadrupole. In smaller polyaromatic molecules the atomic and CH polarity quadrupoles are comparable in magnitude.[2]

In an infinite and perfectly planar graphene sheet, the quadrupolar contributions arising from individual carbon atoms add up in such a way that the overall electrostatic potential (ESP) near the surface vanishes completely. However, here we are interested in finite and possibly corrugated graphene leaves. In a small polyaromatic molecule, the atomic quadrupolar contributions sum to create a molecular electrostatic potential similar to the one depicted in Fig. 2. The ESP of larger graphene flakes has similar features. We will now consider the long-range and short-range parts of the ESP of finite graphene flakes separately and discuss how they change with model size.

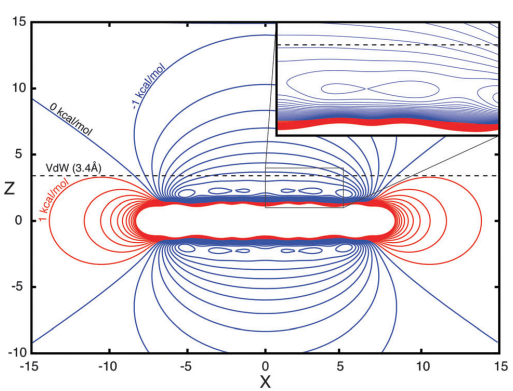

Fig. 2 Electrostatic potential around a small polyaromatic molecule (coronene). The dotted line is plotted 3.4 Å above the graphene surface, *i.e.*, at a typical vdW distance.

In the long range limit, *i.e.*, at distances that are large compared to the size of the graphene flake itself, ESP decays as R^{-3}. Here, the electrostatic field in the z direction (see Fig. 2) is characterized by a macroscopic quadrupole, Q_{zz}^{Macro}, which is simply the sum of the individual carbon atomic quadrupoles, Q_{zz} ($Q_{zz}^{\mathrm{Macro}} = NQ_{zz}$). It should be noted that the R^{-3} decay in the z direction can only be observed very far from the graphene surface, for instance at tens of μm for μm-sized flakes, *i.e.*, far from the vdW contact region. Although the macroscopic quadrupole has not been reported for a single graphene flake, a value of $Q_{zz} = (-3.03 \pm 0.10) \times 10^{-40}$ Cm^2 per carbon atom has been calculated from macroscopic quadrupole measured by Whitehouse and Buckingham for graphite particles.[3] We assumed that this value also applied for the graphene atomic quadrupole.

When approaching the graphene flake surface, the distance dependence of the electrostatic potential weakens (see also the discussion below). The region corresponding to the weaker distance dependence of the electrostatic potential is very wide, ranging from the surface to about one fifth of the flake diameter in the z direction. In this work, we focused mainly on the contact vdW region about 3.4 Å above the surface (indicated by a dashed line in Fig. 2). As the size of the graphene flake increases, the electrostatic potential in this region asymptotically approaches zero, as noted above. Thus, despite bearing a sizeable macroscopic quadrupole moment, the quadrupolar contribution to intermolecular interactions at its surface almost vanishes for large perfectly planar graphene flakes.

Closer to the graphene surface, at the distances typical for vdW interactions, a periodically varying microscopic field arises due to the atomic structure of the surface. The inset of Fig. 2 shows this periodic component as a mild undulation in the ESP contours when passing from one carbon atom to another. Albeit rather weak, the periodic quadrupolar component has been shown to influence the adsorption of gases on a graphite surface.[4–6] According to Vernov and Steele,[4] it has little effect on the adsorption energies but substantially alters barriers to the free translation and location of energy minima of N_2 and H_2O molecules on graphite. Later, Do and Do[5] considered the polarization of an adsorbed fluid (argon) by the periodic quadrupolar field and showed that dipoles induced in the adsorbed gas repel each other and reduce the stability of the adsorbed layer (surface mediation effect). In this article, we do not discuss the periodic component (although it is included in our simulations) but rather focus on the strength of the quadrupolar potential as a function of the finite flake size and corrugation.

To investigate the importance of quadrupolar interactions of graphene flakes with the surrounding medium, we chose to model liquid phase exfoliation in two solvents that differ in the sign of their Q_{zz} quadrupole tensor components, namely benzene and hexafluorobenzene (C_6F_6). Liquid phase exfoliation is a process in which solubilized graphene mono- and multi-layers are produced upon sonication of graphite in suitable solvents. This process is an important potential method for the

large scale and low cost production of medium sized graphene flakes. The key to this technology is finding an efficient, cheap and environment friendly solvent for solubilizing graphene to concentrations above 1 mg ml^{-1}, which is currently challenging.[7] A number of solvents for graphene solubilization have been studied experimentally[8,9] and theoretically.[10,11] It has been suggested that the best solvents are those whose surface energies are close to that of graphene itself (68 mJ m^{-2}),[12] thus minimizing mixing enthalpy. Even better predictions are obtained by using Hansen solubility parameters;[13] approximate values of $\delta_{D,G} \sim 18$ $MPa^{1/2}$, $\delta_{P,G} \sim 10$ $MPa^{1/2}$ and $\delta_{H,G} \sim 7$ $MPa^{1/2}$ have been suggested by Coleman's group,[14] leading to the discovery of a number of new efficient solvents for graphene.[12]

Benzene and C_6F_6 represent a particularly interesting pair of exfoliation solvents. They have reasonably similar Hansen solubility parameters (benzene: $\delta_{D,G} \sim 18.0$ $MPa^{1/2}$, $\delta_{P,G} \sim 0.0$ $MPa^{1/2}$ and $\delta_{H,G} \sim 2.0$ $MPa^{1/2}$; C_6F_6: $\delta_{D,G} \sim 16.9$ $MPa^{1/2}$, $\delta_{P,G} \sim 0.0$ $MPa^{1/2}$ and $\delta_{H,G} \sim 0.0$ $MPa^{1/2}$),[13] and therefore are expected to exhibit similar exfoliation efficiencies. Nevertheless, experiments have shown that whereas C_6F_6 is quite a good exfoliation solvent, benzene is a rather poor one.[9] Interestingly, benzene and C_6F_6 differ in their quadrupole moment, which is of similar magnitude but has opposite sign. Therefore, we decided to test whether this fact can explain the observed difference in exfoliation efficiencies of these two solvents. In molecular mechanics, this could easily be tested by comparing simulations with and without atomic quadrupoles placed on the graphene model.

Our paper is organized as follows. First, we analyze the electrostatic potential at different locations near to graphene flakes as a function of size and corrugation. Then, we estimate Gibbs energy changes of graphene flake exfoliation with and without a quadrupole moment by pulling a free graphene leaf from the surface. After that, the influence of a quadrupole on the solvation energy of graphene leaves of different sizes in different solvents is estimated using alchemical transformation of the quadrupole in a solvent. Finally we estimate exfoliation/association barrier heights by pulling fixed coplanar sheets in different solvents.

2. Methods

Several different structures were chosen to represent graphene flakes and supporting graphene in this study. Graphene flakes were represented by circumcoronene (denoted as C54) or by a larger 35 × 35 Å rectangular flake with 478 carbon atoms (denoted as C478). The periodic supporting graphene was modeled as a 50 × 50 Å rectangular graphene flake (C1008) in simulations including circumcoronene and as a 70 × 70 Å graphene flake (C2040) in simulations including C478. A single graphene sheet was used to model the graphite support. Exfoliation energies of graphite were shown to be somewhat higher (by about 18%),[15] but this should not affect our results because we are interested in the relative effect of the electrostatic component rather than the exfoliation energy itself.

Molecular dynamics simulations were performed within the Gromacs 4.5 software package.[16] After equilibration in the NPT ensemble (P = 1.0 bar, T = 298.15 K), production runs were performed in the NVT ensemble (T = 298.15 K). All atom GAFF force field parameters[17] were used for carbon atoms in circumcoronene and graphene flakes and the SPC/E model was used for water.[18] Parameters for C_6F_6 were taken from the literature,[19] and for benzene, GAFF parameters were used for vdW spheres and RED[20] parameters were used for charges. The integration step for all simulations was 2 fs and the interval for data collection was set to 0.5 ps. The cutoff distance for the direct electrostatics and vdW potential was set to 10 Å. The particle mesh Ewald method was used to calculate the indirect electrostatic potential beyond the cutoff distance. Bonds to hydrogen atoms were constrained during the MD simulations using the non-iterative LINCS algorithm.

The quadrupole moment of the graphene surface was represented by a pair of virtual sites placed above and below each carbon atom. The charges and distances of the virtual sites were chosen to reproduce the experimental value of the graphite quadrupole moment $Q_{zz} = (-3.03 \pm 0.10) \times 10^{-40}$ Cm^2 measured by Whitehouse and Buckingham.[3] A positive charge ($0.52e$) was placed at each carbon atom and two negative charges ($-0.26e$) were placed 0.6 Å above and below the graphene plane. The same values were used for all molecules in the present study.

2.1. Alchemical transformation

Alchemical transformation was used to estimate the effect of the quadrupole moment on solvation energies of graphene flakes in benzene, C_6F_6 and water. The method is based on thermodynamic integration (TI) of derivatives of the Hamiltonian with respect to a mixing parameter lambda, which was used to interpolate the state with and without the quadrupole moment. We used the 5-point Gaussian quadrature. Each simulation for a given lambda was equilibrated for 2.5 ns and the sampling period for data collection was 7.5 ns.

2.2. Graphene peeling

The potential of mean force (PMF) for peeling of the C54 and C478 molecules from an infinite graphene support was calculated using restrained MD simulations in an explicit solvent. As a reaction coordinate, we chose the z-coordinate of one of the outer carbon atoms, which was slowly pulled in the normal direction from the graphene surface. The reaction coordinate was divided into 43 windows separated by 0.48 Å (C54) or 165 windows separated by 0.34 Å (C478). For each window, 16 ns (C54) or 6 ns (C478) MD simulations were carried out. The umbrella integration method[21] was used to reconstruct the PMF of peeling.

2.3. Thermodynamic integration

The PMF of exfoliation of two carbon sheets (C54) constrained to be coparallel was calculated using constrained MD simulations in benzene and C_6F_6 explicit solvents. The 14 Å long reaction coordinate was divided into 52 windows with unequal spacing in order to improve sampling of the regions with rapidly changing force. Each window was equilibrated for 2.5 ns and 7.5 ns was used for data collection. The total force

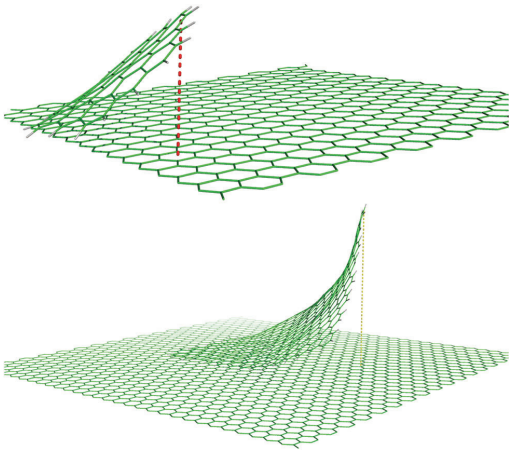

Fig. 3 Peeling of graphene flakes (C54 and C478) from an infinite graphene sheet.

acting on the center of mass of a C54 sheet was collected every 0.5 ps. The average force in each window was integrated using the cubic spline method.

3. Results and discussion

3.1. Electrostatics of finite graphene sheets

A typical size of a graphene flake exfoliated by sonication is about 1 μm^2, which corresponds to about 40 million carbon atoms. Flakes are usually irregularly shaped, with straight edges; a rectangular flake would have less than 10 000 atoms along its edge (1 μm, 10 000 Å). Fig. 4 illustrates how the electrostatic potential above the center of a graphene sheet decays as a function of the distance from the surface, z. Results are shown for rectangular sheets with several edge sizes, a, ranging from 10 to 10 000 Å. With increasing size of the flake, the distance dependence of the potential near to the surface weakens and its amplitude decreases. To estimate the relative importance of this potential for intermolecular interactions, we can compare it with the strength of typical vdW interactions, which dominate binding in graphite: each carbon atom contributes about 1.4 kcal mol^{-1} (or 61 meV per atom) to the cohesion energy of graphite.[22] Fig. 4 shows that for sheets smaller than 100 × 100 Å, the electrostatic interaction with a unit charge is more than 1 kcal mol^{-1}, which is comparable to the dispersion interaction with a carbon-like atom. On the other hand, for sheets larger than 1000 × 1000 Å, the electrostatic interaction with a unit charge is much weaker than 1 kcal mol^{-1} and for a 1 μm flake, it becomes negligible. Interaction of this quadrupolar field with uncharged molecules will usually be even weaker.

Next, we examined the potential near the graphene edge. Fig. 5 shows a plot of the electrostatic potential as a function of the distance from the flake edge. The electrostatic potential was calculated 3.4 Å above the surface, corresponding to typical vdW distances. Results for different sizes of flakes, a, are plotted

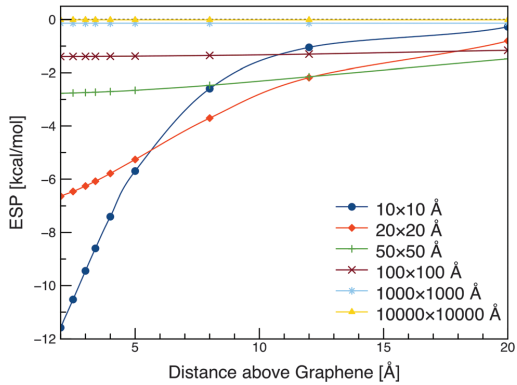

Fig. 4 Electrostatic quadrupolar potential above the surface of a graphene sheet as a function of the distance from the surface, and size of the sheet.

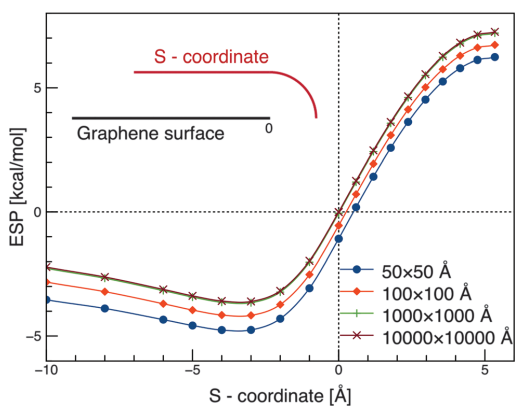

Fig. 5 Electrostatic potential next to the surface (3.4 Å) of a graphene sheet near to an edge as a function of the distance from the edge (S-coordinate) and size of the sheet. The S-coordinate is negative above graphene and positive when leaving the flake.

in different colors. These results show that for a very large flake, the potential near the edge converges to a finite value of about −3.6 kcal mol^{-1} and for smaller flakes, it is even larger. Thus, electrostatic interactions with graphene edges may be important even for relatively large planar sheets. This may result in different adsorption properties of the edges as compared to the rest of the surface.

3.2. Electrostatics of corrugated graphene

Unlike the ideal planar model described above, real graphene exhibits out-of-plane undulations, often called corrugation. The corrugation height has been estimated from experiment as about 1 nm and the length of the "wave" roughly between 5 and 10 nm for free graphene *in vacuo*.[23] As a result of this corrugation, cancellation of the electrostatic quadrupole in real

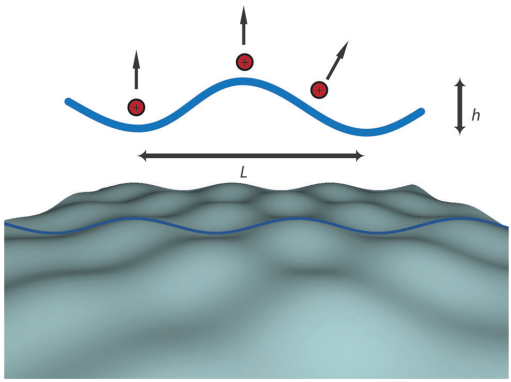

Fig. 6 The model of undulated graphene. Corrugation was represented as an undulation of height h = 1 nm and length L = 8 nm. The electrostatic potential was calculated 3.4 Å above the surface at three distinct locations, *i.e.*, the "valley", the "peak", and the inflex point.

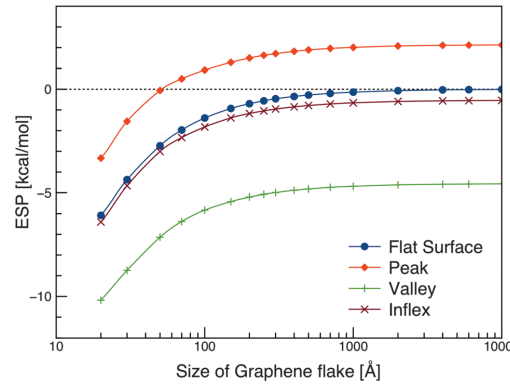

Fig. 8 Electrostatic potential close to the surface (3.4 Å) of a corrugated graphene sheet as a function of the sheet size. Potential above the peak (red), valley (green) and in the inflex of a ripple (violet) is compared with the potential above a perfectly planar sheet of the same size.

graphene is expected to be imperfect. We attempted to estimate the effect of the graphene undulation on the electrostatic potential near to the surface (3.4 Å above the surface). We chose to examine three distinct locations on the undulated landscape, the "peak", the inflex point and the "valley" (see Fig. 6). Corrugation was modeled as sinusoidal in both the x and y directions with an undulation height of 1 nm and 8 nm period.

Fig. 7 shows ESP at these three locations as a function of distance from a rectangular flake (1000 × 1000 Å). For comparison, we also show ESP of a perfectly planar flake of the same size (blue line). As expected, the potential next to the corrugated graphene was predicted to be substantially larger than that above the planar sheet. The absolute value was largest in the valley, somewhat smaller above the peak and very small near the inflex. Interestingly, whereas ESP was always negative above the planar carbon sheets, it was positive at the top of the peak, then changed sign near the inflex and acquired a negative value in the valley. It also decayed more rapidly with distance than ESP of a planar sheet.

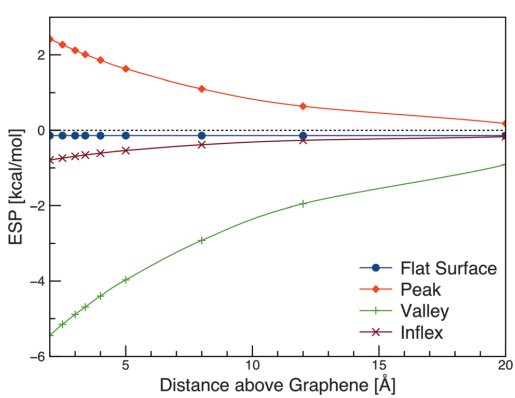

Fig. 7 Electrostatic potential as a function of distance from a corrugated graphene sheet (1000 × 1000 Å) above the peak (red), valley (green) and in the inflex (violet) of a ripple compared with the potential above a perfectly planar sheet of the same size.

Fig. 8 shows ESP above a rectangular graphene flake as a function of its size. The most important difference compared to planar graphene is that the potential does not converge to zero but to a finite value with increasing sheet size. For our simple model, ESP converged to about 2 kcal mol^{-1} per unit charge above the peak and about −4.5 kcal mol^{-1} per unit charge in the valley. Note that this value is only a very rough estimate because corrugation in real graphene is irregular and probably highly environment-dependant. Nevertheless, it is fairly large and may potentially make a sizeable contribution to the total interaction energy when graphene interacts with polar or charged molecules.

The quadrupolar electrostatic potential of corrugated graphene can be compared with that of benzene and polyaromatic molecules (Fig. 9). Among polyaromatic hydrocarbons, ESP was found to be largest for coronene and only somewhat smaller for benzene, circumcoronene (C-coronene) and dicircumcoronene (DC-coronene) (3.4 Å above surface in the middle of the molecule). The value for graphitic carbon is taken from Whitehouse and Buckingham.[3] In the case of corrugated graphene, the value of ESP in the valley was comparable to that of benzene, and the values above the peak and near the edge were smaller in magnitude, but still significant. Because benzene's quadrupole is known to play a very important role in its intermolecular interactions, it is likely that quadrupolar electrostatic interactions are also important for molecular interactions with corrugated graphene.

Electric field of graphene's quadrupole may become sizeable not only near edges or due to corrugation but every time the graphene sheet is disturbed from planarity. This happens at graphene folds or wrinkles but also in processes in which the

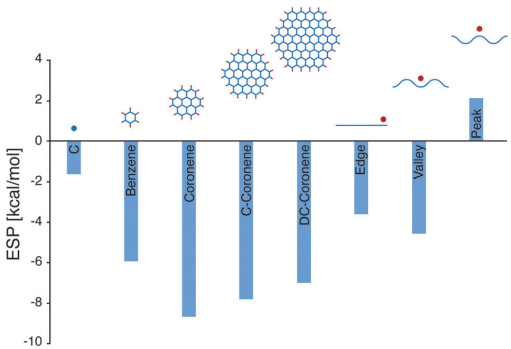

Fig. 9 Comparison of ESP near a graphene edge and of corrugated graphene with ESPs of aromatic hydrocarbons (calculated 3.4 Å above the surface, in the middle of the molecule).

graphene sheet is mechanically stressed, *e.g.*, during sonication induced exfoliation. In all these cases, quadrupolar interactions may need to be considered. Here we should note that when graphene is deformed, rearrangement of its electronic density may also generate dipole moment and other multipoles, which may significantly contribute to the total electric field. However, because these effects cannot be estimated at the force field level, we do not discuss them here. The magnitude of the quadrupolar contribution described in this work may be easily compared with other effects when their estimates become available.

3.3. Role of the quadrupole in MD simulations

The quadrupole moment of carbon atoms in graphene is usually neglected in MD simulations with classical force fields. Therefore, it is important to determine what role it may play and whether neglecting it is a safe approximation. In the present work, we focused mainly on interactions with benzene and C_6F_6, which differ in sign of their molecular quadrupole (Q_{zz}). In particular, we examined whether different exfoliation capabilities of these two solvents may be explained by interactions with the graphene quadrupole. We also attempted to estimate the quadrupole contribution to solvation energies of small graphene flakes by alchemical transformation and TI, and the PMF of graphene exfoliation considering two different exfoliation coordinates. Some calculations were also performed in water.

3.3.1. Potential of mean force of graphene peeling. The mechanism of liquid phase exfoliation is not yet fully understood and many different pathways may be possible. One idealized pathway is that the leaving sheet is gradually peeled from the support. To model this process, we pulled two small model molecules (circumcoronene and the rectangular flake C478) from the support by one of the outer carbon atoms (see Fig. 3 in Methods) and calculated PMF of this process by the umbrella integration technique (Fig. 10).

The PMF of peeling in C_6F_6 exhibited a deep minimum at the contact distance (about 3.4 Å) and then increased monotonically

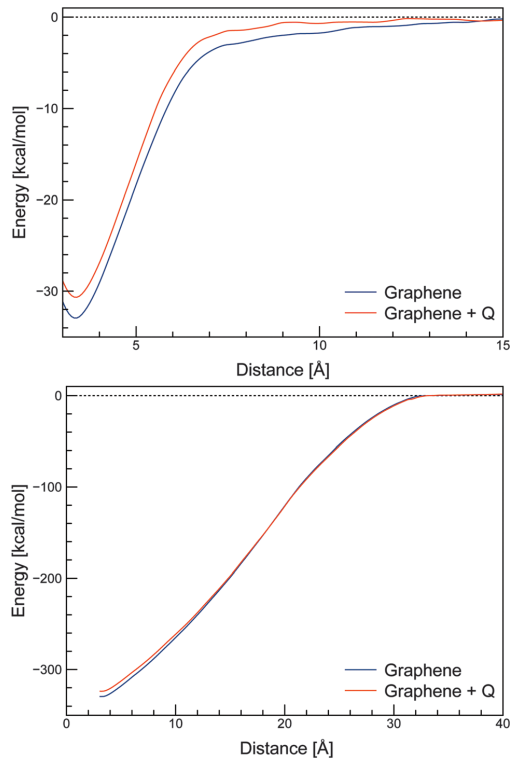

Fig. 10 Calculated PMF of exfoliation of circumcoronene (top) and C478 (bottom) in C_6F_6. A distance of about 3.4 Å corresponds to a stacked bilayer.

and reached the exfoliated state without a barrier. The exfoliated state was predicted to be thermodynamically unstable, consistent with results of MD simulations for other organic solvents.[10] The stabilization energy per carbon atom was about −0.61 kcal mol^{-1} for the circumcoronene model and −0.69 kcal mol^{-1} for C478. When quadrupoles were included on the peeled leaves, the exfoliated state was stabilized by electrostatics and the stabilization energies changed by 0.04 kcal mol^{-1} (from −0.61 to −0.57 kcal mol^{-1}) for C54 and by 0.01 kcal mol^{-1} (from −0.69 to −0.68 kcal mol^{-1}) for the C478 flake. Apparently, the quadrupolar contribution is relatively small in C_6F_6 and tends to decrease with the size of the simulated flake. Therefore, neglect of quadrupole moment is probably a reasonable approximation in this case.

3.3.2. Quadrupole contribution to solvation. The contribution of the quadrupolar moment to graphene's solvation energy was estimated by thermodynamic integration of alchemical transformation. Here we gradually grew atomic quadrupoles and integrated the accompanying change of Gibbs energy. To obtain a deeper insight, we simulated growth of both the natural graphene atomic quadrupoles (denoted as Q), and quadrupoles of the same absolute value but of opposite sign

Table 1 Change in Gibbs energy of solvation when quadrupoles are introduced, ΔG, for C54 and C478 in different solvents

	Circumcoronene (54 C atoms)		35 × 35 Å (478 C atoms)	
ΔG (kcal mol^{-1})	$0 \rightarrow Q$	$0 \rightarrow -Q$	$0 \rightarrow Q$	$0 \rightarrow -Q$
C_6F_6	−2.6	0.2	−8.6	0.4
C_6H_6	−0.1	−2.2		
Water	−4.9			

(denoted as $-Q$). The graphene flake models were not constrained, and thus were free to form ripples. Table 1 shows results for circumcoronene (C54) and the C478 flake, in water, benzene and C_6F_6.

Comparison of the simulations with reversed quadrupoles (Q and $-Q$) indicated competing electrostatic and polarization contributions to solvation. The polarization contribution (here only orientation solvent polarization) is always stabilizing. On the other hand, electrostatic interactions can be either stabilizing or destabilizing, depending on the orientation of the solute and solvent quadrupoles (we assume prevailing coplanar solvent orientation with the surface). Here, the interaction is stabilizing for the natural quadrupole on C54 (Q) in C_6F_6 and the opposite quadrupole ($-Q$) in benzene. The electrostatic and polarization contributions to solvation were apparently of similar magnitude, which resulted in almost complete cancellation in the cases where the electrostatic component was destabilizing (C54(Q) in benzene and C54($-Q$) in C_6F_6).

For benzene and C_6F_6, the quadrupolar contribution to solvation was relatively small and decreased with the flake size (contributions per C atom for C54 and C478 were −0.05 and −0.02, respectively, see Table 1). We did not calculate the total solvation energy directly, but a rough estimate can be obtained from the above estimated exfoliation energy and interaction energy ($\Delta G_{solv} \approx \Delta G_{exf} + E_{int}$). This gives about −22 kcal mol^{-1} for C54. Thus, the quadrupolar contribution to solvation in C_6F_6 was estimated to be only about 12% and is expected to be much smaller for larger graphene flakes. Higher results for water indicate that electrostatic interactions are more important in polar solvents, as expected. Nevertheless, it appears that neglecting quadrupolar interactions in force field calculations introduces only a relatively minor error in solvation energies and is probably a justified approximation.

3.3.3. Potential of mean force of coparallel flakes. The PMF of graphene plates can provide important information relevant to stability of graphene colloid in a given solvent.[10] Here, the graphene flakes were modeled using two circumcoronene molecules, which were kept planar and coparallel. One of the circumcoronenes bore atomic quadrupoles, whereas the other did not. The circumcoronene without quadrupoles represented a flat support, for which the electrostatic field cancels out due to its planarity. The circumcoronene with atomic quadrupoles mimicked the approaching (or leaving) graphene sheet, which may be corrugated or bent, and thus exhibit a local quadrupolar field. For comparison, we also calculated PMF for a model in which both circumcoronene molecules were without quadrupoles, as in the classical force field.

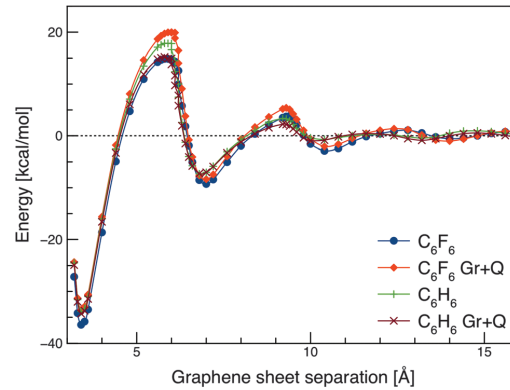

Fig. 11 PMF of separation of two circumcoronene molecules calculated in C_6F_6 with (red) and without quadrupoles (blue) and in benzene with (brown) and without quadrupoles (green) on the approaching circumcoronene.

Fig. 11 shows PMF in two different solvents, benzene and C_6F_6, calculated both with and without atomic quadrupoles on the approaching molecule. The exfoliation energy in C_6F_6 was very similar to that obtained in the peeling calculation described above (Fig. 10), *i.e.*, about 0.67 kcal mol^{-1} per carbon atom. Interestingly, the exfoliation energies in benzene and C_6F_6 were very similar. This means that the experimentally observed difference between the exfoliation efficiencies in the two solvents cannot be explained by thermodynamic stabilization of the exfoliated state. Nevertheless, the good stability of the graphene dispersion in C_6F_6 may be partly explained by kinetic considerations, as discussed below.

Inclusion of quadrupoles had notable effects on several characteristics of the PMF curves. Consistent with the results shown above (using a different exfoliation trajectory, Fig. 10), the exfoliation energy in C_6F_6 decreased only slightly (by about 3 kcal mol^{-1}, or 5%) when quadrupoles were included. However, inclusion of quadrupoles had a more pronounced effect on the barrier heights. Let us consider an association barrier at around 6 Å, which separates the solvent separated minimum at around 7 Å from the contact minimum at 3.4 Å. The height of this barrier has been shown to play an important role in kinetic theory of graphene colloid aggregation because it contributes to colloid stability.[10] When quadrupoles were neglected, benzene provided a slightly larger barrier height than C_6F_6, which suggests slower aggregation in benzene. Interestingly, when quadrupoles were considered, the height of this barrier increased by 4.2 kcal mol^{-1} (17%) in C_6F_6, whereas in benzene it decreased by 2.7 kcal mol^{-1} (11%) (note that these are rough estimates only as they are model-dependent). As a result, the expected association rate would be slower in C_6F_6 than in benzene when quadrupoles are included, as opposed to the situation when quadrupoles are neglected.

Because of the sensitivity of reaction rates to barrier heights, the almost 7 kcal mol^{-1} change may lead to a significant decrease of the aggregation rate in C_6F_6, resulting in better kinetic stability of graphene colloid in this solvent. Thus, kinetic aspects may partially explain the experimentally observed better exfoliation capabilities of C_6F_6, which cannot be explained by thermodynamic considerations, as discussed above.

4. Conclusions

In this study, we investigated the effect of graphene's electric quadrupole moment arising from its π electron distribution on intermolecular interactions. The magnitude of the graphene quadrupolar field was studied as a function of model size and corrugation. For an infinite and perfectly planar graphene sheet, the quadrupolar field near the surface vanishes with increasing sheet size, and therefore does not contribute to intermolecular interactions. However, in small graphene sheets the electric quadrupolar field decreases with increasing sheet size only slowly and may have a significant effect for small flakes, nanoribbons or near the edges of flakes. In corrugated graphene, the quadrupolar field does not vanish even for infinite sheets, and in the valleys of the corrugation, it reaches values comparable to those known for a benzene molecule. Because cancellation of the quadrupolar field near a graphene surface is disturbed by the curvature of the surface, significant electrostatic contributions may be expected near to graphene bends and folds. These results indicate that quadrupolar interactions may need to be considered when modeling intermolecular interactions with corrugated or bent graphene.

The effect of neglecting quadrupoles was tested in MD simulations of graphene exfoliation/aggregation in two similar solvents, benzene and C_6F_6. Inclusion of explicit quadrupoles made only a small contribution to the solvation energy of exfoliated flakes, of the order of a few percent. Although the electrostatic contribution thermodynamically favors solubilization of graphene in C_6F_6 when compared to benzene, stabilization is too small to explain the striking difference between the observed exfoliation efficiencies of these two solvents. However, considering quadrupoles had a marked effect on the PMF of graphene aggregation. Without quadrupoles, benzene exhibited a higher association barrier than C_6F_6, but when quadrupoles were included, the barrier height in C_6F_6 became substantially higher than that in benzene. Because the aggregation barrier height contributes to the kinetic stability of the exfoliated state, quadrupolar interactions may need to be taken into account when accurate modeling of graphene aggregation is needed.

It should be noted that current pairwise additive empirical potentials also neglect other effects which may play important roles in molecular interactions with graphene, such as polarization, charge redistribution in graphene upon corrugation, or charge transfer between interacting molecules. Some of these effects may be sizeable and comparable in magnitude with the quadrupolar contribution. The main purpose of this work was to isolate the quadrupolar contribution and estimate its magnitude separate from the above mentioned effects.

In conclusion, corrugated or bent graphene exhibits an electric quadrupole moment that may be important for intermolecular interactions. Our results will help to assess errors due to omission of quadrupolar electrostatic interactions in force field MD simulations and improve the general understanding of the importance of quadrupolar moments in molecular interactions with graphene.

Acknowledgements

This work was supported by grant P208/10/1742, from the Grant Agency of the Czech Republic. Further funding was provided by the Operational Program Research and Development for Innovations of the European Regional Development Fund *via* projects CZ.1.05/2.1.00/03.0058 and CZ.1.07/2.3.00/20.0017 administered by the Ministry of Education, Youth and Sports of the Czech Republic and a student project of Palacky University (PrF_2013_028).

References

1 V. Georgakilas, M. Otyepka, A. B. Bourlinos, V. Chandra, N. Kim, K. C. Kemp, P. Hobza, R. Zboril and K. S. Kim, *Chem. Rev.*, 2012, **112**, 6156–6214.
2 G. R. Jenness and K. D. Jordan, *J. Phys. Chem. C*, 2009, **113**, 10242–10248.
3 D. B. Whitehouse and A. D. Buckingham, *J. Chem. Soc., Faraday Trans.*, 1993, **89**, 1909.
4 A. Vernov and W. A. Steele, *Langmuir*, 1992, **8**, 155–159.
5 D. D. Do and H. D. Do, *Colloids Surf., A*, 2007, **300**, 50–59.
6 D. Nicholson, R. F. Cracknell and N. G. Parsonage, *Mol. Simul.*, 1990, **5**, 307–314.
7 U. Khan, A. O'Neill, M. Lotya, S. De and J. N. Coleman, *Small*, 2010, **6**, 864–871.
8 J. N. Coleman, *Adv. Funct. Mater.*, 2009, **19**, 3680–3695.
9 A. B. Bourlinos, V. Georgakilas, R. Zboril, T. A. Steriotis and A. K. Stubos, *Small*, 2009, **5**, 1841–1845.
10 C. Shih, S. Lin, M. S. Strano and D. Blankschtein, *J. Am. Chem. Soc.*, 2010, **132**, 14638–14648.
11 A. Schlierf, H. Yang, E. Gebremedhn, E. Treossi, L. Ortolani, L. Chen, A. Minoia, V. Morandi, P. Samorì, C. Casiraghi, D. Beljonne and V. Palermo, *Nanoscale*, 2013, **5**, 4205–4216.
12 J. N. Coleman, *Acc. Chem. Res.*, 2013, **46**, 14–22.
13 C. Hansen, *Hansen Solubility Parameters: A User's Handbook*, CRC Press, Boca Raton, Florida, 2nd edn, 2007, p. 544.
14 Y. Hernandez, M. Lotya, D. Rickard, S. D. Bergin and J. N. Coleman, *Langmuir*, 2010, **26**, 3208–3213.
15 L. A. Girifalco and R. A. Lad, *J. Chem. Phys.*, 1956, **25**, 693.

16 D. Van Der Spoel, E. Lindahl, B. Hess, G. Groenhof, A. E. Mark and H. J. C. Berendsen, *J. Comput. Chem.*, 2005, **26**, 1701–1718.
17 J. Wang, R. M. Wolf, J. W. Caldwell, P. A. Kollman and D. A. Case, *J. Comput. Chem.*, 2004, **25**, 1157–1174.
18 H. J. C. Berendsen, J. R. Grigera and T. P. Straatsma, *J. Phys. Chem.*, 1987, **91**, 6269–6271.
19 D. Dellis, I. Skarmoutsos and J. Samios, *J. Mol. Liq.*, 2010, **153**, 25–30.
20 F.-Y. Dupradeau, A. Pigache, T. Zaffran, C. Savineau, R. Lelong, N. Grivel, D. Lelong, W. Rosanski and P. Cieplak, *Phys. Chem. Chem. Phys.*, 2010, **12**, 7821–7839.
21 J. Kästner and W. Thiel, *J. Chem. Phys.*, 2005, **123**, 144104.
22 R. Zacharia, H. Ulbricht and T. Hertel, *Phys. Rev. B: Condens. Matter Mater. Phys.*, 2004, **69**, 155406.
23 J. C. Meyer, A. K. Geim, M. I. Katsnelson, K. S. Novoselov, T. J. Booth and S. Roth, *Nature*, 2007, **446**, 60–63.

JACS
JOURNAL OF THE AMERICAN CHEMICAL SOCIETY

Article

pubs.acs.org/JACS

Adsorption of Small Organic Molecules on Graphene

Petr Lazar,[‡] František Karlický,[‡] Petr Jurečka, Mikuláš Kocman, Eva Otyepková, Klára Šafářová, and Michal Otyepka*

Regional Centre of Advanced Technologies and Materials, Department of Physical Chemistry, Faculty of Science, Palacký University Olomouc, 771 46 Olomouc, Czech Republic

Supporting Information

ABSTRACT: We present a combined experimental and theoretical quantification of the adsorption enthalpies of seven organic molecules (acetone, acetonitrile, dichloromethane, ethanol, ethyl acetate, hexane, and toluene) on graphene. Adsorption enthalpies were measured by inverse gas chromatography and ranged from −5.9 kcal/mol for dichloromethane to −13.5 kcal/mol for toluene. The strength of interaction between graphene and the organic molecules was estimated by density functional theory (PBE, B97D, M06-2X, and optB88-vdW), wave function theory (MP2, SCS(MI)-MP2, MP2.5, MP2.X, and CCSD(T)), and empirical calculations (OPLS-AA) using two graphene models: coronene and infinite graphene. Symmetry-adapted perturbation theory calculations indicated that the interactions were governed by London dispersive forces (amounting to ∼60% of attractive interactions), even for the polar molecules. The results also showed that the adsorption enthalpies were largely controlled by the interaction energy. Adsorption enthalpies obtained from *ab initio* molecular dynamics employing non-local optB88-vdW functional were in excellent agreement with the experimental data, indicating that the functional can cover physical phenomena behind adsorption of organic molecules on graphene sufficiently well.

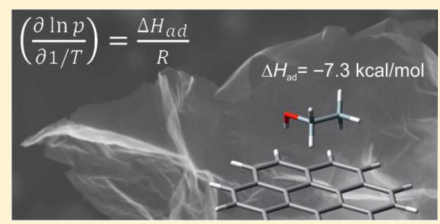

INTRODUCTION

Since its discovery, graphene[1] has been demonstrated to have promising applications in diverse disciplines, ranging from electronics to medicine.[2,3] It has been shown that the potential applications of graphene can be extensively broadened by various modes of functionalization, including non-covalent binding (adsorption) of molecules and nanoparticles.[4] One particularly interesting branch of research is the development of graphene-based chemical detectors, which can achieve such a high level of sensitivity that individual molecules adsorbed on graphene can be detected.[5,6] However, further progress requires quantification and understanding of the interaction of adsorbed molecules with graphene.

Quantification and identification of the nature of the interaction of adsorbed molecules on graphene pose several challenges from a theoretical perspective. Adsorption of small single molecules on graphene can be evaluated by quantum mechanical calculations based on density functional theory (DFT).[7,8] DFT can readily accommodate the periodic boundary conditions necessary to model a graphene sheet and can, in principle, calculate the adsorption properties of an arbitrary molecule. However, the reliability of the results obtained with the most widely used exchange-correlation DFT functionals, i.e., local density approximation (LDA) and generalized gradient approximation (GGA),[9,10] is often inadequate. In particular, omission of non-local electron correlations can severely affect the calculated adsorption properties because the interaction of guest molecules with graphene involves a large component of London dispersive forces of non-local nature. Recently, several techniques have been developed to combat this shortcoming, ranging from empirical corrections[11] and addition of a non-local correlation core (vdW-DF)[12] up to fully non-local and computationally expensive methods, such as random phase approximation.[13,14] However, there is a current lack of suitable experimental data with which to assess the performance of these methods.

In this paper, we present a combined experimental and theoretical study of the adsorption of seven small organic molecules onto graphene, which aimed to identify the magnitude and nature of the interaction. We used inverse gas chromatography to determine the adsorption enthalpies of gas-phase molecules to graphene flakes. This method allows adsorption enthalpies of volatile organic compounds onto a given surface to be measured directly and has previously been used to determine surface and interaction properties of various carbon-based materials, e.g., graphite,[15,16] carbon nanotubes,[17] and activated carbon.[18] However, to date, no reports have analyzed the interaction of molecules with graphene. To address this deficiency, we performed *ab initio* molecular dynamics (AIMD) simulations based on DFT to identify energetically favorable configurations of adsorbed molecules and evaluate the adsorption energies. In particular, we investigated use of the optB88-vdW DFT functional, which includes a contribution from non-local correlations.[19] For comparison, we also evaluated the adsorption properties using

Received: March 29, 2013
Published: April 9, 2013

dx.doi.org/10.1021/ja403162r | J. Am. Chem. Soc. 2013, 135, 6372−6377

an empirical force field typically used to analyze the interaction of graphene with large assemblies, such as nucleobases[20,21] or large molecules.[22,23] In addition, we calculated the properties of molecules adsorbed on coronene, which has been suggested to be a suitable small model of graphene.[24−28] The coronene model also allows the treatment of non-local correlations via the benchmark CCSD(T) method and evaluation of the contributions to the enthalpy of adsorption arising from zero-point and thermal vibrations. The nature of the interaction was examined in further detail using the symmetry-adapted perturbation theory (SAPT) method.[29]

EXPERIMENTAL AND COMPUTATIONAL METHODS

Differential isosteric adsorption enthalpies (heats of adsorption), ΔH_{ads}, were measured by inverse gas chromatography (iGC) using an SMS-iGC 2000 instrument (Surface Measurement Systems, UK) equipped with an SMS silylated column (diameter 4 mm, length 30 cm) containing 18.8 mg of graphene flakes (Graphenesupermarket, AO-1) with a surface area of 510 m^2/g. Measurements were carried out with *n*-hexane (Merck, LiChrosolv for LC, ≥98%), toluene (Sigma-Aldrich, Chromasolv for HPLC, 99.9%), dichloromethane (Merck, LiChrosolv for LC, ≥99.9%), ethyl acetate (Lach:ner, for HPLC, min. 99.8%), ethanol (Merck, gradient grade LiChrosolv for LC, ≥99.9%), and acetonitrile (Lach:ner, HPLC supergradient, min. 99.9%).

The adsorption enthalpies ΔH_{ads} for a given coverage ν can be calculated from the Clausius−Clapeyron equation:

$$\left(\frac{\partial P}{\partial T}\right)_{\nu} = \frac{\Delta H_{ad}}{T\Delta V} \tag{1}$$

where T is the thermodynamic temperature. Assuming ideal gas behavior and that ΔV is approximately equal to the volume of vapor in the gas phase, this equation can be rewritten as

$$\left(\frac{\partial \ln P}{\partial 1/T}\right)_{\nu} = \frac{\Delta H_{ad}}{R} \tag{2}$$

where R is the universal gas constant and P is pressure. The adsorption enthalpy can then be derived from a plot of $\ln P$ vs $1/T$. Further details on how $\ln P$ can be calculated from elution times measured by iGC can be found in the literature.[30,31]

Scanning electron microscopy (SEM) images were captured on a Hitachi 6600 FEG microscope operating in the secondary electron mode and using an accelerating voltage of 5 kV. Energy dispersive X-ray spectra (EDS) were also captured on this microscope by using a NORAN System 7 X-ray microanalysis system and an accelerating voltage of 5 kV. The SEM sample comprised a dried powder sample mounted on an aluminum holder with double-sided adhesive carbon tape.

Benchmark wave function calculations were performed for model complexes on coronene using the TurboMole 6.3 program[32] and Molpro 2012 package.[33] The CCSD(T)/CBS estimate was obtained by extrapolating[34] the cc-pV(T,Q)Z/MP2 energies and correcting for higher order correlation effects obtained at the CCSD(T)/cc-pVDZ level.[35] MP2.5/CBS and MP2.X/CBS energies were evaluated analogically, with the correction term obtained at the MP3/cc-pVDZ level.[36] The SCS(MI)-MP2 method was used with parameters of c_{OS} = 0.4 and c_{SS} = 1.29, as recommended for cc-pV(T,Q)Z extrapolation.[37] All energies were corrected for the basis set superposition error by using the counterpoise correction[38] (see Supporting Information for rigorous definitions and details). Geometry optimizations were carried out with cc-pVDZ and cc-pVTZ basis sets for MP2 and M06-2X,[39] and B97D,[40] respectively, using the Gaussian09 package.[41] Frequency calculations were performed at the B97D/cc-pVTZ level to determine the zero-point energy ($\Delta\Delta E_0$), thermal ($\Delta\Delta E_T$), and enthalpy ($\Delta\Delta E_H$) corrections. These corrections contribute to the enthalpy ΔH and internal energy ΔU as follows:

$$\Delta H = \Delta E + \Delta\Delta E_0 + \Delta\Delta E_T + \Delta\Delta E_H \tag{3}$$

$$\Delta U = \Delta E + \Delta\Delta E_0 + \Delta\Delta E_T$$

where ΔE stands for the electronic energy. All electronic energies discussed in the text are *adsorption* (i.e., *stabilization*) *energies*, ΔE, defined as the energy difference between the complex and infinitely separated fragments (graphene/coronene and molecule), whereas the *interaction energy*, ΔE_{int}, corresponds to fragments with the geometry of the complex. The difference between the adsorption and interaction energies is termed the *deformation energy*, E_{def}, of the fragments, i.e., $\Delta E = \Delta E_{int} + E_{def}^{gr} + E_{def}^{mol}$ (see Supporting Information for further details).

SAPT decomposition allows the interaction energy to be partitioned into physically meaningful components. Here, we used DFT-SAPT[42−45] implemented in the Molpro program package.[33] The components obtained from the SAPT calculation were gathered into four terms corresponding to electrostatics, exchange repulsion, induction, and dispersion:

$$E^{SAPT} = E_{elst} + E_{exch\text{-}rep} + E_{ind} + E_{disp} \tag{4}$$

where E_{elst} is $E_{elst}^{(1)}$, $E_{exch\text{-}rep}$ is $E_{exch\text{-}rep}^{(1)}$, E_{ind} is $E_{ind}^{(2)} + E_{exch\text{-}ind}^{(2)} + \delta(\mathrm{HF})$, and E_{disp} is $E_{disp}^{(2)} + E_{exch\text{-}disp}^{(2)}$ (for more details on DFT-SAPT, see the references above). We used the LPBE0AC exchange-correlation potential[42−49] for monomer calculations and a cc-pVTZ basis set.

DFT calculations on graphene were performed using the projector-augmented wave (PAW) method in the Vienna Ab initio Simulation Package (VASP) suite.[50,51] The energy cutoff for the plane-wave (PW) expansion was set to 400 eV, as further increasing the energy cutoff to 500 eV resulted in no change in the calculated adsorption energies. The graphene sheet was modeled using a 4×4 supercell (32 carbon atoms) with a calculated C−C bond length of 1.44 Å. The periodically repeated sheets were separated by 15 Å of vacuum. The AIMD simulation was used to mimic finite temperature effects; molecules were placed onto a graphene sheet, and the system was treated as a canonical (NVT) ensemble. The temperature in the simulation was set to 333 K, which was typical of the temperature used in the experiment. AIMD simulations were performed for at least 5 ps with a time step of 1 fs. Adsorption energies were obtained by quenching low-energy configurations from the AIMD run (ΔE^{AIMD}) and by time-averaging Kohn−Sham energies $\Delta\langle E^{AIMD}\rangle$ obtained in the AIMD simulation. In order to determine enthalpies of adsorption ΔH^{AIMD}, we corrected the adsorption energies on graphene, ΔE^{AIMD}, by the zero-point ($\Delta\Delta E_0$) and thermal ($\Delta\Delta E_T$) corrections from the coronene model and $-RT$ ($\sim\Delta\Delta E_H$). The $\Delta\langle E^{AIMD}\rangle$ obtained from the AIMD simulations intrinsically included thermal corrections. Thus, the respective enthalpy $\Delta\langle H^{AIMD}\rangle$ was calculated by adding zero-point energy and $-RT$ corrections only.

Force field (FF) simulations were performed using all-atom optimal potentials for liquid simulation (OPLS-AA).[52] Structures and topologies of the molecules were taken from the Gromacs Molecule & Liquid Database.[53,54] Graphene was modeled by 3936 atoms, which were kept in fixed positions in a planar hexagonal lattice with a bond distance of 1.4 Å. Periodic boundary conditions were applied in all three dimensions of the simulation box, which had a size of 100 × 100 × 130 Å. Intermolecular interactions were calculated using the Lennard-Jones potential described by Chang and Steele[55] with a cutoff radius of 10.0 Å. The Newtonian equations of motion were integrated using a 2 fs time step. Each MD run was equilibrated for 0.2 ns, and the energy $\Delta\langle E^{FF}\rangle$ of the molecule−graphene interaction was calculated as an average of 5000 values over 1 ns of simulation time. All simulations were performed with a constant volume and a temperature of 323 K. The adsorption enthalpies from force field simulations were calculated as follows:

$$\Delta\langle H^{FF}\rangle = \Delta\langle E^{FF}\rangle - RT \tag{5}$$

where $-RT$ corresponds to the enthalpy correction ($\Delta\Delta E_H$).

dx.doi.org/10.1021/ja403162r | J. Am. Chem. Soc. 2013, 135, 6372−6377

RESULTS AND DISCUSSION

Experiment. The adsorption enthalpies (ΔH_{ads}) of the organic molecules to graphene flakes (Figure S1) measured by iGC ranged from −5.9 to −13.5 kcal/mol (Table 1).

Table 1. Experimental Adsorption Enthalpies (in kcal/mol) and Their Respective Confidence Intervals (at α = 0.05) for Seven Molecules, Measured by Inverse Gas Chromatography in the Specified Temperature Ranges (T_{min}−T_{max} in K)

compound	ΔH_{ads}	T_{min}−T_{max}
acetone	−8.2 ± 0.3	303−333
acetonitrile	−7.6 ± 0.3	303−343
dichloromethane	−5.9 ± 0.5	303−343
ethanol	−7.3 ± 0.7	303−343
ethyl acetate	−11.5 ± 0.2	303−343
hexane	−12.2 ± 0.2	333−373
toluene	−13.5 ± 0.3	343−383

Dichloromethane had the lowest ΔH_{ads}, followed by ethanol, acetonitrile, acetone, ethyl acetate, hexane, and last toluene, which displayed the highest affinity to graphene. Each measurement was conducted at five (four for acetone) temperatures (Table 1) at low coverage ν (~2.0%), and plots of $\ln P$ against $1/T$ (Figures S2−S8) were linear for each molecule with a coefficient of determination (r^2) above 0.99, except for ethanol ($r^2 \approx 0.98$).

The same ΔH_{ads} values were obtained in consecutive independent measurements under constant conditions, confirming the reproducibility of the results. The estimated experimental error in the adsorption enthalpies was, on average, less than 0.4 kcal/mol (Table 1). The values of ΔH_{ads} depended on coverage (see Figure 1 for ΔH_{ads} of

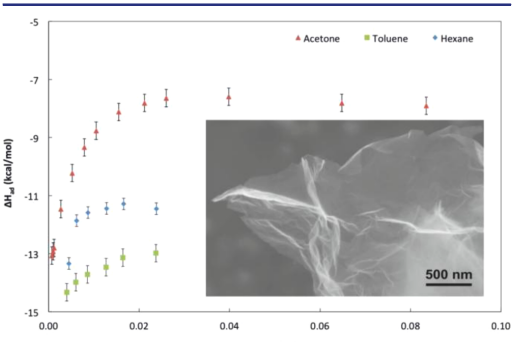

Figure 1. Adsorption enthalpies (ΔH_{ads}) of acetone, toluene, and hexane on graphene flakes vs coverage, showing saturation at ~2% coverage. Inset: SEM image of the graphene flake.

acetone, toluene, and hexane). ΔH_{ads} was more negative at very low coverage, indicating that adsorption initially occurred onto high surface energy sites (e.g., sides and edges) of the graphene flakes but increased with increasing coverage. Once the high surface energy positions were filled, molecules then adsorbed onto the graphene surface, as manifested by the constant ΔH_{ads} value. A slight deviation from this behavior was observed for ethanol: after an initial drop, ΔH_{ads} slowly increased with increasing coverage (data not shown). This can be attributed to clustering of ethanol molecules (via hydrogen bonds) on the surface, which is also reflected in the large error bars observed for ethanol (Table 1). This may also explain the deviation of the $\ln P$ vs $1/T$ plot for ethanol from linearity (albeit not statistically significant at α = 0.05). Consequently, the ΔH_{ads} value of ethanol measured at low temperatures was lower (−9.1 kcal/mol) than that at higher temperatures (−5.2 kcal/mol).

Computations on Coronene Model. In order to unravel the nature of the interaction between the studied molecules and a graphene-like support, we performed calculations on a finite model system, i.e., coronene. The calculated geometries of molecules allowed to relax and adsorb on coronene are displayed in Figure 2. The coronene model enabled

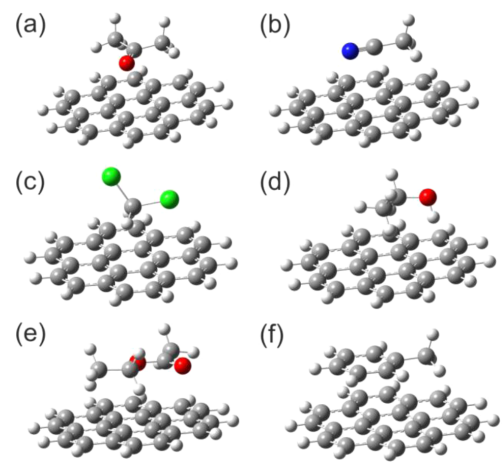

Figure 2. Calculated geometries of (a) acetone, (b) acetonitrile, (c) dichloromethane, (d) ethanol, (e) ethyl acetate, and (f) toluene adsorbed on coronene.

decomposition of the interaction energies by SAPT (Figure 3a), and computation of zero-point energy, and thermal and enthalpy corrections (Figure 3b,c), needed to convert calculated energies of adsorption into *enthalpies* of adsorption. The coronene model also enabled the strength of the interaction to be evaluated by various *ab initio* methods up to the CCSD(T) level and identification of a DFT functional suitable for the description of molecules adsorbed on graphene (Table 2, Figure 3d).

Figure 3a shows the contributions of dispersion, induction, and electrostatics calculated by SAPT to the total attractive energy. For instance, the dispersion contribution (in %) was calculated as $E_{disp}/(E_{disp} + E_{ind} + E_{elst})$. Clearly, the dispersion stabilization was dominant as it contributed more than 60% of the total attractive interaction for all the complexes considered, including those that were polar. The second largest attractive contribution was due to electrostatics, which was very large even for nonpolar molecules such as hexane. This indicates that most of the electrostatic attraction originates from large overlap (or penetration) electrostatics, which is a consequence of quite short intermolecular distances caused by strong dispersion attraction. The induction (or polarization) interaction was comparatively small in all cases. Full SAPT data are shown in Table S1.

The contributions to the enthalpy of adsorption (ΔH) according to equation 3 are displayed in Figure 3b,c. The zero-

dx.doi.org/10.1021/ja403162r | J. Am. Chem. Soc. 2013, 135, 6372−6377

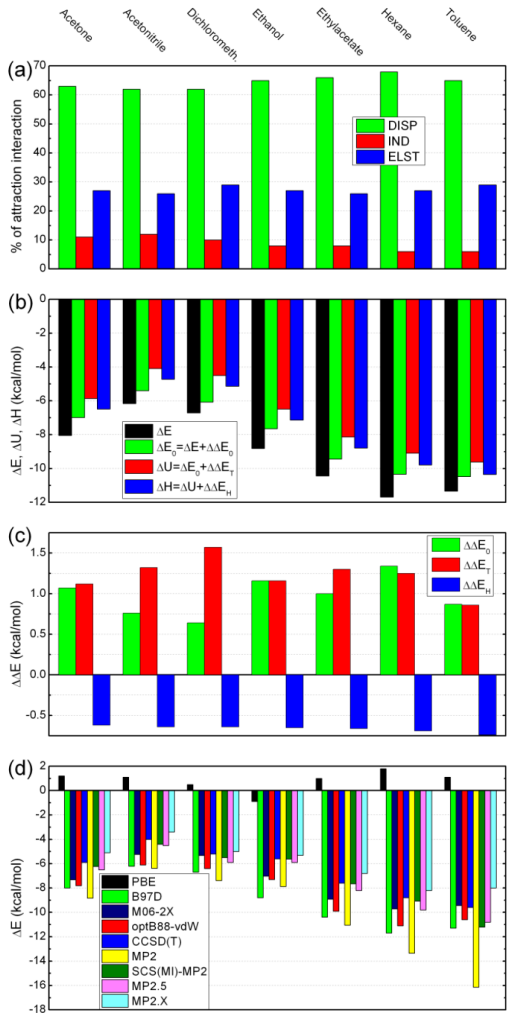

Figure 3. (a) Decomposition of the attractive contributions to the adsorption energy from SAPT. (b) Adsorption energies/enthalpies showing the contributions of the zero-point energy ($\Delta\Delta E_0$), thermal ($\Delta\Delta E_T$), and enthalpy ($\Delta\Delta E_H$) corrections. (c) Effects of the corrections to the adsorption energies. (d) Adsorption energies of the seven studied molecules on coronene calculated by various methods.

point energy corrections ($\Delta\Delta E_0$) were similar for all molecules and increased the adsorption energy by about 0.8−1.3 kcal/mol. Thermal corrections ($\Delta\Delta E_T$) further increased the final adsorption enthalpies by 0.9−1.6 kcal/mol. On the other hand, enthalpy corrections ($\Delta\Delta E_H$) had an opposite effect, decreasing the energies by ~ -0.7 kcal/mol, i.e., by an amount similar to $-RT$ for an ideal gas. As a result, each correction had a similar magnitude for all molecules on coronene. Thus, the adsorption enthalpies (ΔH) were predominantly controlled by the adsorption energies (ΔE).

Table 2. Interaction Energies of Seven Different Molecules on Coronene (ΔE_{int} in kcal/mol) Calculated with the optB88-vdW Functional, M06-2X Functional, SCS(MI)-MP2/CBS Method, and CCSD(T)/CBS Estimate

compound	optB88-vdW/PW	M06-2X/cc-pVTZ	SCS(MI)-MP2/CBS[a]	CCSD(T)/CBS[a]
acetone	−8.5	−7.5	−7.9	−7.6
acetonitrile	−6.6	−5.4	−6.6	−6.2
dichloromethane	−6.8	−5.4	−7.0	−6.7
ethanol	−7.8	−7.1	−7.1	−7.1
ethyl acetate	−10.5	−9.1	−9.7	−9.7
hexane	−11.6	−9.9	−10.7	−10.4
toluene	−12.1	−9.7	−13.5	−11.9

[a]B97D geometries.

Figure 3d displays the calculated adsorption (stabilization) energies ΔE (obtained by adding monomer deformation energies to the interaction energies; see Methods and Supporting Information for definitions) of molecules on coronene. All methods reproduced the experimental order of adsorption energies. Compared to the CCSD(T) method, which provides the most physically robust description of dispersion interactions, the SCS(MI)-MP2, MP2.5, and MP2.X methods gave very reliable results with mean errors (MEs) of 0.4, 0.7, and 0.7 kcal/mol, respectively. However, it should be noted that the MP2 method gave consistently lower adsorption energies, reflecting the known tendency of MP2 to overestimate the dispersion contribution to the correlation energy.[56]

Comparison of adsorption energies calculated by DFT functionals with the reference CCSD(T) data showed that only functionals incorporating non-local dispersive electron correlation effects provided reasonable results. Adsorption energies ΔE calculated by the widely used semi-local GGA functional PBE were positive (except for ethanol; see Figure 3d), although geometry optimizations with the PBE functional found minima corresponding to adsorbed states of the molecules. In this case, slightly negative interaction energies ΔE_{int} (between −0.4 and −3.2 kcal/mol) were counterbalanced by positive deformation energies. Adsorption energies predicted by the B97D functional, which accounts for London dispersive forces by empirical corrections, were in close agreement with CCSD(T) values, with a ME of 2.4 kcal/mol. However, such empirical corrections are pairwise additive, which limits their use for larger systems.[57] The optB88-vdW functional, which includes a non-local core to account for non-local correlation effects (as well as many-body vdW energy), provided better adsorption energies compared to the CCSD(T) method (ME = 1.8 kcal/mol) and therefore was used for the simulations of molecules on graphene. It should be noted that vdW-DF[12]-based functionals have been shown to be highly sensitive to the exchange component, particularly in the case of metal−graphene interactions.[58,59] Hybrid meta-GGA M06-2X functional, which accounts for dispersion using a reparametrized exchange-correlation functional, gave the lowest ME of 0.9 kcal/mol with respect to the CCSD(T)/CBS estimate of adsorption energies.

For the sake of completeness, we also compared interaction energies ΔE_{int} (i.e., energies not including the deformation energies) obtained by the optB88-vdW, M06-2X, and SCS(MI)-MP2 methods (i.e., the best-performing functionals and wave function-based method) against those calculated from the

dx.doi.org/10.1021/ja403162r | J. Am. Chem. Soc. 2013, 135, 6372−6377

Table 3. Adsorption Energies ΔE (and Enthalpies ΔH, see text for details, both in kcal/mol) Obtained by Quenching AIMD Simulations (ΔE^{AIMD} and ΔH^{AIMD}), Averaging Energies Obtained in AIMD Simulations ($\Delta\langle E^{AIMD}\rangle$ and $\Delta\langle H^{AIMD}\rangle$), and from Force Field Simulations ($\Delta\langle H^{FF}\rangle$); Experimental Adsorption Enthalpies ΔH_{ads} Are Also Listed

compound	$\Delta\langle H^{FF}\rangle$	ΔE^{AIMD}	$\Delta\langle E^{AIMD}\rangle$	ΔH^{AIMD}	$\Delta\langle H^{AIMD}\rangle$	ΔH_{ads}
acetone	−6.6	−9.3	−8.3	−7.8	−7.9	−8.2 ± 0.3
acetonitrile	−5.0	−8.0	−6.9	−6.6	−6.8	−7.6 ± 0.3
dichloromethane	−6.3	−7.2	−5.8	−5.7	−5.8	−5.9 ± 0.5
ethanol	−5.0	−7.9	−6.9	−6.2	−6.4	−7.3 ± 0.7
ethyl acetate	−9.4	−13.1	−11.5	−11.5	−11.2	−11.5 ± 0.2
hexane	−10.2					−12.2 ± 0.2
toluene	−10.5	−15.1	−12.9	−14.0	−12.7	−13.5 ± 0.3

benchmark CCSD(T) method (Table 2). The MEs (0.6, 0.8, and 0.4 kcal/mol for optB88-vdW, M06-2X, and SCS(MI)-MP2, respectively) were lower than the thermochemical accuracy (1 kcal/mol) usually required for such types of calculations. Owing to the high quality (low ME of the energy) and reasonable computational demands, we recommend all three methods for calculations of the interaction energies of organic molecules to coronene. Full data sets of the adsorption and interaction energies of molecules on coronene are provided in Tables S3 and S4.

Computations on Graphene. The adsorption enthalpies of molecules on graphene were initially calculated using the empirical OPLS-AA force field. The resulting enthalpies $\Delta\langle H^{FF}\rangle$ (Table 3) correlated to the experimental data with a correlation coefficient of r = 0.93. Compared to the experimental data, the force field energies were underestimated by an average ME of 1.9 kcal/mol. This might be due to the neglect of polarization energy in the pairwise additive force fields[60] and other limitations of classical force fields.[57] Nevertheless, the OPLS-AA force field was able to recognize weakly and strongly bound molecules, and thus may be suitable for semi-quantitative estimates of the interaction energies of large molecules with graphene.

Based on the above-mentioned results, we applied the optB88-vdW functional to obtain the adsorption enthalpies of molecules on graphene at a quantum mechanical level by AIMD. The starting configurations were adopted as the geometries obtained from the molecule−coronene system optimizations (Figure 2). All molecules remained bound to the graphene surface during the AIMD simulations, with the average surface−molecule distance corresponding to physisorption. It should be noted that, in test AIMD with the standard PBE functional,[49] the molecules spontaneously detached from the graphene surface, which underlines the importance of non-local dispersive correlations. Adsorption energies obtained by quenching low-energy AIMD configurations (ΔE^{AIMD}) and time-averaged energies from AIMD runs ($\Delta\langle E^{AIMD}\rangle$) are reported in Table 3. The time-averaged energies intrinsically included a contribution from thermal vibrations ($\Delta\Delta E_T$) to the internal energy, which slightly increased the adsorption energy ($\Delta E^{AIMD} < \Delta\langle E^{AIMD}\rangle$; Table 3). However, the adsorbed molecules did not alter the electronic structure of graphene, as shown by the band structure (Supporting Information, Figure S9).

The close agreement between experimental and calculated values of the adsorption enthalpies ΔH^{AIMD} and $\Delta\langle H^{AIMD}\rangle$, obtained from ΔE^{AIMD} and $\Delta\langle E^{AIMD}\rangle$, respectively, by adding appropriate corrections (see Methods section for details), indicates that thermal vibrations were well described, even by using the harmonic approximation on the coronene model. Theoretical enthalpies of adsorption followed the same order as the measured adsorption enthalpies, with the strongest binding being that of toluene and the weakest binding for dichloromethane. Moreover, the absolute values of the calculated adsorption enthalpies were in excellent agreement with the experimental values (r = 0.99, ME = 0.4 kcal/mol for $\Delta\langle H^{AIMD}\rangle$ and r = 0.99, ME = 0.5 kcal/mol for ΔH^{AIMD}). This agreement shows that modern DFT functionals that include non-local dispersive interactions can reliably treat even difficult systems, such as a molecule adsorbed on a two-dimensional graphene sheet.

CONCLUSIONS

Inverse gas chromatography measurements provided experimental values for the adsorption enthalpies of seven organic molecules on graphene flakes with an error less than 0.7 kcal/mol (ME = 0.4 kcal/mol). Molecule−coronene systems were modeled to calculate the strength and nature of the interaction together with the effect of zero-point energy, thermal vibration, and enthalpy corrections to the adsorption enthalpy. SAPT calculations showed that all the considered complexes were predominantly stabilized by dispersion, which contributes more than 60% to the attractive energy, even in polar complexes. The change in zero-point energy upon adsorption was similar for each molecule and led to an increase of the adsorption energy by about 0.8−1.3 kcal/mol. Thermal vibrations further increased the energy by 0.9−1.6 kcal/mol. Thermal correction to the enthalpy had an opposite effect, decreasing the energy by ∼ −0.7 kcal/mol, equivalent to $-RT$ for an ideal gas. As these contributions were similar (and rather small) for all the considered molecules, we concluded that the adsorption enthalpy is mainly controlled by the interaction energy. *Ab initio* MD simulations of molecules on graphene were performed using the optB88-vdW functional. We found that the order and absolute values of the theoretical adsorption enthalpies were in excellent agreement with the experimental values, indicating that the non-local electron correlation is crucial for proper description of the adsorption to graphene at the DFT level.

ASSOCIATED CONTENT

Supporting Information

Figure S1, SEM images and EDS spectra of graphene flakes; Figures S2−S8, measured slopes of $\ln P$ against $1/T$ for each molecule; Figure S9, band structures; details on energy calculations; Table S1, SAPT components; Table S2, adsorption enthalpy contributions; Tables S3 and S4, adsorption and interaction energies on coronene; and Table S5, adsorption geometries of molecules on coronene. This

material is available free of charge via the Internet at http://pubs.acs.org.

AUTHOR INFORMATION

Corresponding Author

michal.otyepka@upol.cz

Author Contributions

‡P.L. and F.K. contributed equally.

Notes

The authors declare no competing financial interest.

ACKNOWLEDGMENTS

This work was supported by the Grant Agency of the Czech Republic (P208/12/G016 and P208/10/1742), the Operational Program Research and Development for Innovations−European Regional Development Fund (CZ.1.05/2.1.00/03.0058), the Operational Program Education for Competitiveness−European Social Fund (CZ.1.07/2.3.00/20.0017), and a student project of Palacký University (PrF_2013_028).

REFERENCES

(1) Novoselov, K. S.; Geim, A. K.; Morozov, S. V.; Jiang, D.; Zhang, Y.; Dubonos, S. V.; Grigorieva, I. V.; Firsov, A. A. *Science* **2004**, *306*, 666.

(2) Geim, A. K.; Novoselov, K. S. *Nat. Mater.* **2007**, *6*, 183.

(3) Novoselov, K. S.; Falko, V. I.; Colombo, L.; Gellert, P. R.; Schwab, M. G.; Kim, K. *Nature* **2012**, *490*, 192.

(4) Georgakilas, V.; Otyepka, M.; Bourlinos, A. B.; Chandra, V.; Kim, N.; Kemp, K. C.; Hobza, P.; Zboril, R.; Kim, K. S. *Chem. Rev.* **2012**, *112*, 6156.

(5) Schedin, F.; Geim, A. K.; Morozov, S. V.; Hill, E. W.; Blake, P.; Katsnelson, M. I.; Novoselov, K. S. *Nat. Mater.* **2007**, *6*, 652.

(6) Myung, S.; Yin, P. T.; Kim, C.; Park, J.; Solanki, A.; Reyes, P. I.; Lu, Y. C.; Kim, K. S.; Lee, K. B. *Adv. Mater.* **2012**, *24*, 6081.

(7) Hohenberg, P.; Kohn, W. *Phys. Rev. B* **1964**, *136*, B864.

(8) Kohn, W.; Sham, L. J. *Phys. Rev.* **1965**, *140*, 1133.

(9) Burke, K. *J. Chem. Phys.* **2012**, *136*, 150901.

(10) Cohen, A. J.; Mori-Sanchez, P.; Yang, W. T. *Chem. Rev.* **2012**, *112*, 289.

(11) Grimme, S. *Wires Comput. Mol. Sci.* **2011**, *1*, 211.

(12) Dion, M.; Rydberg, H.; Schroder, E.; Langreth, D. C.; Lundqvist, B. I. *Phys. Rev. Lett.* **2004**, *92*, 246401.

(13) Eshuis, H.; Bates, J. E.; Furche, F. *Theor. Chem. Acc.* **2012**, *131*, 1084.

(14) Ren, X. G.; Rinke, P.; Joas, C.; Scheffler, M. *J. Mater. Sci.* **2012**, *47*, 7447.

(15) Papirer, E.; Brendle, E.; Ozil, F.; Balard, H. *Carbon* **1999**, *37*, 1265.

(16) Balard, H.; Maafa, D.; Santini, A.; Donnet, J. B. *J. Chromatogr. A* **2008**, *1198−1199*, 173.

(17) Menzel, R.; Bismarck, A.; Shaffer, M. S. P. *Carbon* **2012**, *50*, 3416.

(18) Díaz, E.; Ordóñez, S.; Vega, A.; Coca, J. *J. Chromatogr. A* **2004**, *1049*, 139.

(19) Klimes, J.; Bowler, D. R.; Michaelides, A. *Phys. Rev. B* **2011**, *83*, 195313.

(20) Antony, J.; Grimme, S. *Phys. Chem. Chem. Phys.* **2008**, *10*, 2722.

(21) Umadevi, D.; Sastry, G. N. *J. Phys. Chem. Lett.* **2011**, *2*, 1572.

(22) Min, S. K.; Kim, W. Y.; Cho, Y.; Kim, K. S. *Nature Nanotechnol.* **2011**, *6*, 162.

(23) Zhang, T.; Xue, Q.; Zhang, S.; Dong, M. *Nano Today* **2012**, *7*, 180.

(24) Janowski, T.; Pulay, P. *J. Am. Chem. Soc.* **2012**, *134*, 17520.

(25) Smith, D. G. A.; Patkowski, K. *J. Chem. Theory Comput.* **2013**, *9*, 370.

(26) Kysilka, J.; Rubes, M.; Grajciar, L.; Nachtigall, P.; Bludsky, O. *J. Phys. Chem. A* **2011**, *115*, 11387.

(27) Voloshina, E.; Usvyat, D.; Schutz, M.; Dedkov, Y.; Paulus, B. *Phys. Chem. Chem. Phys.* **2011**, *13*, 12041.

(28) Podeszwa, R. *J. Chem. Phys.* **2010**, *132*, 044704.

(29) Szalewicz, K. *Wires Comput. Mol. Sci.* **2012**, *2*, 254.

(30) Panzer, U.; Schreiber, H. P. *Macromolecules* **1992**, *25*, 3633.

(31) Conder, J. R.; Young, C. L. *Physicochemical measurement by gas chromatography*; Wiley: New York, 1979.

(32) Ahlrichs, R.; Bar, M.; Haser, M.; Horn, H.; Kolmel, C. *Chem. Phys. Lett.* **1989**, *162*, 165.

(33) Werner, H. J.; Knowles, P. J.; Knizia, G.; Manby, F. R.; Schutz, M. *MOLPRO*, version 2012.1, a package of ab initio programs, 2012; http://www.molpro.net.

(34) Halkier, A.; Helgaker, T.; Jørgensen, P.; Klopper, W.; Koch, H.; Olsen, J.; Wilson, A. K. *Chem. Phys. Lett.* **1998**, *286*, 243.

(35) Jurecka, P.; Hobza, P. *J. Am. Chem. Soc.* **2003**, *125*, 15608.

(36) Riley, K. E.; Rezac, J.; Hobza, P. *Phys. Chem. Chem. Phys.* **2011**, *13*, 21121.

(37) Distasio, R. A.; Head-Gordon, M. *Mol. Phys.* **2007**, *105*, 1073.

(38) Boys, S. F.; Bernardi, F. *Mol. Phys.* **1970**, *19*, 553.

(39) Zhao, Y.; Truhlar, D. *Theor. Chem. Acc.* **2008**, *120*, 215.

(40) Grimme, S. *J. Comput. Chem.* **2006**, *27*, 1787.

(41) Frisch, M. J.; Trucks, G. W.; Schlegel, H. B.; Scuseria, G. E.; Robb, M. A.; Cheeseman, J. R.; Scalmani, G.; Barone, V.; Mennucci, B.; Petersson, G. A.; Nakatsuji, H.; Caricato, M.; Li, X.; Hratchian, H. P.; Izmaylov, A. F.; Bloino, J.; Zheng, G.; Sonnenberg, J. L.; Hada, M.; Ehara, M.; Toyota, K.; Fukuda, R.; Hasegawa, J.; Ishida, M.; Nakajima, T.; Honda, Y.; Kitao, O.; Nakai, H.; Vreven, T.; Montgomery, J. A.; Peralta, J. E.; Ogliaro, F.; Bearpark, M.; Heyd, J. J.; Brothers, E.; Kudin, K. N.; Staroverov, V. N.; Kobayashi, R.; Normand, J.; Raghavachari, K.; Rendell, A.; Burant, J. C.; Iyengar, S. S.; Tomasi, J.; Cossi, M.; Rega, N.; Millam, J. M.; Klene, M.; Knox, J. E.; Cross, J. B.; Bakken, V.; Adamo, C.; Jaramillo, J.; Gomperts, R.; Stratmann, R. E.; Yazyev, O.; Austin, A. J.; Cammi, R.; Pomelli, C.; Ochterski, J. W.; Martin, R. L.; Morokuma, K.; Zakrzewski, V. G.; Voth, G. A.; Salvador, P.; Dannenberg, J. J.; Dapprich, S.; Daniels, A. D.; Farkas; Foresman, J. B.; Ortiz, J. V.; Cioslowski, J.; Fox, D. J. *Gaussian 09*, Revision A.02; Wallingford CT, 2009.

(42) Hesselmann, A.; Jansen, G. *Chem. Phys. Lett.* **2002**, *362*, 319.

(43) Hesselmann, A.; Jansen, G. *Chem. Phys. Lett.* **2002**, *357*, 464.

(44) Hesselmann, A.; Jansen, G. *Chem. Phys. Lett.* **2003**, *367*, 778.

(45) Hesselmann, A.; Jansen, G.; Schutz, M. *J. Chem. Phys.* **2005**, *122*, 014103.

(46) Della Sala, F.; Gorling, A. *J. Chem. Phys.* **2001**, *115*, 5718.

(47) Gruning, M.; Gritsenko, O. V.; van Gisbergen, S. J. A.; Baerends, E. J. *J. Chem. Phys.* **2001**, *114*, 652.

(48) Adamo, C.; Barone, V. *J. Chem. Phys.* **1999**, *110*, 6158.

(49) Perdew, J. P.; Burke, K.; Ernzerhof, M. *Phys. Rev. Lett.* **1997**, *78*, 1396.

(50) Blochl, P. E. *Phys. Rev. B* **1994**, *50*, 17953.

(51) Kresse, G.; Joubert, D. *Phys. Rev. B* **1999**, *59*, 1758.

(52) Jorgensen, W. L.; Tirado-Rives, J. *Proc. Natl. Acad. Sci. U.S.A.* **2005**, *102*, 6665.

(53) Caleman, C.; van Maaren, P. J.; Hong, M. Y.; Hub, J. S.; Costa, L. T.; van der Spoel, D. *J. Chem. Theory Comput.* **2012**, *8*, 61.

(54) van der Spoel, D.; van Maaren, P. J.; Caleman, C. *Bioinformatics* **2012**, *28*, 752.

(55) Cheng, A.; Steele, W. A. *J. Chem. Phys.* **1990**, *92*, 3858.

(56) Riley, K. E.; Pitonak, M.; Jurecka, P.; Hobza, P. *Chem. Rev.* **2010**, *110*, 5023.

(57) DiStasio, R. A.; von Lilienfeld, O. A.; Tkatchenko, A. *Proc. Natl. Acad. Sci. U.S.A.* **2012**, *109*, 14791.

(58) Granatier, J.; Lazar, P.; Otyepka, M.; Hobza, P. *J. Chem. Theory Comput.* **2011**, *7*, 3743.

(59) Granatier, J.; Lazar, P.; Prucek, R.; Safarova, K.; Zboril, R.; Otyepka, M.; Hobza, P. *J. Phys. Chem. C* **2012**, *116*, 14151.

(60) Zgarbova, M.; Otyepka, M.; Sponer, J.; Hobza, P.; Jurecka, P. *Phys. Chem. Chem. Phys.* **2010**, *12*, 10476.

Choosing a Density Functional for Modeling Adsorptive Hydrogen Storage: Reference Coupled Cluster and Diffusion Quantum Monte Carlo Calculations, and a Comparison of Dispersion-Corrected Density Functionals

Mikuláš Kocman[1], Petr Jurečka[1,*], Matůš Dubecký[1], Michal Otyepka[1], Yeonchoo Cho[2], Kwang S. Kim[3]

[1] Regional Centre of Advanced Technologies and Materials, Department of Physical Chemistry, Faculty of Science, Palacky University, 17. listopadu 12, 77146 Olomouc, Czech Republic
[2] Center for Superfunctional Materials, Department of Chemistry and Department of Physics, Pohang University of Science and Technology, Hyojadong, Namgu, Pohang 790-784, Korea
[3] Center for Superfunctional Materials, Department of Chemistry, Ulsan National Institute of Science and Technology (UNIST),UNIST-gil 50, Ulsan 689-798, Korea

E-mail: petr.jurecka@upol.cz

Abstract

Hydrogen storage in carbonaceous materials and their derivatives is currently a widely investigated topic. Rational design of novel adsorptive materials is often attempted with the help of computational chemistry tools, in particular density functional theory (DFT). However, different exchange-correlation functionals provide a very wide range of hydrogen binding energies. The aim of this article is to offer high level QM reference data based on coupled-clusters singles and doubles calculations with perturbative triple excitations, CCSD(T), and a complete basis set limit estimate that can be used to assess the accuracy of various DFT-based predictions. Reference binding curves are calculated for two model compounds representing weak and strong hydrogen adsorption: coronene (-4.7 kJ/mol per H_2), and coronene modified with boron and lithium (-14.3 kJ/mol). The reference data are compared to results obtained with widely used density functionals including pure DFT, M06, DFT-D3, PBE-TS, optB88-vdW, vdW-DF and vdW-DF2. Dispersion correction, either empirical or density-based, improves description in both types of complexes. However, density-based dispersion schemes such as vdW-DF2, PBE-TS or optB88-vdW provide more accurate results for the more strongly bound coronene/boron/lithium…hydrogen complex, which is probably a better model for prospective high-capacity graphene based sorbents. Our results may serve as a guide for choosing suitable DFT methods for quickly evaluating hydrogen binding potential and as a reference for assessing the accuracy of the previously published DFT results.

1. Introduction

Recent progress in graphene-related nanotechnologies has fuelled interest in graphene-based sorption materials. One potential application of graphene nanostructures is in hydrogen storage devices. To be practical, these devices should match or exceed the target gravimetric capacity specified by the U.S. Department of Energy (DOE). In addition, they should adsorb molecular hydrogen reversibly. In the case of physisorption, the adsorption energy of molecular hydrogen should ideally be around 15 kJ/mol per H_2 in order to achieve the target capacity while still being weak enough to allow hydrogen release under relatively mild conditions.[1] Since the interaction energy of molecular hydrogen with a pristine graphene surface is only about 4 kJ/mol, several modifications of graphene have been proposed to

increase the strength of this interaction.[2–8] While graphene surfaces can be doped with many elements, light elements such as boron, lithium, calcium or magnesium must be used to achieve the required gravimetric capacity.

In addition to experimental studies, there have been many attempts to use computational methods to design novel materials for hydrogen storage.[5–12] Typically, such studies use quantum mechanical (QM) methods to predict the geometries and properties of carbonaceous structures that incorporate light elements in order to enhance their interactions with molecular hydrogen.[5–9,11,12] A crucial quantity when designing graphene based sorption materials is the interaction energy, which can be related to the adsorption capacity of the studied material. Interaction energies are readily calculated using a wide variety of quantum chemical methods at various levels of accuracy and reliability.

The most popular tool for preliminary evaluation of hydrogen adsorption energy is density functional theory (DFT). This method is widely used due to its modest computational demands and ability to simulate reasonably large periodic structures. Unfortunately, the applicability of most current DFT functionals is limited by their inability to describe London dispersion forces. Because dispersion (long-range correlation) is an important part of the noncovalent binding energy to graphene-like materials, the reliability of results obtained with such DFT methods is often questionable. Note, however, that studies focusing on hydrogen chemisorption[13,14] are less sensitive to the quality of modeling of vdW interactions.

Considerable effort has been invested in the development of DFT methods that can describe dispersion interactions in recent years and many different solutions have been suggested.[15–27] Dispersion can be included either in the form of a pairwise empirical correction,[15–17] or with reduced empiricism at various levels of accuracy and computer demands.[18–23] For instance, an empirical DFT/CC scheme[24] described the interactions between molecular hydrogen and carbon nanostructures very accurately.[25] Unfortunately, the availability of dispersion-corrected DFT schemes in current software tools is still limited and so they are rarely used (for an example, see ref [26]). Moreover, the accuracy of many of these schemes is not well tested or understood. Therefore, it would be desirable to have a suitable benchmark for adsorptive hydrogen binding that would enable us to meaningfully compare different methods.

Accurate wave function theory QM methods can provide robust and reliable estimates of noncovalent binding. However, very high levels of theory and considerable computer resources are needed to accurately describe weak dispersion interactions. Note that the popular and relatively affordable MP2 method is known to overestimate the dispersion contribution to the interaction energy[28] and thus is not suitable for benchmark calculations. Very accurate results can be obtained with the CCSD(T) method,[29] but only when large atomic basis sets are employed.[30] This makes calculations extremely demanding owing to the steep scaling of CCSD(T) demands ($\approx O(N^7)$). One viable compromise is to estimate the CCSD(T) result at the complete basis set (CBS) limit by combining MP2/CBS extrapolation with corrections for higher-order correlation effects calculated using a smaller basis set,[31] and also other possibilities exist.[30] However, studies of this type are limited to relatively small model systems, typically polyaromatic molecules, and are not suitable for production calculations.

Quantum Monte Carlo (QMC) calculations provide an alternative and largely independent source of theoretical reference data on interaction energies. The well-established diffusion Monte Carlo method with fixed node approximation[32,33] (FN-DMC) covers essentially all dynamic correlations and is thus (in this particular respect) equivalent to a full configuration interaction calculation using a complete basis set. FN-DMC calculations have successfully been used to study the interactions of atomic hydrogen (both chemi- and physisorption) with coronene and graphene.[34] While FN-DMC calculations are extremely time-consuming when

very high accuracy (below 1 kJ/mol) is required,[35] they can provide invaluable help in situations where the accuracy of wave function based methods is not well established.

In this work we calculated reference dissociation curves for the physisorption of molecular hydrogen on two different model compounds, coronene and coronene modified with boron and lithium (coroB_2Li_2, Figure 1). Whereas coronene exhibits the weak hydrogen adsorption typical of unmodified carbonaceous materials, the coroneneB_2Li_2 molecule exhibits much stronger molecular hydrogen binding characteristic of modified sorption materials. Reference interaction energies were obtained using the high-level CCSD(T)/CBS method and FN-DMC calculations were performed to verify the wave function results for one complex. These reference results were then used to evaluate the performance of several standard DFT functionals along with some more recently developed DFT-based methods that include dispersion corrections.

2. Methods

Structures. All structures were optimized using the TPSS functional augmented with an empirical dispersion term using the B-0.93-35 parameters[17] and the cc-pVQZ basis set. During this optimization, the distance between the hydrogen atoms of molecular hydrogen was held at its CCSD(T)/AVQZ-optimized value (0.742Å).[25] Symmetric structures with two H_2 molecules placed above and below the coronene base (Figure 1) were used to reduce the demands of the time-consuming CCSD(T) calculations by exploiting symmetry (the accuracy of this approximation is discussed below). Starting from the resulting optimized structures, geometries for a distance-dependent scan were generated by varying only the intermolecular separation between the sorbent and hydrogen molecules (2.5, 2.8, 3.1, 3.4, 3.7, 4.0, 5.0 and 7.0 Å). Interaction energies were calculated as the difference in energy between the complex and the isolated coronene as one subsystem and two isolated hydrogen molecules as the second. The interaction per H_2 molecule was then calculated as half of this interaction energy. The error due to the presence of the second H_2 molecule was found to be smaller than 0.05 kJ/mol at the MP2/CBS level.

Figure 1. Model systems: coronene…$2H_2$ and coroB_2Li_2…$2H_2$.

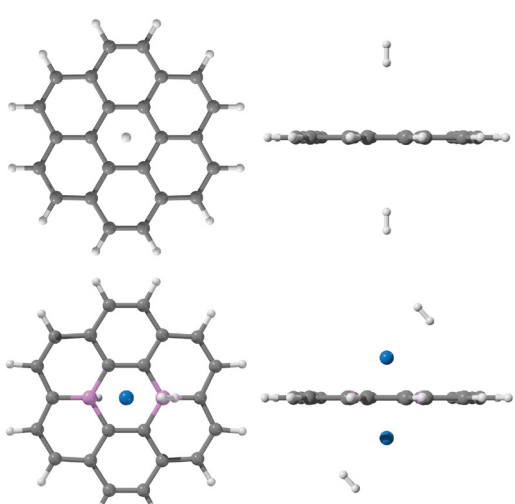

Reference CCSD(T)/CBS Calculations. Reference QM interaction energies were calculated according to Eq. 1.

$$\Delta E_{\mathrm{CBS}}^{\mathrm{CCSD(T)}} = \Delta E_{\mathrm{CBS}}^{\mathrm{MP2}} + (\Delta E^{\mathrm{CCSD(T)}} - \Delta E^{\mathrm{MP2}})|_{\mathrm{small\ basis}} \qquad \text{Eq. 1}$$

The MP2 energy at the complete basis set (CBS) limit ($\Delta E_{\mathrm{CBS}}^{\mathrm{MP2}}$) was obtained using the 2-point extrapolation scheme of Halkier and Helgaker, in which HF and correlation energies are extrapolated separately.[36,37] The correction for higher order correlation effects was calculated as the difference between the CCSD(T) and MP2 energies obtained using a smaller basis set. The use of a smaller basis set is justified by the weak basis set dependence of this contribution.[38] The CCSD(T)/CBS evaluation is described in more detail elsewhere.[31] For the MP2 calculations, the hydrogen molecules and the inner ring atoms of coronene (6 carbon atoms) and coroB_2Li_2 (4 carbon, 2 boron, and 2 lithium atoms) were described using the aug-cc-pVXZ basis sets (X=T,Q), while the remaining carbon and hydrogen atoms were described using the cc-pVXZ (X=T,Q) basis sets. In the CCSD(T) calculations, we used the QZVPP basis set for the H_2 molecules, the TZVPP basis set for the inner ring atoms of coronene and coroB_2Li_2, and the TZVP basis set for the remaining atoms. Counterpoise correction was used in all calculations. CCSD(T) and MP2 calculations were performed using the TurboMole 6.3 software package.[39,40]

Reference Quantum Monte Carlo Calculations. Benchmark diffusion quantum Monte Carlo ground-state projection calculations[35] for the coronene…$2H_2$ complex were performed using the single-determinant Slater-Jastrow trial wave functions, which are known to provide an optimal cost/accuracy tradeoff (cf. e.g. ref [41]). B3LYP orbitals obtained with the aug-cc-pVTZ basis set were used and the core electrons were replaced by the appropriate effective core potentials.[42] The explicit correlation Jastrow functions with electron-nucleus (e-n) and electron-electron (e-e) terms were exhaustively variationally optimized for the complex and its constituents, respectively. The employed protocol exhibits favorable scaling, $\propto O(N^3)$ where N is the number of electrons, and relies on fixed-node error cancellation.[35] It is known to be suitable for benchmark calculations of noncovalent interaction energies in large closed-shell complexes.[43] The statistical error is reported as ± the standard deviation (σ).

SAPT Decomposition of Interaction Energies. The components of the interaction energy between the sorbent and H_2 molecules were determined by the DFT-SAPT method of Hesselmann and Jansen[44–47] as implemented in the Molpro software package.[48] In DFT-SAPT, the monomer is described using density functional theory (DFT) and the intermolecular interactions by SAPT (Symmetry Adapted Perturbation Theory).[49] The total interaction energy is then given by the sum of the following terms (Eq. 2)

$$E^{SAPT} = E_{elst}^{(1)} + E_{exch}^{(1)} + E_{ind}^{(2)} + E_{exch-ind}^{(2)} + E_{disp}^{(2)} + E_{exch-disp}^{(2)} + \delta(HF), \qquad \text{(Eq. 2)}$$

where $E_{elst}^{(1)}$ is the electrostatic contribution, $E_{exch}^{(1)}$ is the exchange repulsion contribution, $E_{ind}^{(2)}$ is the induction or polarization contribution, $E_{disp}^{(2)}$ is the dispersion contribution, and $E_{exch\text{-}ind}^{(2)}$ and $E_{exch\text{-}disp}^{(2)}$ are exchange-induction and exchange-dispersion mixing terms. The δ(HF) term approximates higher order induction contributions. Here, these contributions are conveniently contracted into four terms: $E_{elst} = E_{elst}^{(1)}$, $E_{exch} = E_{exch}^{(1)}$, $E_{ind} = E_{ind}^{(2)} + E_{exch\text{-}ind}^{(2)} + \delta(HF)$ and $E_{disp} = E_{disp}^{(2)} + E_{exch\text{-}disp}^{(2)}$. All DFT-SAPT calculations were done using the cc-pVTZ basis set and PBE0AC density functional[45,50,51] with the asymptotically correct LB94 xc-potential of van Leeuwen and Baerends[52] and a gradient-controlled shift procedure.[53]

DFT calculations. Some of the most commonly used density functionals were evaluated: the LDA SVWN functional,[54,55] the GGA functionals BLYP,[56,57] PBE,[50] B97-D[58] and PW91,[59] the hybrid functionals B3LYP[60] and PBE0,[51] and the meta-GGA functionals TPSS[61] and M06.[62] All DFT calculations were performed using the def2-QZVP basis set and some were also performed using the def2-TZVP basis set for comparative purposes.

Calculations using Grimme's empirical dispersion correction (DFT-D3) were performed with the basis set recommended by the authors (def2-QZVP) in conjunction with Johnson and Becke damping,[20,63,64] both with and without damped Axilrod-Teller-Muto based three-body terms.[16] Counterpoise correction was not applied.

Calculations with the Tkatchenko-Scheffler[21] dispersion correction and PBE functional (PBE-TS) were performed using the FHI-aims code[65] with a tier 2 basis set and a tight grid. The VASP code[66] was used to calculate vdW-DF,[18] vdW-DF2[67] and optB88-vdW[68] interaction energies in a 20x20x25 Å rectangular box with a 500 Ry cutoff.

3. Results and Discussion

Nature of Binding in Model Complexes. Knowing the nature of hydrogen's interactions with different types of sorbents may help us to understand the performance of various density functional based methods. It has been shown that dispersion interactions dominate the binding of both polar and non-polar solvent molecules to coronene,[69,70] and may also be important in hydrogen storage materials.[71] Because H_2 is a nonpolar molecule we would expect dispersion forces to similarly dominate the stabilizing interaction in the coronene…$2H_2$ complex. However, in the coroB_2Li_2 complex hydrogen binds to positively charged lithium atoms. As such, the polarization contribution may also be important in this case. To assess the relative importance of these stabilizing contributions in our two model complexes, we decomposed the total interaction energy into physically meaningful contributions using the DFT-SAPT method. The interaction energy can be decomposed into four basic components: electrostatic, induction (or polarization), dispersion and repulsion.

Table 1 shows that dispersion is, as expected, by far the most important contribution in the coronene…$2H_2$ complex, accounting for about 75% of its total stabilization. The second largest contribution (18%) is from electrostatic stabilization. This comes in part from the overlap (penetration) effect and in part from the interaction of coronene's molecular quadrupole with that of the H_2 molecule. Note that while the quadrupolar component is important for small model compounds such as benzene or coronene, it will be close to zero for infinite planar graphene sheets due to the cancellation of the quadrupolar field in this case. For this reason the coronene molecule may not be a fully representative model for interactions with infinite graphene. However, it should also be noted that quadrupolar interactions may become sizeable even in graphene, either on the edges of finite graphene flakes or when the graphene is corrugated as is often the case.[72]

The situation with the coroB_2Li_2 complex is different. While the dispersion contribution is still quite large in this case, the polarization and electrostatic contributions are equally important; their combined stabilizing contribution is about twice that of dispersion. Because of its additional induction and electrostatic stabilization, this complex is much more stable than coronene…$2H_2$.

Table 1. Components of the interaction energy (kJ/mol per H_2) in model complexes obtained using SAPT decomposition at the equilibrium geometry.

Complex	$E_{Exch\text{-}rep}$	E_{Elst}	E_{Ind}	E_{Disp}	E_{Tot}
coronene…$2H_2$	6.5	-1.8	-0.8	-7.4	-3.5
coroB_2Li_2…$2H_2$	22.0	-13.0	-12.1	-10.9	-14.0

The calculations described above show that the nature of hydrogen binding in nonpolar and polar complexes is very different. This should be reflected in the performance of DFT functionals for the two binding situations. As we show below, DFT methods without explicit dispersion correction perform poorly for the dispersion-dominated coronene complex but their results for the dispersion/induction-stabilized coroB_2Li_2 complex are in much better (albeit imperfect) agreement with reference calculations.

Reference CCSD(T)/CBS and FN-DMC calculations. The reference dissociation curves obtained at the CCSD(T)/CBS level are shown in Figure 2. For the coronene…$2H_2$ complex, our calculations predict an interaction energy of -4.68 kJ/mol per H_2 molecule. This result is comparable to other CCSD(T)/CBS estimates that have been published for smaller model systems. As expected, the calculated binding energy for coronene is greater than that reported for benzene (-4.34 kJ/mol) or naphthalene (-4.42 kJ/mol).[25] Our reference value is also in relatively good agreement with the partly empirical DFT/CC estimate for coronene obtained by the same authors (-4.94 kJ/mol), particularly given that the DFT/CC potential was found to overestimate the interaction energy of hydrogen with graphene by 0.2 kJ/mol.[73]

The reliability of the CCSD(T)/CBS estimate was confirmed by a single point DMC calculation on the coronene…$2H_2$ complex at the equilibrium separation (3.1 Å). The DMC run provided an interaction energy of -4.31 ± 0.7 kJ/mol, in good agreement with the wave function result. Note that the CCSD(T)/CBS and DMC methods are quite different in nature but are both regarded as benchmark-quality approaches. As such, this good agreement gives us confidence in the accuracy of our result.

Comparison of our theoretical estimates with experimental data is less straightforward. First, experimental data are available only for the interaction of molecular hydrogen with graphite (-51.7 ± 0.5 meV, or -4.99 ± 0.05 kJ/mol);[74] its interaction with graphene is expected to be around 9 % weaker.[75] Second, the interaction of H_2 with graphene is expected to be somewhat stronger than with our model molecule, coronene; the difference between the two is estimated to be -0.5 kJ/mol based on DFT/CC calculations.[25] With these two corrections accounted for we obtain a value of -4.7 kJ/mol, which is in good agreement with the above experimental value.

Reference interaction curves for the more polar coroB_2Li_2…$2H_2$ complex are also shown in Figure 2. The accuracy of these results should be similar to those for the complex of coronene with molecular hydrogen. The estimated interaction energy is -14.25 kJ/mol per H_2 molecule. Note that this large interaction energy is close to the optimal value suggested by Bhathia et al.[1] (15 kJ/mol), so the coroB_2Li_2…$2H_2$ complex should be a good model system for studying adsorptive hydrogen storage.

Pure DFT Functionals. Let us start with the dispersion-bound complex of molecular hydrogen with coronene. Given the importance of dispersion in this complex, it can be expected that the widely used LDA, GGA, meta-GGA and hybrid density functionals will not describe it correctly. Indeed, as shown in Figure 2 all GGA based functionals with the def2-QZVP atomic basis set either predict that hydrogen does not bind (BLYP, B3LYP) or underestimate its binding to varying extents, depending on the level of error cancellation in

their exchange-correlation parts. Similar results were obtained with the smaller def2-TZVP basis set (not shown). In addition, the equilibrium binding distances predicted by these functionals are too long. The M06 meta-GGA functional developed by Truhlar's group yields the best agreement with the reference curve and also predicts the right intermolecular distance. However, even M06 underestimates binding quite significantly, by more than 50%. Thus, none of the pure (dispersion uncorrected) functionals can be recommended for the investigation of weak H_2 binding to nonpolar carbonaceous sorbents.

The SVWN LDA functional is also unsuitable for describing hydrogen adsorption on nonpolar adsorbents. According to Figure 2, it overestimates the binding energy in the coronene…$2H_2$ complex by about 50% and also predicts too short an equilibrium distance. Strong overestimation of binding by SVWN has been reported previously, and its source has been traced to the erroneous exchange functional.[76] Therefore, predicted sorption energies on novel materials obtained with this functional will probably be unrealistically large.

Figure 2. DFT/def2-QZVP interaction energies compared to CCSD(T)/CBS reference data for the coronene…$2H_2$ (top) and coroB_2Li_2…$2H_2$ (bottom) complexes. Interaction energies are given per one H_2 molecule.

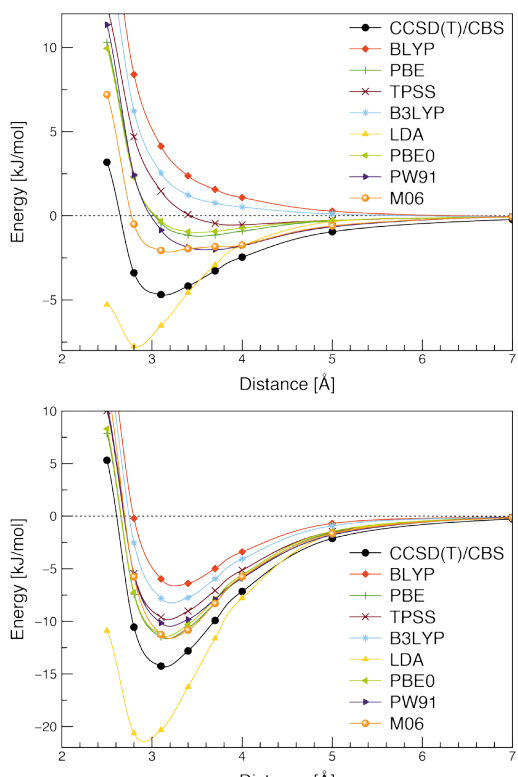

Next, we compare the performance of different functionals for the coroB_2Li_2…$2H_2$ complex, in which molecular hydrogen is bound much more strongly than in the coronene complex (-14.3 kJ/mol vs. -4.7 kJ/mol). As shown above, this is largely due to additional stabilization arising from electrostatics and polarization. Because standard DFT functionals describe polarization-bound complexes relatively well (although some error cancellation is

involved),[77] we would expect them to perform comparatively well for this complex. Indeed, Figure 2 shows that in this case all tested functionals predict bonding and none of them is purely repulsive. The best agreement is achieved with the M06, PBE and PBE0 functionals, which underestimate the interaction energy by about 20% relative to the reference CCSD(T)/CBS data and predict the correct intermolecular separation. The PW91 and TPSS functionals also predict relatively accurate binding distances but substantially underestimate the interaction energy. The other functionals predict only weak binding, giving less than half of the reference interaction energy. As before, the SVWN functional strongly overestimates the interaction energy.

These results clearly show that none of the tested DFT functionals is capable of accurately describing hydrogen physisorption in both dispersion and polarization binding scenarios. The best results are obtained with M06, but even this functional substantially underestimates the strength of binding in both complexes. The other DFT functionals, which have often been used to estimate adsorption strength in the literature, predict excessively weak binding. The only exception is SVWN, which strongly overestimates the interaction energy. Thus, none of the standard and widely used DFT functionals can be used to accurately estimate hydrogen adsorption on carbonaceous materials.

Functionals with Empirical Dispersion Correction. The DFT-D3 method developed by Grimme was tested because it is a very widely available empirical dispersion scheme and can be combined with various commonly used DFT functionals. The B97-D functional was also evaluated. Figure 3 shows the results obtained with the density functionals for which the optimized D3 correction was available. The LDA approximation was not considered because it overbinds both complexes and further dispersion stabilization would only worsen the results. As expected, the dispersion correction improved the overall accuracy of the DFT predictions for both the dispersion-bound and the dispersion/polarization-bound complex. All functionals predicted equilibrium geometries very close to the CCSD(T)/CBS reference. In the case of the nonpolar coronene…$2H_2$ complex, the PBE-D3, PBE0-D3 and B97-D functionals overestimated the interaction energy by up to 20% (with B97-D), whereas BLYP-D3 and B3LYP-D3 provided remarkably accurate results. Interestingly, all of the tested functionals gave very similar results for the polar coroB_2Li_2…$2H_2$ complex, overestimating the interaction energy by about 17%. Thus, although the empirical correction provided clear improvements, none of the tested combinations accurately described the more complicated binding situation in the dispersion/induction complex, so the adsorption capacities obtained with these methods for more polar sorption materials will probably be somewhat overestimated. Overall, the best results were obtained using the BLYP+D and B3LYP+D combinations with Becke-Johnson damping.

Figure 3. DFT-D3/def2-QZVP interaction energies compared to CCSD(T)/CBS reference data for the coronene…$2H_2$ (top) and coroB_2Li_2…$2H_2$ (bottom) complexes. Interaction energies are given per one H_2 molecule.

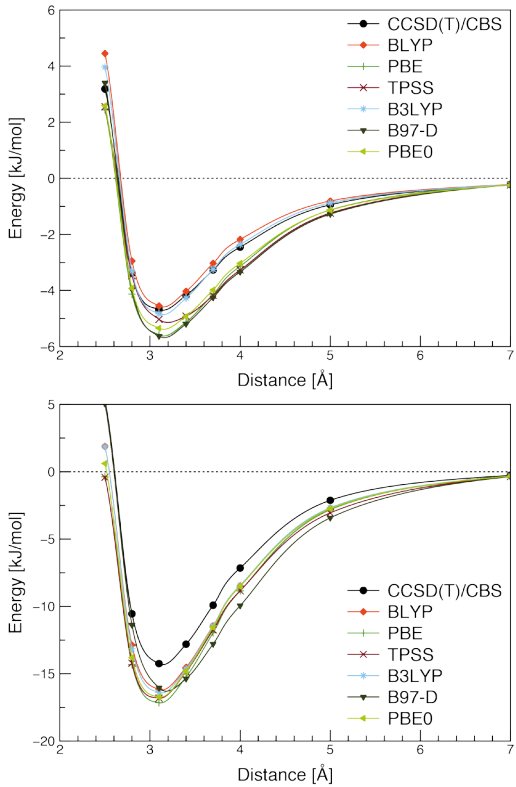

Importance of the Three-Body Dispersion Term. Optionally, DFT-D3 calculations can be performed using an empirical correction for three-body dispersion based on the Axilrod-Teller-Muto formula (see above). Interaction energy curves for selected DFT-D3 combinations are shown in Figure S1. Inclusion of the three-body terms slightly weakens the predicted interaction regardless of the DFT-D3 functional used. Thus, three body terms somewhat improved the agreement between the DFT-D3 functionals and the reference calculations when the DFT-D3 calculations were too attractive and vice versa. However, this effect was very modest, amounting to around 0.2 kJ/mol on average. It therefore seems that it is not essential to include the three-body dispersion correction and that it is more important to select a good combination of DFT functional and two-body D3 correction.

Functionals with Density-Based Dispersion Correction. Several density functionals in which the dispersion correction is at least partially derived from the DFT electron density are now available in widely used quantum chemistry packages. Here we tested the vdW-DF functional of Dion et al.,[18] its newer version vdW-DF2,[67] a reparameterization of vdW-DF developed by Klimes et al.[68] (optB88-vdW), and the PBE+TS functional of Tkatchenko and Scheffler.[21] Results obtained for both complexes with these functionals are shown in Figure 4.

All four of these density functionals overestimated the binding energy in the nonpolar coronene…$2H_2$ complex. The largest discrepancy was seen for vdW-DF, which predicted an interaction energy (-6.6 kJ/mol) that is 40% greater than the CCSD(T)/CBS reference value of -4.7 kJ/mol. This functional also overestimated the equilibrium separation by about 30%. The more recent dispersion-corrected density functionals performed better and all yielded quite

similar results. Their estimated interaction energies (and, in parentheses, the extent to which they exceeded the reference value) were: vdW-DF2 -5.5 kJ/mol (15%), optB88+vdW -5.9 kJ/mol (26%) and PBE+TS -6.0 kJ/mol (28%). This represents a significant improvement compared to pure DFT functionals. The density-based dispersion functionals also overestimated the interaction energy in the more polar coroB_2Li_2 …$2H_2$ complex. However, while the absolute overestimation is comparable to that for the nonpolar coronene…$2H_2$ complex, the relative overestimation is much smaller. Interestingly, the vdW-DF functional gave the most accurate result for the coroB_2Li_2 …$2H_2$ complex despite being the least accurate density-based functional for the nonpolar complex. The greatest overestimation for the polar complex was observed with PBE+TS (-1.5 kJ/mol, 10%). All four functionals predicted the correct equilibrium separation.

While the tested density-based dispersion functionals are less accurate than the best DFT-D3 combinations for the weakly bound coronene…$2H_2$, they better describe the stronger binding in the more polar coroB_2Li_2 …$2H_2$ complex. Because the latter is probably a better model for high-capacity hydrogen storage materials, the recent functionals with density-based dispersion corrections may be good choices for modeling such substances. It should be noted that these methods are less empirical and therefore potentially more robust towards unusual binding situations that deviate strongly from those considered when creating empirical parameterizations such as DFT-D3.

Figure 4. PBE+TS, vdW-DF, vdW-DF2 and optB88-vdW interaction energies compared to CCSD(T)/CBS reference data for the coronene…$2H_2$ (top) and coroB_2Li_2…$2H_2$ (bottom) complexes. Interaction energies are given per one H_2 molecule.

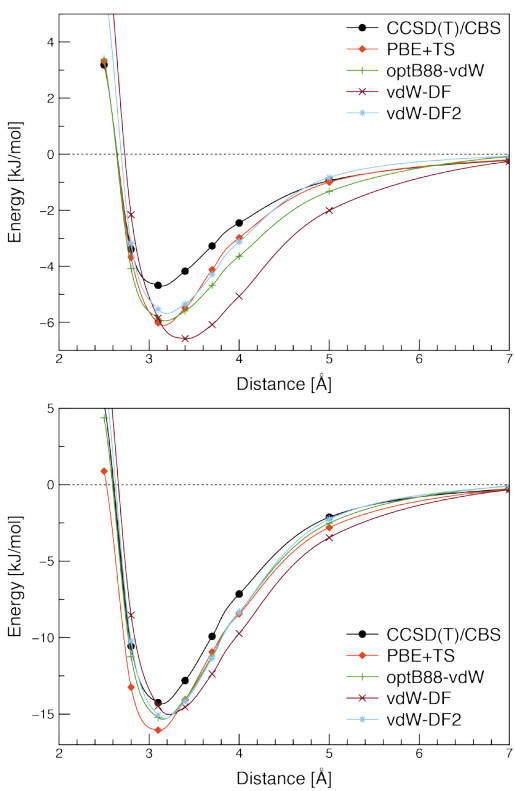

4. Conclusions

The accuracy of various DFT based approaches for estimating the adsorption energies of molecular hydrogen to two model compounds was assessed by comparison to high-level wave function theory and Diffusion Quantum Monte Carlo reference calculations. Two binding scenarios were considered: weak dispersion-dominated binding to a coronene molecule and strong polarization-dominated binding to a coroB_2Li_2 molecule.

In the weak binding case, the common GGA, meta-GGA and hybrid functionals significantly underestimate the interaction energy and cannot be recommended for quantitative estimates. It is important to emphasize that the frequently used pure LDA functional strongly overbinds hydrogen and predicts excessively short intermolecular separations in both types of complexes. As such, its use is generally not recommended. Predictions based on LDA calculations would result in unrealistically favorable binding of molecular hydrogen. Various types of dispersion corrections to DFT, whether empirical or non-empirical, generally improve the predicted binding energies and geometries, and several schemes provide very accurate results. In particular, the BLYP-D3 and B3LYP-D3 results with Becke-Johnson damping were quite close to the CCSD(T)/CBS reference values. Among the tested non-empirical dispersion correction schemes, the vdW-DF2, TS+PBE and optB88+vdW performed best and provide significantly better results than pure DFT functionals. Nevertheless, they somewhat overestimate the binding energy and their overall accuracy was lower than that of the best empirical DFT-D3 combinations.

The more polar coroB_2Li_2…$2H_2$ complex is probably a better model for potential high capacity graphene-based sorbent materials. In this case, the DFT functionals without dispersion correction underestimate binding, although to a lesser extent than for the coronene…$2H_2$ complex. The best functionals in this case are M06, PBE and PBE0, which underestimate the binding strength by less than 20 %. The inclusion of dispersion corrections also increases the overall accuracy of the predictions for this more polar complex. The most accurate dispersion-corrected functionals were the density-based vdW-DF2 and optB88+vdW. The empirical BLYP-D3 and B3LYP-D3 functionals also provided acceptable results, although they overestimate the interaction energies by an appreciable margin.

Our results may serve as a guide for choosing a suitable DFT method for quickly predicting the strength of hydrogen binding in new materials and as a reference for assessing the accuracy of previously published DFT results.

Acknowledgements. This work was supported by grant P208/12/G016 from the Grant Agency of the Czech Republic (P.J., M.O.), by the Operational Program Research and Development for Innovations of the European Regional Development Fund (CZ.1.05/2.1.00/03.0058) and project No. CZ.1.07/2.3.00/20.0058, administered by the Ministry of Education, Youth and Sports of the Czech Republic. Further funding was provided by NRF (National Honor Scientist Program: 2010-0020414).

References

1. S. K. Bhatia and A. L. Myers, *Langmuir*, 2006, **22**, 1688–1700.

2. K. C. Kemp, H. Seema, M. Saleh, N. H. Le, K. Mahesh, V. Chandra, and K. S. Kim, *Nanoscale*, 2013, **5**, 3149–3171.

3. H. M. Lee, D. Y. Kim, C. Pak, N. J. Singh, and K. S. Kim, *J. Chem. Theory Comput.*, 2011, **7**, 969–978.

4. V. Georgakilas, M. Otyepka, A. B. Bourlinos, V. Chandra, N. Kim, K. C. Kemp, P. Hobza, R. Zboril, and K. S. Kim, *Chem. Rev.*, 2012, **112**, 6156–6214.

5. Y.-H. Kim, Y. Zhao, A. Williamson, M. Heben, and S. Zhang, *Phys. Rev. Lett.*, 2006, **96**, 016102.

6. A. Du, Z. Zhu, and S. C. Smith, *J. Am. Chem. Soc.*, 2010, **132**, 2876–2877.

7. W.-Q. Deng, X. Xu, and W. Goddard, *Phys. Rev. Lett.*, 2004, **92**, 166103.

8. B. Kuchta, L. Firlej, S. Roszak, and P. Pfeifer, *Adsorption*, 2010, **16**, 413–421.

9. L. Firlej, S. Roszak, B. Kuchta, P. Pfeifer, and C. Wexler, *J. Chem. Phys.*, 2009, **131**, 164702.

10. S. Patchkovskii, J. S. Tse, S. N. Yurchenko, L. Zhechkov, T. Heine, and G. Seifert, *Proc. Natl. Acad. Sci. U. S. A.*, 2005, **102**, 10439–10444.

11. H. Lee, J. Ihm, M. L. Cohen, and S. G. Louie, *Nano Lett.*, 2010, **10**, 793–798.

12. I. Cabria, M. J. López, and J. A. Alonso, *J. Chem. Phys.*, 2005, **123**, 204721.

13. M. Bonfanti, R. Martinazzo, G. F. Tantardini, and A. Ponti, *J. Phys. Chem. C*, 2007, **111**, 5825–5829.

14. G. M. Psofogiannakis, T. a Steriotis, A. B. Bourlinos, E. P. Kouvelos, G. C. Charalambopoulou, A. K. Stubos, and G. E. Froudakis, *Nanoscale*, 2011, **3**, 933–936.

15. S. Grimme, *J. Comput. Chem.*, 2004, **25**, 1463–1473.

16. S. Grimme, J. Antony, S. Ehrlich, and H. Krieg, *J. Chem. Phys.*, 2010, **132**, 154104.

17. P. Jurecka, J. Cerný, P. Hobza, and D. R. Salahub, *J. Comput. Chem.*, 2007, **28**, 555–569.

18. M. Dion, H. Rydberg, E. Schröder, D. C. Langreth, and B. I. Lundqvist, *Phys. Rev. Lett.*, 2004, **92**, 246401.

19. A. D. Becke and E. R. Johnson, *J. Chem. Phys.*, 2007, **127**, 154108.

20. E. R. Johnson and A. D. Becke, *J. Chem. Phys.*, 2005, **123**, 24101.

21. A. Tkatchenko and M. Scheffler, *Phys. Rev. Lett.*, 2009, **102**, 073005.

22. S. N. Steinmann and C. Corminboeuf, *J. Chem. Theory Comput.*, 2010, **6**, 1990–2001.

23. A. Tkatchenko, D. Alfè, and K. S. Kim, *J. Chem. Theory Comput.*, 2012, **8**, 4317–4322.

24. O. Bludský, M. Rubes, P. Soldán, and P. Nachtigall, *J. Chem. Phys.*, 2008, **128**, 114102.

25. M. Rubes and O. Bludský, *Chemphyschem*, 2009, **10**, 1868–1873.

26. R. M. Ferullo, N. F. Domancich, and N. J. Castellani, *Chem. Phys. Lett.*, 2010, **500**, 283–286.

27. F. Tran, J. Weber, T. a. Wesołowski, F. Cheikh, Y. Ellinger, and F. Pauzat, *J. Phys. Chem. B*, 2002, **106**, 8689–8696.

28. O. Hübner, A. Glöss, M. Fichtner, and W. Klopper, *J. Phys. Chem. A*, 2004, **108**, 3019–3023.

29. R. J. Bartlett, J. D. Watts, S. A. Kucharski, and J. Noga, *Chem. Phys. Lett.*, 1990, **165**, 513–522.

30. K. E. Riley, M. Pitonák, P. Jurecka, and P. Hobza, *Chem. Rev.*, 2010, **110**, 5023–5063.

31. P. Jurecka and P. Hobza, *J. Am. Chem. Soc.*, 2003, **125**, 15608–15613.

32. W. Foulkes, L. Mitas, R. Needs, and G. Rajagopal, *Rev. Mod. Phys.*, 2001, **73**, 33–83.

33. B. M. Austin, D. Y. Zubarev, and W. A. Lester, *Chem. Rev.*, 2012, **112**, 263–288.

34. J. Ma, A. Michaelides, and D. Alfè, *J. Chem. Phys.*, 2011, **134**, 134701.

35. M. Dubecký, P. Jurečka, R. Derian, P. Hobza, M. Otyepka, and L. Mitas, *J. Chem. Theory Comput.*, 2013, **9**, 4287–4292.

36. A. Halkier, T. Helgaker, P. Jørgensen, W. Klopper, and J. Olsen, *Chem. Phys. Lett.*, 1999, **302**, 437–446.

37. A. Halkier, T. Helgaker, P. Jørgensen, W. Klopper, H. Koch, J. Olsen, and A. K. Wilson, *Chem. Phys. Lett.*, 1998, **286**, 243–252.

38. P. Jurečka and P. Hobza, *Chem. Phys. Lett.*, 2002, **365**, 89–94.

39.

40. R. Ahlrichs, M. Bär, M. Häser, H. Horn, and C. Kölmel, *Chem. Phys. Lett.*, 1989, **162**, 165–169.

41. L. Horváthová, M. Dubecký, L. Mitas, and I. Štich, *Phys. Rev. Lett.*, 2012, **109**, 053001.

42. M. Burkatzki, C. Filippi, and M. Dolg, *J. Chem. Phys.*, 2007, **126**, 234105.

43. J. Řezáč and P. Hobza, *J. Chem. Theory Comput.*, 2013, **9**, 2151–2155.

44. A. Hesselmann and G. Jansen, *Chem. Phys. Lett.*, 2002, **362**, 319–325.

45. A. Hesselmann and G. Jansen, *Chem. Phys. Lett.*, 2002, **357**, 464–470.

46. A. Hesselmann and G. Jansen, *Chem. Phys. Lett.*, 2003, **367**, 778–784.

47. A. Hesselmann, G. Jansen, and M. Schütz, *J. Chem. Phys.*, 2005, **122**, 14103.

48. H.-J. Werner, P. J. Knowles, G. Knizia, F. R. Manby, M. Schütz, and others, 2012.

49. B. Jeziorski, R. Moszynski, and K. Szalewicz, *Chem. Rev.*, 1994, **94**, 1887–1930.

50. J. P. Perdew, K. Burke, and M. Ernzerhof, *Phys. Rev. Lett.*, 1996, **77**, 3865–3868.

51. C. Adamo and V. Barone, *J. Chem. Phys.*, 1999, **110**, 6158.

52. R. van Leeuwen and E. J. Baerends, *Phys. Rev. A*, 1994, **49**, 2421–2431.

53. M. Grüning, O. V. Gritsenko, S. J. A. van Gisbergen, and E. J. Baerends, *J. Chem. Phys.*, 2001, **114**, 652.

54. J. Slater, *Phys. Rev.*, 1951, **81**, 385–390.

55. S. H. Vosko, L. Wilk, and M. Nusair, *Can. J. Phys.*, 1980, **58**, 1200–1211.

56. A. D. Becke, *Phys. Rev. A*, 1988, **38**, 3098–3100.

57. C. Lee, W. Yang, and R. G. Parr, *Phys. Rev. B*, 1988, **37**, 785–789.

58. S. Grimme, *J. Comput. Chem.*, 2006, **27**, 1787–1799.

59. J. P. Perdew, *Electronic Structure of Solids '91*, Akademie Verlag, Berlin, P. Ziesche., 1991.

60. A. D. Becke, *J. Chem. Phys.*, 1993, **98**, 5648.

61. J. Tao, J. Perdew, V. Staroverov, and G. Scuseria, *Phys. Rev. Lett.*, 2003, **91**, 146401.

62. Y. Zhao and D. G. Truhlar, *Theor. Chem. Acc.*, 2007, **120**, 215–241.

63. A. D. Becke and E. R. Johnson, *J. Chem. Phys.*, 2005, **123**, 154101.

64. E. R. Johnson and A. D. Becke, *J. Chem. Phys.*, 2006, **124**, 174104.

65. V. Blum, R. Gehrke, F. Hanke, P. Havu, V. Havu, X. Ren, K. Reuter, and M. Scheffler, *Comput. Phys. Commun.*, 2009, **180**, 2175–2196.

66. G. Kresse and J. Furthmüller, *Phys. Rev. B. Condens. Matter*, 1996, **54**, 11169–11186.

67. K. Lee, É. D. Murray, L. Kong, B. I. Lundqvist, and D. C. Langreth, *Phys. Rev. B*, 2010, **82**, 081101.

68. J. Klimeš, D. R. Bowler, and A. Michaelides, *J. Phys. Condens. Matter*, 2010, **22**, 022201.

69. P. Lazar, F. Karlický, P. Jurečka, M. Kocman, E. Otyepková, K. Safářová, and M. Otyepka, *J. Am. Chem. Soc.*, 2013, **135**, 6372–6377.

70. J. Antony and S. Grimme, *Phys. Chem. Chem. Phys.*, 2008, **10**, 2722–2729.

71. R. C. Lochan and M. Head-Gordon, *Phys. Chem. Chem. Phys.*, 2006, **8**, 1357–1370.

72. M. Kocman, M. Pykal, and P. Jurečka, *Phys. Chem. Chem. Phys.*, 2014, **16**, 3144–3152.

73. V. Spirko, M. Rubes, and O. Bludský, *J. Chem. Phys.*, 2010, **132**, 194708.

74. L. Mattera, F. Rosatelli, C. Salvo, F. Tommasini, U. Valbusa, and G. Vidali, *Surf. Sci.*, 1980, **93**, 515–525.

75. E. Ghio, L. Mattera, C. Salvo, F. Tommasini, and U. Valbusa, *J. Chem. Phys.*, 1980, **73**, 556.

76. Y. Zhang, W. Pan, and W. Yang, *J. Chem. Phys.*, 1997, **107**, 7921–7925.

77. S. N. Steinmann, C. Piemontesi, A. Delachat, and C. Corminboeuf, *J. Chem. Theory Comput.*, 2012, **8**, 1629–1640.